INHIBITION OF BACTERIAL HEPTOSE SYNTHESIS

INHIBITION OF BACTERIAL HEPTOSE SYNTHESIS

By

GLADYS P. DE LEON, B. Sc.

A Thesis

Submitted to the School of Graduate Studies

In partial Fulfilment of the Requirements

For the Degree

Master of Science

McMaster University

MASTER OF SCIENCE (2005) McMaster University

(Biochemistry) Hamilton, Ontario

TITLE: Inhibition of Bacterial Heptose synthesis

AUTHOR: Gladys P. de Leon, B. Sc. (McMaster University)

SUPERVISOR: Professor G.D. Wright

NUMBER OF PAGES: xiii, 107

Abstract

Lipopolysaccharide (LPS) a major non-protein component of the outer membrane of Gram-negative bacteria, defines many of the host-bacterium interactions and provides an effective barrier by inhibiting diffusion of bile salts, detergents, and lipophilic antibiotics. The heptose molecule is an essential component of the bacterial LPS inner core and the synthesis of this subunit is an attractive antimicrobial target. A major challenge to exploit this pathway for antibiotic discoveries has been the unavailability of substrates.

TktA, GmhA, HldE and GmhB proteins involved in the biosynthesis of the LPS precursor ADP-D-*glycero*-β-*manno*-heptose have been cloned and overexpressed in *Escherichia coli* to develop a simultaneous *in vitro* assay suitable for high-throughput screening (HTS) of small molecules. Readily accessible ribose-5-phosphate and fructose-6-phosphate were used as substrates for the heptose pathway and to circumvent the obstacles of substrate availability and stability. We have optimized an *in-vitro* pathway assay and report its use to screen a small molecule library that identifies the first reported inhibitor of heptose synthesis. The inhibitor, 2-Methyl-6-methylamino-7-oxo-7*H*-naphthol [1,2,3-*de*]quinoline-4-sulfonic acid was determined to be a competitive inhibitor of the HldE kinase with K_i of 63 ± 8 μM. This assay enables probing an important biochemical pathway that otherwise would be highly challenging and allows for efficient detection of novel LPS inhibitors that could potentially lead into antimicrobial treatment.

This study also exploited structure-based drug design via protein crystallization. The crystal apoprotein structure of GmhA was determined to a 1.95 Å resolution. The

GmhA with the substrate bound was determined to a 2.79 Å resolution which is the first reported structure of this protein bound with the substrate. By applying knowledge and techniques earned from a combination of advances in assay development, compound library development, robotic instrumentation and protein crystallization, identification and modification of novel inhibitors is possible and has the potential to advance antibiotic research.

Acknowledgements

First and foremost, I would like to give all the credits to my Creator for all the blessings and for making it possible for me to enjoy life with a purpose.

I would like to thank my dad for encouraging me to become a stronger person everyday, for being my coach, my idol, my inspiration, and for sacrificing everything to be where I am right now. My mom for her understanding and support, although she is far away her prayers and words give me comfort at night. My brother and sister for their understanding and putting up with a lot of missed occasions and especially being bossed around when I'm home visiting.

Very special thanks to my supervisor, Dr. Gerry Wright, for giving me this opportunity to work in this project, to be part of this dynamic lab and I will carry on as a proud Wright lab alumni. His guidance and encouragement have made me do things I never thought I can possibly do and I will always remember this experience. I would also like to thank my committee members, Dr. Eric Brown and Dr. Miguel Valvano, for all the help and suggestions. Thanks also to Dr. Murray Junop for helping me with protein crystallization and for taking the time to teach me new techniques and theory.

Thanks to everyone in the Wright lab both past and present for making this experience an unforgettable one. I would like to personally thank Kalinka for all the help and for being such a kind person. Thanks to Ishac for all the help and for making me laugh -"we'll talk online" and to Tariq for not only putting up with me but also for the all good times and the pranks! I would like to thank Ian for the all the advice, the guidance and most especially for making our bay the 'best bay ever!' P.S. Molly rocks.

The yeast lover girls Laura and Denise for the salsa and facial memories; to Bays 1 and 2 occupants, Rae, Linda, Xiao Dong for all the help, Sherry for making sure we have enough P1 buffer and Jay (jay of death) for keeping me up-to-date in the punk music scene. Thanks to Jennifer for being my Hollywood daily gossip correspondent, for the great time in Hawaii and for being such a cool friend which is so bananas! To Tushar for the great times every Paycheck Thursday and may you carry on the legacy. Special thanks to Vanessa, not only for being one of the first person to talk to me in the lab but also for the science talks, the grant writing marathon, and for being such a great friend.

Last and certainly not the least, my cousins, Julie, Brian, Cherry and Cathy, my amazing friends, Elaine, Catherine, Vaneeta, Dorothy, Maricor, Candice and the rest of the crew for the great friendship throughout so many years, great parties, night outs, long phone conversations and for laughing with me about anything. Without whom I may have loosened my cool. Thanks guys!

Table of Contents

List of Figures

List of Tables

1. Introduction

1.1 Medical problems caused by multi-drug resistant Gram-negative bacteria

The rate of multi-drug resistant (MDR) pathogens continues to grow at an alarming rate. According to the World Health Organization's (WHO) 2000 report on infectious disease, pneumonia, which can be caused by MDR bacteria remains the number one killer world wide (59). The presence of opportunistic pathogens such as *Psedomonas aeruginosa, Staphylococcus aureus, Haemophilus influenza* and *Burkholderia cepacia* is associated with a deterioration of lung function, causing severe chronic lung inflammation in cystic fibrosis patients (10, 13, 41, 46, 47). Gram-negative bacteria are also responsible for infections of the central nervous system (CNS) such as meningitis and meningoencephalitis, bacterial endocarditis and other biofilm diseases (9, 37). Resistance of Gram-negative bacteria to hydrophobic molecules such as antibiotics and oligopeptides is attributed to the low permeability of the outer membrane (OM) (1, 14, 15, 25, 28, 30-32, 34, 39, 43, 52, 60). Despite advances in medicine and technology, infectious diseases pose a deadlier threat to human life than war and famine. Although prevention through vaccination continues to be the ultimate weapon against infection and drug resistance, no vaccines are available to prevent five of the top six major infectious killers.

1.2 Outer membrane of Gram-negative bacteria

1.2.1 Composition

The cell envelope of Gram-negative bacteria consists of an inner membrane (IM) and an OM separated by the peptidoglycan layer in the periplasm (Figure 1-1). The OM of Gram-negative bacteria lies outside the peptidoglycan layer and displays an asymmetric lipid morphology. The inner leaflet of the OM is composed of phospholipids while the outer leaflet is made up of lipopolysaccharide (LPS). The phospholipid components of the OM are similar to those of the cytoplasmic membrane, the only difference being a slight enrichment in phosphatidylethanolamine (30, 39, 40, 43, 60).

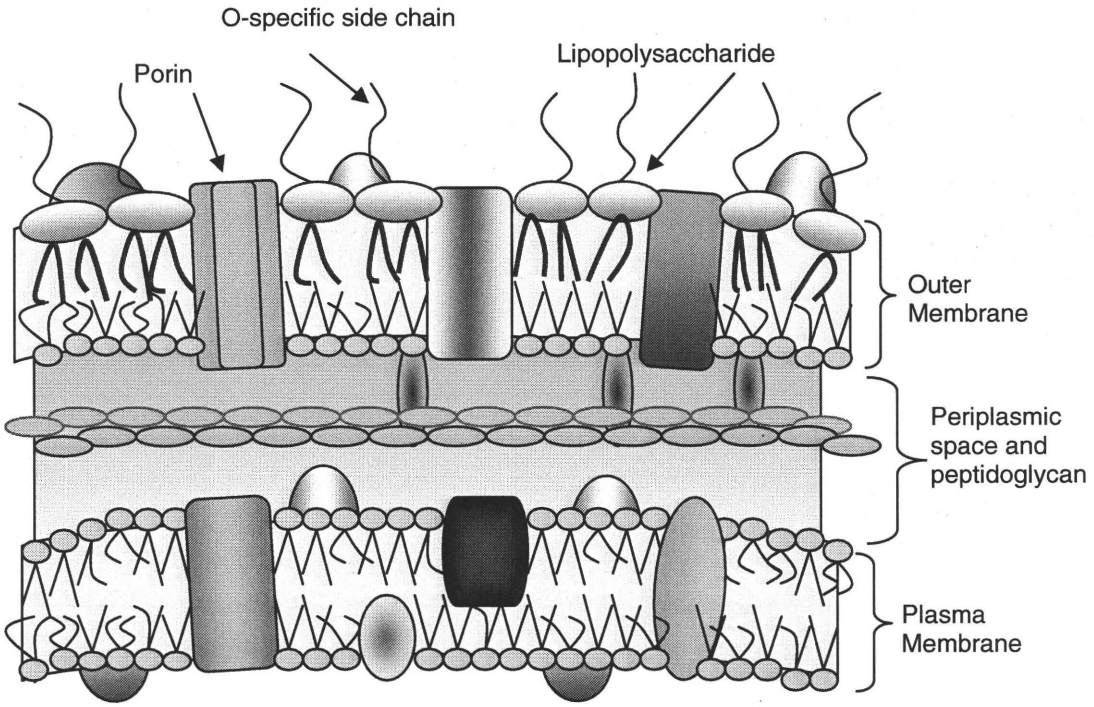

Figure 1-1. Cell envelope structure of most Gram-negative bacteria. The cell envelope of Gram-negative bacteria is divided into three main sections: the plasma membrane, the periplasmic space and peptidoglycan, and the outer membrane. Gram-negative bacteria have a unique outer membrane composed primarily of lipopolysaccharide (LPS) and membrane proteins. LPS is exclusive to Gram-negative bacteria and is attributed to the resistance of these pathogens to several antibiotics which are effective against most Gram-positive organisms (15, 30, 39, 50, 55, 60).

LPS, a complex of glycolipids found on the outer leaflet of the bilayer, plays an important role in the structural integrity and is characteristic of the Gram-negative bacterial cell envelope (15, 39, 40, 60). It is divided into three main components, the anchor lipid-A, the core oligosaccharide region, and the O-specific polysaccharide chain also known as the O-antigen (Figure 1-2).

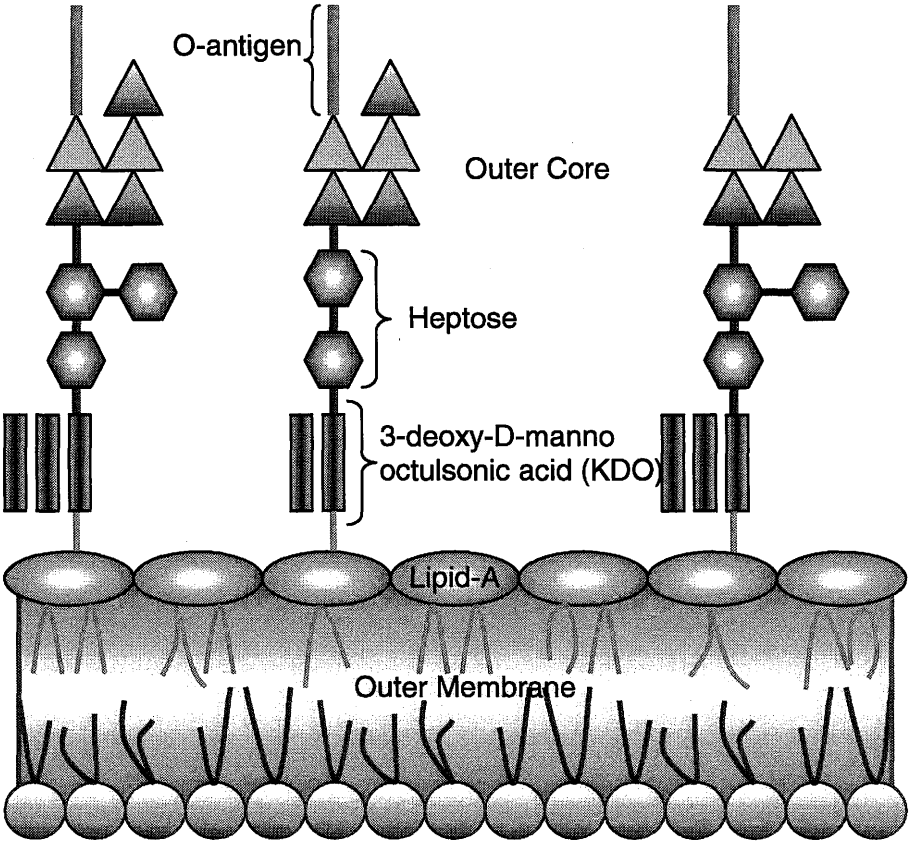

Figure 1-2. Gram-negative bacterial outer membrane structure. The asymmetric lipid bilayer is composed of phospholipids in the inner leaflet and lipopolysaccharide (LPS) in the outer leaflet. LPS is sub-divided into three components: lipid-A, core-oligosaccharide, and O-antigen. Lipid-A anchors the LPS molecule to the membrane. The core oligosaccharide domain, attached directly above lipid-A, is further divided into two domains. The inner-core is composed of two or three residues of 3-deoxy-D-manno-octulsonic acid (KDO) and two or three residues of L-*glycero*-D-*manno*-heptose (labelled as Heptose above). The outer-core domain is made up of hexose and hexosamine sugars. The O-antigen, the least conserved of the LPS components, is located above the outer-core domain and is composed of diverse oligosaccharides repeats.

1.2.2 Lipid-A

The lipid-A is a hydrophobic membrane anchor opposite the inner phospholipid leaflet layer of the OM. This universally conserved region of the LPS contributes to the structural integrity of the bacterial membrane by providing low fluidity of the outer membrane (39). Lipid-A possesses a backbone composed of a β,1'-6 linked acylated, phosphorylated and glycosylated glucosamine disaccharide (39, 40) (Figure 1-2). The enzymology and molecular genetics of the conserved biosynthesis of lipid-A are best characterized in *E. coli* and it has been well documented in several review articles (30-32, 34, 35, 39, 40, 52, 60).

1.2.3 Core Oligosaccharide

Attached to the lipid-A is the core oligosaccharide, which is further subdivided into three substituents: the inner-core domain, consisting of two residues of 3-deoxy-D-*manno*-octulosonic acid (KDO), and, depending on the particular species, two or three residues of L-*glycero*-D-*manno*-heptose (Heptose) (15, 22, 30, 31, 40, 43, 52, 56, 60). The KDO and heptose provide an effective membrane barrier by protecting the bacterial cells from antibiotics, bile salts, detergents and digestive enzymes (31). There has been substantial developments in understanding the enzymology and molecular biology of the inner core mostly in *E. coli* and *S. enterica,* particularly in the enzymes involved in the biosynthesis of the heptose region (3, 5, 19, 21, 22, 36, 49, 55, 56). Such advancements will be further discussed in detail later in this paper.

The outer-core domain is located external to the heptose region, and usually consists of hexoses and hexoamines (Figure 1-2). The specific role of the outer-core other than being a membrane barrier is not clear since there are no substantial studies that have been conducted on the sugars in this domain. The inner-core component of the LPS molecule is relatively conserved among many enteric and non-enteric bacteria except in *Acinetobacter, Legionella* and *Rhizobium* (32, 56). While the outer-core shows structural diversity, the sugars in the O-antigen region are even more diverse (39).

1.2.4 O-antigen

Attached to the core-oligosaccharide region is the O-antigen region component of LPS (Figure 1-2). The addition of the O-antigen to the nascent lipid-A-core at the periplasmic face of the cytoplasmic membrane completes biosynthesis of the LPS molecule. The O-antigen is a structurally diverse polymer, composed of oligosaccharide repeats that protect invading bacteria from lytic components resulting from the activation of the complement cascade (39). The chemistry of the O-antigen (i.e. chain length) has also been reported to affect the assembly of the membrane attack complex and influences invasiveness and subsequent inter- and intracellular spread via polar localization in *Shigella flexneri* (60). The oligosaccharide diversity in the surface O-antigens of Gram-negative bacteria is observed due to the variability within the repeat unit such as type, linkage and substitution of its sugar components leading to an enormous number of possible O-antigen structures (39, 60). The variability and diversity of this region of the

LPS is not surprising considering that the O-antigen is more exposed to selective pressure of host responses, bacteriophages, and environmental stresses (39, 40).

1.3 Roles of Lipopolysaccharides

1.3.1 Structural and functional integrity of the outer membrane

One of the major roles of LPS is to provide structural and functional integrity to the Gram-negative OM. First, LPS ensures the proper assembly and structure of membrane porins like OmpF, OmpC and PhoE in *E. coli* and OprF in *P. aeruginosa*, LamB (maltose channel), ScrY (sucrose channel), gated channels and membrane protein receptors (31, 32, 60). These proteins are essential for bacterial survival and growth since they are required for the influx of nutrients and efflux of waste products and harmful molecules. The importance of the LPS molecule, especially the phosphorylated sugar substituents in membrane protein assembly, is evident in the X-ray structure of LPS in complex with membrane porin FhuA. In 2000, Ferguson and colleagues concluded that the basic amino acid side chains that play an important role in the interaction between the LPS and FhuA are also conserved in other LPS-binding proteins (14, 32). This X-ray analysis emphasized that the negative charges on the LPS molecules play an important role in protein stability and hence, provides the structural and functional integrity of Gram-negative OM and its protein components.

1.3.2 LPS as an effective membrane barrier

An interesting feature of the LPS layer is that it acts as both as an endotoxin, for example contributing to bacterial sepsis, and as a component of the bacterial outer membrane barrier. These related characteristics are attributed to the way the LPS molecules aggregate while interacting with cells, antibiotics, and antimicrobial peptides (51). The proximal part of the core (KDO and heptose) and the lipid-A backbone contain a large number of anionic groups (33). It is proposed that these negatively charged phosphoryl substituents allow neighbouring LPS molecules to be cross-linked by divalent cations such as Ca^{2+} or Mg^{2+} (60) (Figure 1-3). The cross-linking divalent cations bridge the LPS molecule to aggregate in such a way that would impart stability to the Gram-negative outer membrane and a decrease in fluidity. In turn, the packing properties of the LPS molecules provide Gram-negative bacteria with an effective permeability barrier against hydrophobic antibiotics and oligopeptides (31, 52, 60) (Figure 1-3).

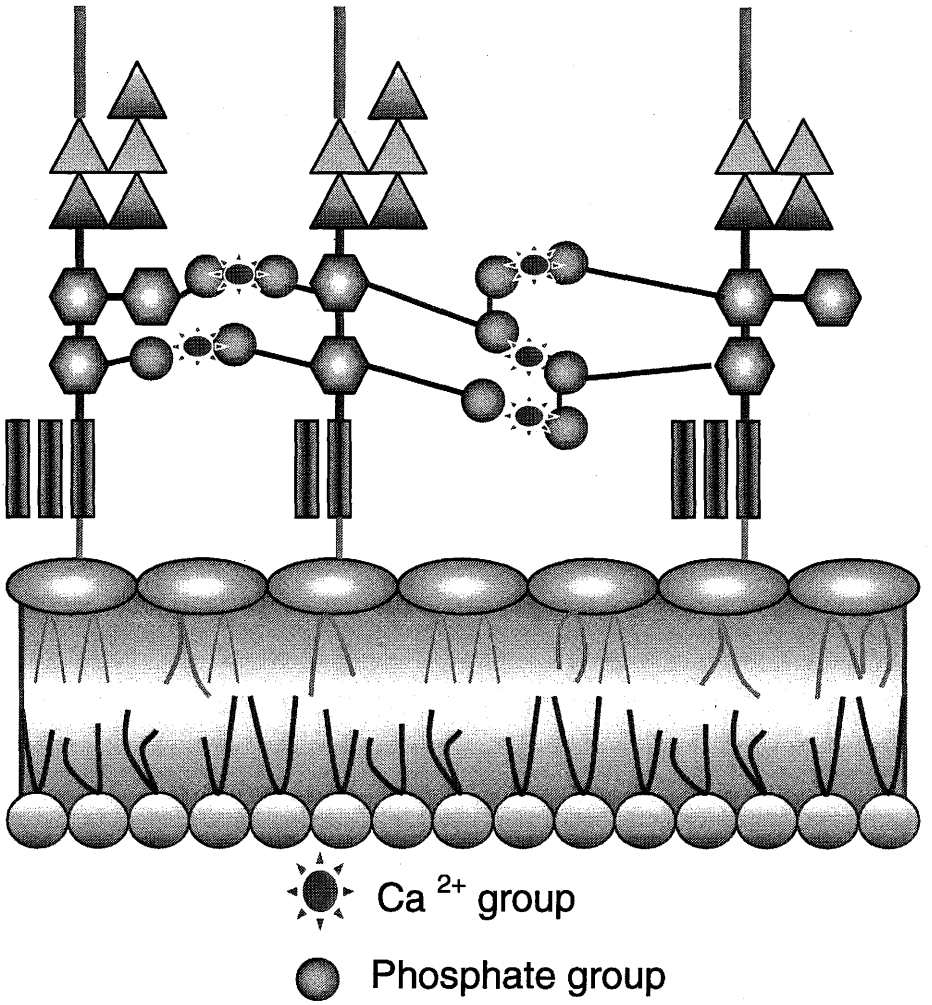

Figure 1-3. Crosslinking of the LPS molecules. Cross-section of the inner-core component of the Gram-negative bacterial outer membrane showing clusters of phosphate groups. The phosphate groups branch out from different heptose sugar promoting LPS crosslinking by divalent cations, Ca^{2+} and/or Mg^{2+}. Note that the KDO and lipid-A constituents also contain phosphorylation, but these are not shown in the diagram for simplicity.

The glucosamine disaccharides of lipid-A are typically phosphorylated at the 1 and 4' position, while some of the KDO and heptose in the inner-core are phosphorylated or carry phosphoethanolamine or pyrophosphoethanolamine substituents (31, 32, 38, 60) The barrier function of the OM has been documented extensively for the past 30 years.

The Nikaido group (32) suggested that with the acidic lipids, the neutralization and bridging of the negative charges by Ca^{2+} or Mg^{2+} is the major factor in determining lateral interaction between the lipids and hence the fluidity and melting behaviour of the bilayer. A parallel observation was reported earlier by Papahadjopolons *et al.* (32). The acidic lipid phosphatidylserine increases melting point by more than 50°C when 1 mM Ca^{2+} was added to the solution, increasing LPS cross-linking of the phosphate constituents. Furthermore, several findings over the past three decades strongly support that the removal of most of the cations from LPS by ethylene-diamine-tetraacetic acid (EDTA) treatment disrupts the aggregation and packing properties of the LPS molecules resulting in a leaky membrane (1, 8, 25, 40, 54).

1.3.3 Preventing drug access and developing antibiotic resistance

The presence of long unsaturated fatty acyl chains and the bridging of the LPS molecules result in strong lateral interaction between LPS molecules, producing a gel-like interior with very low fluidity (32). This characteristic contributes to the resistance of Gram-negatives to many antibiotics that are effective against Gram-positives, which lack the LPS region. For example, Gram-negatives are resistant to macrolides, novobiocin, rifamycins, clindamycin and fusidic acid (31). Due to the ability of the LPS molecule to slow down the diffusion rates of antibiotics, bacteria have the opportunity to combat the small amounts of antibiotic able to penetrate the cell, rather than a larger amount. This also primes the bacteria to develop very high levels of resistance to antibiotics (25, 31, 32, 34, 38). For example, *Pseudomonas aeruginosa* is notorious for being resistant to a large

range of antibiotics, mostly because the permeability of the OM to hydrophilic solutes is about two orders of magnitude lower than that of *E. coli* (32). In addition to a slower diffusion rate, the main porin in *P. aeruginosa*, OprF, which is abundantly present in the OM, allows only a very small diffusion of small molecules, although its exclusion limit is much higher than that of the *E. coli* OmpF (35). These observations have recently been supported through Atomic Force Microscopy (AFM) structural studies. Tong and McIntosh in 2004 (51) performed structural analysis of the interactions of hydrophobic antibiotics and melittin with large unilamellar vesicles (LUVs) composed of LPS and phospholipids. The analysis indicated that the tight packing of the LPS molecules decreases the permeability of the LUVs to hydrophobic antibiotics.

1.4 Molecular and Chemical Studies

1.4.1 Perturbation of the outer membrane permeability barrier

Chemical and molecular studies on the LPS molecule over the past fifty years suggest that disruption of the phosphorylated sugar substituents results in major structural alterations leading to increased membrane permeability. For example, treatment of LPS with the divalent cation chelating agent, EDTA, increases cell permeability to detergents, bile salts, hydrophobic molecules and antibiotics. Early studies by MacGregor and Elliker in 1958 (27) with *P. aeruginosa* indicated that mutants resistant to quaternary ammonium compounds increased in sensitivity to these compounds after treatment with EDTA (27). Treatment with EDTA resulted in disruption of the permeability barrier but not other cell functions as the EDTA treated bacteria remained fully viable (27). These

observations attracted scientists world wide to study the OM permeability to drugs and metabolites that are known to be ineffective against Gram-negative bacteria (25).

It is widely accepted that increased OM permeability is due to the loss of divalent cations, mostly interacting with phosphorylated heptoses that normally cross-link and bridge LPS molecules. It should be emphasized that the electrostatic interactions between the polycationic and polyanionic agents of the LPS at the surface of the outer membrane greatly depends on the ionic strength (32, 52, 53).

Mutational studies in the genes responsible for the biosynthesis of the heptose region are well characterized in *E. coli* and *S. typhimurium.* Mutants of Gram-negative bacteria with an altered or absent heptose region are characterized as having 'deep-rough' LPS phenotypes (5, 26, 33, 38, 55, 60). The deep-rough phenotype consists of a series of characteristics that collectively reflect changes in both composition and structure of the outer membrane, leading to its instability (5, 6, 26, 31, 43, 45, 60).

1.5 ADP-heptose pathway

1.5.1 Molecular genetics of the ADP-heptose biosynthesis

The complete biosynthetic pathway for the activated nucleotide heptose precursor, ADP-L-*glycero*-D-*manno*-heptose, was recently elucidated by Valvano *et. al* in 2002 (56). As illustrated in Figure 1-4, the group proposed that the pathway in *E. coli* occurs via the following steps: i) conversion of D-sedoheptulose-7-phosphate to D-*glycero*-D-*manno*-heptose-7-phosphate by a phosphoheptose isomerase, ii) formation of D-ß-D

heptose-1,7-bisphosphate by a phosphoheptose kinase reaction, iii) dephosphorylation of the hexose diphosphate to D- β-D-heptose-1-phosphate by a bisphosphatase reaction, iv) adenylylation via phosphodiester linkage, and v) epimerisation of ADP-D-*glycero*-β-*manno*-heptose to an activated sugar, ADP-L-*glycero*-β-*manno*-heptose (33, 43, 55). The ADP-heptose serves as a substrate for specific heptosyltransferases that transfer the heptose moiety to the growing inner core molecules after the synthesis of the lipid-A-KDO is complete.

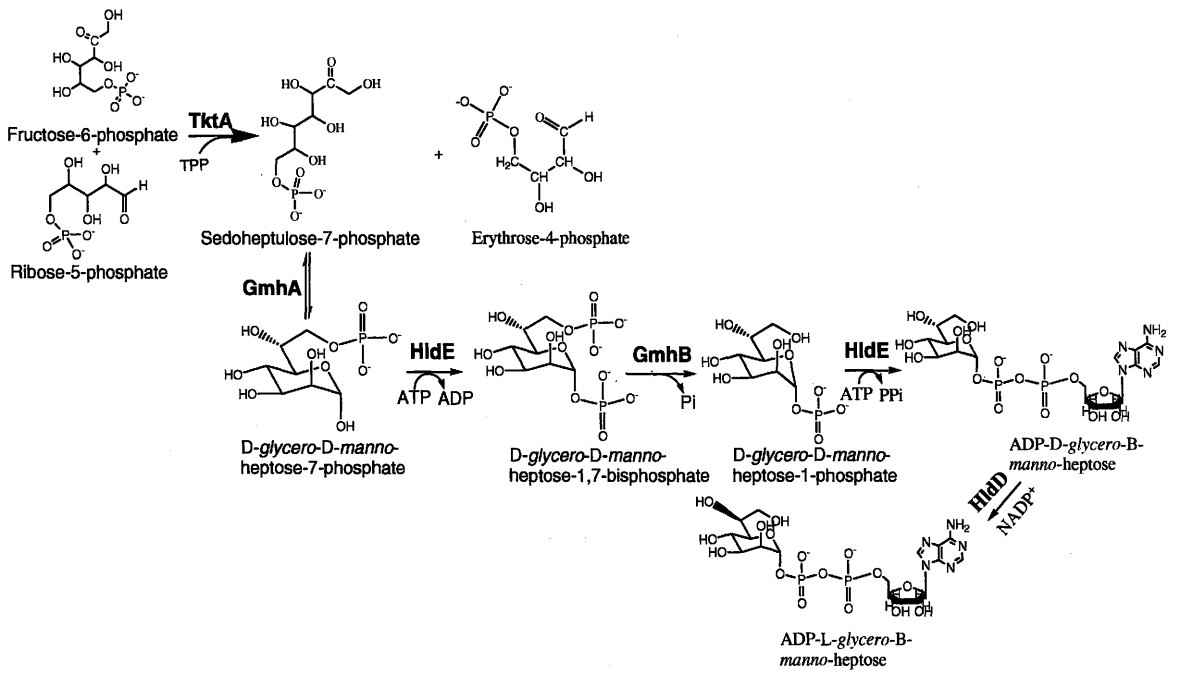

Figure 1-4. The biosynthesis of the ADP-heptose constituent of bacterial lipopolysaccharide. The reaction begins with fructose-6-phosphate and ribose-5-phosphate to synthesize the nucleotide activated sugar ADP-L-*glycero*-β-*manno*-heptose. The nucleotide activated sugar is the precursor for the LPS inner-core domain. The enzymes in the pathway have been shown to be essential for the synthesis of the ADP-heptose constituent, as mutational studies have demonstrated that alteration or deletion of any of the genes produced deep-rough phenotypes which are sensitive to novobiocin.

1.5.2 TktA – Transketolase enzyme

Transketolase (D-sedoheptulose-7-phosphate:D-glyceraldehyde-3-phosphate glycoladehyde transferase) is a key enzyme not only in the non-oxidative pentose pathway but also for the biosynthesis of the ADP-L-*glycero*-β-*manno*-heptose (11, 48). TktA catalyzes several reactions leading to formation of sedoheptulose-7-phosphate (11). For the purpose of this work, the reaction between ribose-5-phosphate and fructose-6-phosphate to synthesize sedoheptulose-7-phosphate is illustrated in Figure 1-4. The importance of TktA in the biosynthesis of ADP-heptose was elucidated in *S. typhimurium* by L. Eidels and J. Osborn (12), who isolated *tktA* mutants that failed to synthesize sedoheptulose-7-phosphate, and consequently produce a heptose deficient LPS.

1.5.3 GmhA – Phosphoheptose isomerase enzyme

The enzyme GmhA is responsible for the first committed step in ADP-heptose biosynthesis, which converts the linear sugar sedoheptulose 7-phosphate to D-glycero-D-manno-heptose-7-phosphate via an isomerase reaction (Figure 1-4). Valvano and Brooke (5) identified that the *gmhA* gene in *E. coli* encodes an enzyme exhibiting phosphoheptose isomerase activity. A strain carrying a *gmhA* deletion displayed high sensitivity to the hydrophobic antibiotic novobiocin and produced an LPS core lacking *glycerol-manno*-heptose and terminal hexoses. They also demonstrated that the *gmhA* gene (formerly known as *lpcA*) is conserved among enteric bacteria including *Enterobacter, Escherichia, Klebsiella, Proteus, Salmonella,* and *Shigella*, suggesting that it is an essential component of the inner-core biosynthetic pathway (5).

1.5.4 HldE - Bifunctional kinase/adenylyl transferase

The second catalytic step committed to the ADP-heptose pathway is phosphorylation of D-*glycero*-D-*manno*-heptose-7-phosphate at position 1 by HldE, a bifunctional kinase/adenylyltrabnsferase enzyme (Figure 1-4). Both enzyme domains of HldE are functionally different and genetically separable. Domain I is involved in the synthesis of D-ß-D heptose-1,7-bisphosphate, whereas domain II catalyzes ADP transfer to form ADP-D-*glycero*-ß-*manno*-heptose (55, 56), and both are involved in the biosynthesis of the LPS core. Valvano and colleagues (55) reported that the insertion of the mini-Tn10 in domain I of the *hldE* gene confers a heptoseless LPS phenotype in *E. coli* K-12. Mutants with a heptoseless inner core are viable, but they display a dramatic reduction in the number of porins. In addition, bacteria did not grow in media containing detergents, bile salts and hydrophobic antibiotic due to the increased permeability of the outer membrane (55). Similar results were obtained by the Kim group (17) using *S. typhimurium.*

The Valvano group (55) also reported that the kinase domain (HldE-A) showed conservation in members of the ribokinase family and the adenylyltransferease (HldE-C) domain showed similarities with the cytidylyltransferase superfamily via BLAST search using the *E. coli* HldE protein as a query. This conservation among bacteria makes the HldE protein a good target for developing novel therapeutics.

1.5.5 GmhB - Heptose-bisphosphate phosphatase enzyme

The *gmhB* gene encodes the heptose-bisphosphate phosphatase enzyme. The enzyme can use either D-*glycero*-α-D-*manno*heptose-1,7-bisphosphate or D-*glycero*-ß-D-*manno*heptose-1, 7-bisphosphate as a substrate to remove the phosphate group at the C-7 position (56) (Figure 1-4). The study by Kneidinger and co-workers (56) confirmed that the GmhB protein is required for the formation of ADP-D-*glycero*-ß–D-*manno*-heptose (21, 56).

Sequence analysis of the GmhB protein performed by Valvano and colleagues (56) indicated that the protein belongs to the haloacid dehydrogenase (HAD) superfamily of hydrolases that contain three highly conserved sequence motifs with core α/ß domains. In addition, the catalytic aspartic acid as well as motif I are highly conserved among the GmhB homologues. This conservation suggests similar structures and mechanism of action as that of the other members of the HAD family, hence *gmhB* appears to be a good target in developing novel antibiotics.

1.6 Research Barriers

Chemical and molecular studies on 'deep-rough' mutations in various organisms such as *S. typhimurium* (12), *E. coli* and *P. aeruginosa* (5, 22, 31, 33, 38, 52, 55, 56, 60) concluded that deep-rough mutants with truncated LPS and reduced phosphorylation show an unstable OM. Thorough research over the past few decades strongly supports the idea that finding inhibitors for the enzymes involved in heptose biosynthesis leading to 'deep-rough' phenotypes are good candidates in developing novel inhibitors. Such inhibitors may act synergistically with conventional antibiotics. However, this approach has some difficulties. Before screening for inhibitors, it is necessary to develop the sugar substrate intermediates for ADP-heptose biosynthesis, which are currently unavailable. Also, an appropriate assay must be developed and subsequently adapted for HTS. The sugar substrate sedoheptulose-7-phosphate was discontinued in 1997 by Sigma-Aldrich, and the sugar intermediates D-*glycero*-D-*manno*-heptose-7-phosphate, D-ß-D heptose-1, 7-bisphosphate, D-ß-D-heptose-1-phosphate and ADP-D-*glycero*-ß–*manno*-heptose (19) are not available commercially. Therefore, the lack of commercial resources limit the understanding and characterization of the enzymes GmhA, HldE, GmhB and HldD in the ADP-heptose pathway, leading to difficulties in finding and evaluating inhibitors that could potentially lead to novel antimicrobial agents.

1.7 Research Objectives

Through a combination of advances in assay development, compound library development, robotic instrumentation, and liquid handling technologies in the 1990s, there has been an increased demand for high throughput inspired protein biochemists to come up with new means to perform multiple assays in a day. Our primary objective in this work was to develop an *in-vitro* assay suitable for high-throughput screening by empirically linking the enzymes in the ADP-heptose biosynthetic pathway to establish an assay in a metabolically relevant direction starting with 1) TktA, 2) GmhA, 3) HldE (Kinase), 4) GmhB, and 5) HldE (adenylyltransferase). This assay could then be used to screen small molecule libraries to identify inhibitors of the ADP-heptose biosynthetic enzymes, which could lead to the development of new antimicrobial agents. Screening the enzymes in tandem avoids problems with substrate availability and stability. This is a great advantage for a screen of the ADP-heptose pathway since the substrates and intermediates are not commercially unavailable as mentioned in the previous section. The transketolase enzyme must be included in the pathway assay since the reaction will be initiated by the commercially available substrates ribose-5-phosphate and fructose-6-phosphate. Also, a screen involving the enzymes in tandem potentially increases the chances of finding inhibitory compounds to more than one enzyme.

2. *Materials and Methods*

2.1 Bacterial Strains and Growth Conditions

Bacterial cultures were grown overnight at 37°C and 250 rpm in Luria Broth (LB) from Sigma (St Louis, MO) supplemented with the appropriate antibiotics at final concentrations of 100 μg/mL ampicillin or 50 μg/mL kanamycin. All antibiotics used for this study were purchased from BioShop Canada, Ltd. (Burlington, ON), unless otherwise noted. *E. coli* BL21 (DE3) cells were used for plasmid propagation and protein overexpression.

2.2 Recombinant DNA methods

Recombinant DNA procedures were performed according to standard methods described by Sambrook *et. al.* (42). Genomic DNA isolated from *E. coli* W3110 cells was used as the template to amplify the *tktA, gmhA, hldE* and *gmhB* genes. Genomic DNA was prepared using the salting-out procedure (42). Plasmid DNA was extracted from overnight cultures of *E. coli* using Qiagen QIAprep Spin Miniprep Kit (Qiagen Inc., Missisauga, ON) according to the manufacturer's instructions. DNA was analyzed by 1% Tris-acetate-ethylenediamine-tetracetic acid (TAE) agarose gel electrophoresis stained with ethidium bromide according to standard methods (42). DNA fragments were excised from the agarose gels and purified using either the Qiagen QIAEXII Gel Extraction Kit or QIAquick Gel Extraction Kit according to manufacturer's instructions. Transformations were performed by electroporation with a Genepulser apparatus from Bio-Rad Laboratories Ltd. (Mississauga, ON) using a 0.2 mm cuvettes. All restriction

endonucleases were obtained from MBI Fermentas (Oakville, ON), except for *Nde* I, which was purchased from New England Biolabs (Pickering, ON). All enzymes were used as suggested by the manufacturer unless otherwise specified.

2.3 Gene Amplification

Three genes encoding the first three enzymes TktA, GmhA and HldE of the ADP-heptose biosynthetic pathway were amplified by Polymerase Chain Reaction (PCR) using *E. coli* W3110 genomic DNA as the template. Reaction mixtures were composed of 1 x Biotools DNA polymerase buffer (Biotools Inc., Edmonton, AB) mixed with 500 ng of chromosomal DNA template in a 50 μL sample volume. The reactions were set-up according to general procedures with modifications in the $MgCl_2$ contents. The oligonucleotide primer annealing temperatures were varied for each gene and were dependent on the calculated melting points (Table 2-1). Primers used for this study were synthesized at MOBIX Central Facility at McMaster University (Hamilton, ON).

Table 2-1. Summary of the forward and reverse primers and their corresponding annealing temperature (°C) used to amplify *tktA*, *gmhA*, *hldE* and *gmhB* genes via PCR.

Gene	Size (bp)	Primers (5'→ 3')	Calculated Annealing Temperature (°C)
tktA	1992	***Forward***: GGGGACAAGTTTGTACAAAAAAGCAGGCTT AGATTACGATTACGATATCCCA ACG GAA ACC CTG TAT TTT CAG GGC TCC TCA CGT AAA GAG CTT GCC ***Reverse***: GGGGACCACTTTGTACAAGAAAGCTGGGTC TTACAGCAGTTCTTTTGCTTTCGC	**52**
gmhA	579	***Forward***: CGCGGATCCATATGTACCAGGATCTTATTC GTAACG ***Reverse***: CGCGGATCCAAGCTTACTTAACCATCTCTTTT TCAATCAAC	**53**
hldE	1434	***Forward***: GGGGACAAGTTTGTACAAAAAAGCAGGCTT AGATTACGATATCCCAACGCAAGAAACCCT GTATTTTCAGGGCAAAGTAACGCTGCCAGA G ***Reverse***: GGGGACCACTTTGTACAAGAAAGCTGGGTC TTAGCCTTTTTTATCCTGTTGG	**44**
gmhB	577	***Forward***: ATGAATTCATATGGCGAAGAGCGTACCCG ***Reverse:*** ATGAATTCAAGCTTAATCATTGTGCCGGTTT TTGCT	**50**

Generally, reactions were incubated at 95 °C for 5 minutes prior to the addition of 1 U Biotools DNA polymerase. The PCR program was designed to have a 30 cycles of the following: 94°C for 1 min, followed by the appropriate annealing temperature (Table 2-1) for 1 min, and 72°C for 2 min to allow for DNA elongation. The reaction was maintained at 72°C for 10 minutes at the end of the 30 cycles and stored at 4°C.

2.4 Plasmid Constructions

Oligonucleotide primers for the amplification of DNA fragments containing the *E. coli* heptose biosynthetic genes *hldE* and *tktA* were designed with *attB1* or *attB2* sites for the insertion into the Gateway donor vector pDONR201 (Invitrogen Life Technologies, Burlington, ON) by homologous recombination (Table 2-1). The PCR products were inserted into pDONR 201 vectors according to the manufacturer's instructions. The resulting plasmids were used to transfer the gene sequence via homologous recombination into the pDEST 17 expression vector (His fusion vector).

Following amplification, the *gmhA* gene was digested with restriction enzymes *Nde* I and *Hind* III at 37°C for 45 min. An additional amount of *Nde* I was added and incubated for an additional 30 min. The endonuclease digestion was followed by a desalting procedure and an overnight ligation was carried-out at 16°C with *Nde* I and *Hind* III digested pET28(a) vector from Novagen (San Diego, CA) treated with 0.25 uL shrimp

alkaline phosphatase (SAP). The pET28(a)-*gmhB* construct was prepared in the same manner by a summer student in the lab, Adam Scott.

2.5 General protein overexpression and purification protocol

The general growth conditions of *E. coli* BL21 (DE3) cells carrying expression plasmids are described in section 2.1. A single colony of *E. coli* BL21 (DE3) containing the desired gene-vector construct was inoculated into 25 mL of LB plus the appropriate antibiotic (Table 2-2) and incubated overnight at 37°C and 250 rpm. A 10 mL aliquot of the overnight culture was inoculated into 1 L LB plus antibiotic, and grown at 37°C and 250 rpm. The culture was induced at OD_{600nm} of ~ 0.55 with isopropyl β-D-thiogalactopyranoside (IPTG) to a final concentration of 1 mM and grown at 16°C for 20 h except for HldE overexpression, which was grown at 37°C for 24 hours.

Cells were harvested by centrifugation at 6,000 rpm for 15 min. The harvested cells were resuspended in 20 mL lysis buffer (Table 2-3) and lysed by three passages through a French Press at a pressure of 10,000 psi. After cell lysis and removal of the membranes by centrifugation, proteins were purified using a 5 mL Hi Trap Chelating HP column (Amersham Bioscience, Piscataway, NJ). For GmhA protein crystallization, a second column was employed to further purify the protein (Section 2.5.2).

Table 2-2. Summary of the plasmids, bacterial strains and antibiotics used for the overexpression of TktA, GmhA, HldE and GmhB proteins.

Protein	TktA	GmhA	HldE	GmhB
Plasmid	pDEST 17 (N-terminal His Tag)	pET 28a(+) (NdeI/ HindIII)	pDEST 17 (N-terminal His Tag)	pET 28a(+) (NdeI/ HindIII)
Bacterial Strain	*E. coli* BL21 (DE3)	*E. coli* BL21 (DE3)	*E. coli* BL21 (DE3)	*E. coli* BL21 (DE3)
Antibiotic resistance gene	Ampicillin	Kanamycin	Ampicillin	Kanamycin

2.5.1 Purification of TktA from recombinant strains

The purification of TktA was carried out using the modified protocol published by Sprenger et al. (48). Harvested cells carrying the pDEST17-*tktA* plasmid were resuspended in 20 mL lysis buffer (Buffer components are described in Table 2-3 below).

The cell free extract was applied directly to a 5 mL HiTrap Chelating Column at a flow rate of 1.0 mL/min. The overexpressed transketolase was eluted at a concentration of 65.5 mM imidazole using a linear gradient. Fractions with TktA protein were collected, analyzed by 15% SDS-polyacrylamide gel electrophoresis, and dialyzed overnight in 20 mM HEPES pH 8.5 at 4 °C. The protein was concentrated to 30 mg/mL using 10,000 MWCO Amicon ultra-15 centrifugation filter from Millipore (Etobicoke, ON) and stored at -20°C in 0.1% DTT and 20% glycerol at a final concentration of 15 mg/mL.

2.5.2 Purification of GmhA from recombinant strains

Cells carrying the pET 28(a)-*gmhA* plasmid were harvested from an overnight culture and resuspended in 20 mL lysis buffer (Table 2-3). After centrifugation, the supernatant was applied onto a 5 mL HiTrap chelating column at a flow rate of 1.0 mL/min. The GmhA protein was eluted at a concentration of 213 mM imidazole using a linear gradient. Fractions containing GmhA, as established by 15% SDS-polyacrylamide gel electrophoresis were pooled and dialyzed overnight in 20 mM HEPES pH 8.0 at 4°C. The dialyzed protein was further concentrated to 20 mg/mL using 10,000 MWCO Amicon ultra-15 centrifugation filter and stored at -20°C with 50% glycerol and 2 mM DTT at a final concentration of 10 mg/mL. An additional purification step for GmhA was performed to set-up crystallization trials. After the first step of purification, the protein was loaded onto a Q-Sepharose column (Amersham Bioscience, Piscataway, NJ) at a rate of 1.0 mL/min and eluted at a concentration of 150 mM KCl_2 using a linear gradient. The column buffer A contained 20 mM HEPES pH 8.0, 1 mM EDTA, 10 mM DTT and buffer B contained components of buffer A with 500 mM KCl_2.

Table 2-3. Lysis buffers and solvent systems used for the purification of the recombinant TktA, GmhA, HldE and GmhB proteins.

Protein	Lysis Buffer	Buffer A	Buffer B
TktA	50 mM HEPES pH 8.5, 1 mM Phenylmethyl sulfonyl fluoride (PMSF), 500 mM NaCl, 20 mM Imidazole, 5mM MgCl2, 0.5 mM Thiamine Pyrophosphate (TPP), 1 mM DTT and 2 mg of DNAse	50 mM HEPES pH 8.5, 500 mM NaCl, 5 mM MgCl2, 0.5 mM TPP, 1mM TPP, 1mM DTT and 20 mM imidazole	50 mM HEPES pH 8.5, 500 mM NaCl, 5 mM MgCl2, 0.5 mM TPP, 1mM TPP, 1mM DTT and 250 mM imidazole.
GmhA	50 mM HEPES pH 8.0, 500 mM NaCl, 20 mM Imidazole, 1mM DTT, 1mM PMSF and 2 mg of DNAse.	50 mM HEPES pH 8.0, 500 mM NaCl and 20 mM imidazole	50 mM HEPES pH 8.0, 500 mM NaCl and 350 mM imidazole
HldE	50 mM HEPES pH 8.0, 500 mM NaCl, 20 mM Imidazole, 1mM DTT, 1mM PMSF and 2 mg of DNAse.	50 mM HEPES pH 8.0, 500 mM NaCl and 20 mM imidazole	50 mM HEPES pH 8.0, 500 mM NaCl and 350 mM imidazole
GmhB	50 mM HEPES pH 8.0, 20 mM Imidazole, 1mM DTT, 1mM PMSF and 2 mg of DNAse.	50 mM HEPES pH 8.0 and 20 mM imidazole	50 mM HEPES pH 8.0 and 350 mM imidazole

2.5.3 Purification of HldE from recombinant strains

Harvested cells from an overnight culture carrying the pDEST17-*hldE* plasmid was resuspended in 20 mL lysis buffer (Table 2-3). The cell free extract was purified by application over a 5 mL HiTrap chelating column using a linear imidazole gradient at a flow rate of 1.0 mL/min. The HldE protein was eluted at an imidazole concentration of 200 mM. The buffer system used for this purification was similar to those used for the purification of GmhA (Table 2-3). Fractions containing the purified HldE protein were analyzed by 13% SDS-polyacrylamide gel and pure fractions were pooled and dialyzed overnight at 4°C in 20 mM HEPES pH 8.0. The dialyzed protein was concentrated to a final concentration of 8.0 mg/mL and stored in 50% Glycerol at -80°C after freezing with liquid nitrogen.

2.5.4 Purification of GmhB from recombinant strains

Purification of GmhB was adapted from the purification protocol performed previously by summer student Adam Scott in our lab. For this purification, the column used was the 5 mL HiTrap Chelating resin. The harvested cells were resuspended in 20 mL lysis buffer (Table 2-3). GmhB was eluted at 139 mM imidazole using flow rate of 1.0 mL/min. Protein fractions containing pure GmhB protein as analyzed by 15% SDS-polyacrilamide gel were pooled and dialyzed overnight in the same manner as GmhA and HldE. The protein was concentrated and stored in 50% glycerol at -20°C to a final concentration of 10 mg/mL.

2.6 Enzymatic synthesis of sedoheptulose-7-phosphate

All chemicals and enzymes used for this experiment were purchased from Sigma (St. Louis, MO). The protocol to synthesize and purify sedoheptulose-7-phosphate was adapted from Lee *et al.* (24). The 2.5 mL reaction in a 25 mL two-neck round bottom flask included 25 mM Tris buffer, pH 8.0, 100 mM D-serine, 35 mM ribose-5-phosphate, 1 mM TPP, 3 mM $MgCl_2$, 70 U catalase and 9 U TktA. The flask was filled with oxygen prior to the initiation with 15 U D-amino acid oxidase (DAO). The reaction was incubated with continuous stirring at room temperature and a 100 µL aliquot was taken every three hours to monitor the production of sedoheptulose-7-phosphate by Liquid Chromatography/ Mass Spectroscopy (LC/MS). After the first three hours, an additional 100 U catalase and 90 µmol ribose-5-phosphate was added. An additional 100 U of catalase was added into the same reaction mixture every 3 hours until the 14^{th} hour of the reaction.

After 6 hours, 90 µmol ribose-5-phosphate, 8 U D-amino acid DAO and 10 U transketolase was added. At the 14^{th} hour, the enzymes were removed by a passage through a PD-10 column (24), and the reaction mixture was applied to an AG-1 x 8 (formate form, 2.5 x 16 cm) column. The column was washed with 50 mL water and the sample was eluted with a gradient of 0.4 N formic acid/ 0.1 N ammonium formate in water. Fractions (1 mL) containing sedoheptulose-7-phospate were pooled and dried by lyophilization and dissolved in water to 5 mL. Ammonium ions were removed by passage through a Dowex 50 (H^+ form, 1.5 x 3 cm) column. The flow-through was

collected and neutralized with 4 N NaOH. After this step, 0.6 mmol barium chloride was added into the solution followed by 80% ethanol. The barium salt was precipitated for 3 hours at 4°C and the barium sedoheptulose 7-phosphate was collected by centrifugation at 3000 rpm. The resulting salt was washed with 25 mL of 80% ethanol. The sample was dried *in vacuo* to obtain the barium sedoheptulose 7-phosphate reaction product.

2.7 High-Performance Anion Exchange Chromatography-with Pulsed Amperometric Detection (HPAEC-PAD) to monitor enzyme activity

The activity of TktA, GmhA and HldE were analyzed using an ED40 electrochemical detector with a disposable gold working electrode from Dionex Corp (Sunnyvale, CA). Monosaccharide phosphates were analyzed using a NaOAC-gradient (100 to 660 mM) in 100 mM NaOH, adapted from Dr. Paul Messner's lab (21, 22).

Assays were performed in 1.5 mL eppendorf tubes with 10 mM fructose-6-phosphate, 5.6 mM ribose-5-phosphate, 1 mM TPP and 5 mM ATP. The assay buffer contained 20 mM HEPES pH 8.0 and 10 mM $MgCl_2$ in a reaction volume of 400 µL. TktA enzyme was added (500 ng) to the reaction mixture and a 20 µL aliquot was diluted with the reaction buffer (110 µL final volume) after 1 hr incubation at 37°C. A sample volume of 20 µL was injected for sugar phosphate analysis. GmhA (500 ng) was then added into the same reaction mixture and after 1 hr of incubation; 20 µL of aliquot was

collected for sample injection. Finally, 500 ng of HldE enzyme was added into the same reaction tube and sugar product was injected into the coloumn in the same manner.

2.8 Assay Development

2.8.1 Optimization of the ADP-heptose pathway assay

Assays were performed in a 96-well microtitre plate. Each reaction consisted of 1 mM fructose-6-phosphate, 140 μM ATP, 0.10 mM TPP, 1 U pyrophosphatase, 5% DMSO, 0.1% Tween-20® in 20 mM HEPES pH 8.0, 10 mM KCl and 10 mM $MgCl_2$ reaction buffer to make a 100 uL reaction volume. The reaction was initiated with 1 mM ribose-5-phosphate. The amount of enzymes added to the mixture were determined empirically by varying the amount of one enzyme while keeping the other three enzymes constant and assaying for inorganic phosphate release. This was performed in a metabolically relevant fashion, by varying the first enzyme, TktA, and keeping the others constant. The amount of the subsequent enzyme, GmhA was determined to just exceed the rate established by the previous enzyme, TktA. The amount of HldE and GmhB were optimized in a similar manner as for GmhA using the assay for inorganic phosphate release. In summary, 2.1 nmole, 2.5 pmole, 32 pmole and 12 pmole of GmhA, GmhB, TktA and HldE respectively were used as the optimum enzymatic levels for HTS.

2.8.2 Kinetic studies

After each enzyme was optimally linked, the steady state kinetic parameters for ribose-5-phosphate, fructose-6-phosphate and ATP were determined by varying one substrate at eight concentrations in duplicate from 0.03 - 4 mM for ATP, and 0.05 – 3 mM for both ribose-5-phosphate and fructose-6-phosphate. Data were fit to Equation 1 for Michaelis-Menten kinetics using the computer software GraFit (23).

$$v = \frac{V_{max}\, S}{(K_m + S)} \qquad (1)$$

The IC_{50} value of β-γ-Methyleneadenosine 5'-triphosphate (AMP-PCP) was determined using eight concentrations ranging from 0.01 to 40 μM; ATP was present at 140 μM, as well as 1 mM ribose-5-phosphate and 1 mM fructose-6-phosphate. Data were fit to the four-parameter Equation 2, using GraFit (23) to calculate the IC_{50} value where A = minimum response plateau, D = maximum response plateau, I = concentration of inhibitor and S = slope factor.

$$y = \frac{A - D}{1 + (I/IC_{50})^{S}} + D \qquad (2)$$

2.8.3 Assay for inorganic phosphate production

All chemicals and enzymes were purchased from Sigma (St Louis, MO), unless specified. Inorganic phosphates are released directly by GmhB and indirectly by HldE (adenylyl transferase domain). The pyrophosphate byproduct of the transferase reaction was hydrolyzed into two inorganic phosphates in the presence of 0.1 U of Baker's yeast pyrophosphatase. The release of three phosphates per one mole of sedoheptulose-7-phosphate was monitored at 660 nm upon the reaction of each phosphate with the molybdate/malachite green complex. The assay buffer contained 20 mM HEPES pH 8.0, 10 mM $MgCl_2$, 10 mM KCl, 1 mM fructose-6-phosphate, 140 μM ATP, 100 μM TPP, 0.1 % TWEEN-20, 5 % dimethylsulfoxide (DMSO) in a final reaction volume of 100 μL in 96-well microtitre plate.

The reaction was initiated by the addition of ribose-5-phosphate, such that the final concentration was 1.0 mM. The reaction was incubated for 10 min at room temperature and quenched by adding 5% trichloroacetic acid at 4˚C. This step was followed by the addition of 200 μL molybdate/malachite green colouring reagent prepared fresh using 0.045 % Malachite Green Hydrochloride and 4.2% Ammonium Molybdate in 4 M HCl. The reaction mixture (final volume of 250 μL) was incubated at room temperature for 5 min prior to absorbance reading at 660 nm. A standard curve was generated using Na_2HPO_4 with amounts ranging from 0 to 10 nmole of phosphate for each set of assays prepared.

2.9 ADP-Heptose pathway screening

2.9.1 Primary screen

A high thoughput screen against 1,000 small molecules was performed at the McMaster High Throughput Screening Laboratory (http://hts.mcmaster.ca) in 96-well plates in duplicate using a Beckman-Coulter Biomek FX Liquid Handler (Fullerton, CA) and a Molecular Devices SpectraMax Plus^{384} (Sunnyvale, CA). Compounds were obtained from Chemical Diversity Labs (San Diego, CA) and were dissolved at 1 mM concentration in DMSO placed in 96-well microtitre plates. Each assay reaction contained 50 μM of a kinase-targeted compound, a master mix containing buffer, Mg^{2+}, enzymes, fructose-6-phosphate, and 140 μM ATP with conditions identical to those in the established optimized pathway assay described above. The reactions were pre-incubated for 8 min at room temperature and initiated by the addition of ribose-5-phosphate at 1 mM final concentration. Low controls (no HldE) and high controls (with HldE) were included in each 96-well microtitre plate and the compound solutions were substituted with DMSO at 5% final concentration. Hits were defined as compounds that showed 60% or less product formation relative to the high controls.

Assay quality was assessed by the determination of the Z' factor:

$$Z' \text{ factor} = 1 - [3\sigma_{high} + 3\sigma_{low} / \text{mean}_{high} - \text{mean}_{low}] \qquad (3)$$

2.9.2 Hit Follow-up

HldE activity in the presence and absence of Compound 1 was determined by coupling the production of ADP with lactate dehydrogenase dependent oxidation of NADH in the presence of phosphoenol pyruvate (PEP) and pyruvate kinase/lactate dehydrogenase (2). The assay mixture was comprised of 0.30 mM NADH, 3 mM PEP, 2.5 U pyruvate kinase, 2.8 U lactate dehydrogenase, 1 mM ribose-5-phosphate and fructose-6-phosphate, 5 nmole GmhA, 0.125 nmole TktA, 300 μM ATP, 20 mM HEPES pH 8.0, 10 mM MgCl and 40 mM KCl to make a 100 μL final volume in 96-well microtitre plates. The mixture was incubated for 10 min in the presence of the inhibitor at seven different concentrations in duplicate, ranging from 0.004 to 1.5 mM. The reaction was initiated by the addition of 300 μM ATP, and the oxidation of NADH was monitored at 340 nm in a Molecular Devices Spectramax microtitre platereader. The IC_{50} value was determined as described in Equation 2 using the computer software GraFit in the same manner as determining the IC_{50} value of AMP-PCP.

The K_i value and mode of inhibition were determined using the same ADP-assay with identical reaction conditions. Briefly, seven ATP concentrations varied from 0.04 to 2.5 mM were used with four Compound 1 concentrations ranging from 0.004 to 5 mM. The mixture was pre-incubated for 10 min and initiated by the addition of ATP at varying concentrations. ADP production catalyzed by the kinase domain of HldE was monitored at 340 nm for 20 minutes, and the mode of inhibition was assessed by generating a double reciprocal plot with individual lines to fit a simple double reciprocal model using

Equation 4. The K_i value was calculated using Equations 4 to 6 with the computer software GraFit.

$$1/v_o = (\alpha K_m/V_{max})\ 1/[S] + 1/V_{max} \quad (4)$$

$$\text{slope} = \alpha K_m/V_{max} \quad (5)$$

$$K_i = I/\alpha - 1 \quad (6)$$

2.10 Paired-Ion Chromatography

2.10.1 Paired-Ion Chromatography (PIC) for product validation

The separation of ATP, ADP and ADP-L-*glycero*-D-*manno*-heptose was performed using a Dionex C18 column (Dionex Corp, Sunnyvale, CA) with a methanol gradient (0 to 30%) pH 7.2 in 100 mM potassium phosphate pH 6.0 and 10 mM tetrabutylammoniumhydrogensulfate (TBAHS). The HPLC program was adapted from from Dr. Eric Brown of the Department of Biochemistry and Biomedical Sciences, McMaster University. The assay was performed in 1.5 mL eppendorf tubes with ribose-5-phosphate and fructose-6-phosphate at concentrations of 1.5 mM, 5 mM ATP and 0.10 mM TPP. The amounts of enzymes used were 4.63, 4.77, 4.96 and 1 nmole for GmhA, GmhB, TktA and HldE respectively. The reaction buffer consisted of 20 mM HEPES pH 8.0, 10 mM $MgCl_2$, 10 mM KCl and 0.1 U Baker's yeast pyrophosphatase to make a 100 µL final volume. The reaction was incubated at room temperature for 30 min and 50 µL of sample was injected into the column for investigation of nucleotide activated sugar at 254 nm.

After establishing the retention times for ATP and ADP, the fraction of the new observed peak, believed to be the ADP-heptose, was collected for further LC/MS analysis.

2.10.2 Hit follow-up for Compound 1

HPLC conditions were developed to identify the enzyme being inhibited by compound 1. A 50 µL sample was injected into a VYDAC protein and peptide C18 column from Dionex Corp (Sunnyvale, CA) using a methanol gradient (5-90%) in 10 mM KH_2PO_4 pH 4.2 and 1 mM TBAHS. The nucleated activated sugar was analyzed using the HPLC program illustrated in the table below.

Table 2-4. PIC-HPLC program developed to analyze the effects of the inhibitor Compound 1 to the LPS pathway.

Time (minutes)	Buffer A %	Buffer B %
0	95	5
5	95	5
20	40	60
22	10	90
24	10	90
25	95	5

2.11 Minimal inhibitory concentration (MIC)

The novobiocin MIC was determined by broth dilution in LB medium. A checkerboard assay was implemented to examine the effects of combinations of the antibiotic novobiocin with Compound 1 on the growth of wild type *E. coli* BW25113. *E. coli* BW25113 was kindly donated by Brown's Laboratory. Two-fold serial dilutions of novobiocin (from 25.6 to 0.1 mg/mL) were prepared in a sterile 96-well microtitre plate. Serial dilutions of Compound 1 in DMSO were also dispensed independently, at concentrations ranging from 256 to 0 ng/mL.

Fresh overnight culture was mixed with 0.85% saline to make a solution with OD_{625nm} within the range of 0.08-0.1. A 100 µL aliquot of the saline solution was mixed into 18.612 mL of Miller/Huntin Broth (MHB). Following this, 96 µL of the mixture was added to each well containing Compound 1 at different concentrations. Then 1 µL of each novobiocin dilution was added into each reaction well. The reaction plate was incubated overnight at 37 °C and any bacterial growth was monitored at 600 nm using a Molecular Devices Spectramax microtitre platereader the following day.

3. *Results*

3.1 Amplification of the tktA, gmhA and hldE genes

Using genomic DNA isolated from *E. coli* W3110 and primer pairs complementary to the 5' terminal and 3' terminal of the *tktA* gene, *gmhA* gene and *hldE* gene, DNA fragments of 2.0 kb, 0.58 kb and 1.4 kb respectively were amplified by PCR (Figure 3-1a, 3-1b and 3-1c). The bands shown on three 1% TAE-agarose gels are consistent with the predicted sizes of *tktA*, *gmhA* and *hldE* in Genbank data base. The correct DNA sequence was verified by sequencing of the entire *tktA*, *gmhA* and *hldE* genes at the MOBIX Central Facility of McMaster University.

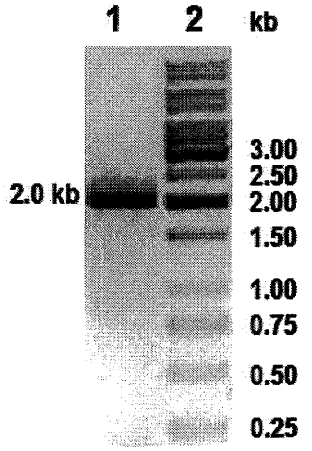

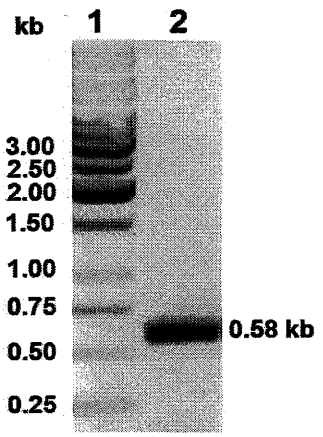

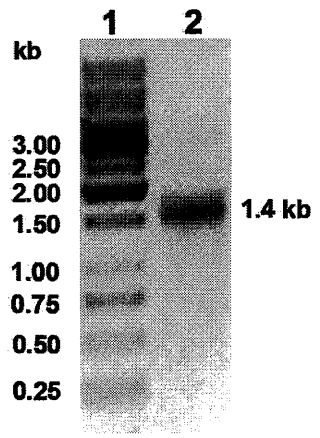

Figure 3-1a **Figure 3-1b** **Figure 3-1c**

Figure 3-1. Amplification of the *tktA, gmhA* and *hldE* genes analyzed on 1% TAE-agarose gels. Figure 3-1a. Amplification of the *tktA* gene; Lane 1 - PCR product of the amplified *tktA* gene with DNA size of 2.0 kilobases. Lane 2 - standard 1 kb molecular size DNA marker. **Figure 3-1b. Amplification of the *gmhA* gene;** Lane 1- standard 1 kb molecular size DNA marker; Lane 2 - PCR product of the amplified *gmhA* gene with DNA size of 0.58 kilobases. **Figure 3-1c. Amplification of the *hldE* gene**; Lane 1- standard 1 kb molecular size DNA marker; Lane 2 - PCR product of *hldE* with DNA size of 1.4 kilobases. The 1% TAE-agarose gels used to analyze *tktA, gmhA* and *hldE* genes were stained with ethidium bromide and visualized with the UV light transilluminator.

3.2 Sub-cloning and overexpression of the TktA, GmhA, HldE and GmhB proteins

The *tktA* gene was inserted into a pDEST17 expression vector via homologous recombination and the construct was transformed into *E. coli* BL21 (DE3) cells. This fuses the *tktA* gene to a sequence encoding an N-terminal His-tag downstream of a bacteriophage T7 promoter for high-level protein expression in *E. coli.* The *hldE* gene was also inserted into a pDEST17 expression vector in the same manner as the sub-cloning of the *tktA* gene.

The *gmhA* gene was inserted into a pET 28 a (+) vector treated with *Nde*I and *Hind*III endonucleases. The construct was transformed into *E. coli* BL21 (DE3) cells. The pET28 a-*gmhA* construct contained a sequence encoding an N-terminal hexa His-tag and a T7 promoter for high-level protein expression. The pET28a-*gmhB* construct was made in the same manner as the pET28a-*gmhA* construct by Adam Scott. The hexa-His tagged TktA, GmhA, HldE and GmhB proteins were overexpressed and purified using a 5 mL HiTrap chelating column. The proteins were analyzed on a 13% SDS-Polyacrylamide gel showing bands consistent with the predicted molecular weights of 72.7 kDa, 20.8 kDa, 51.1 kDa and 21.2 kDa for TktA, GmhA, HldE and GmhB respectively (Figure 3-2) (11, 22, 48, 55).

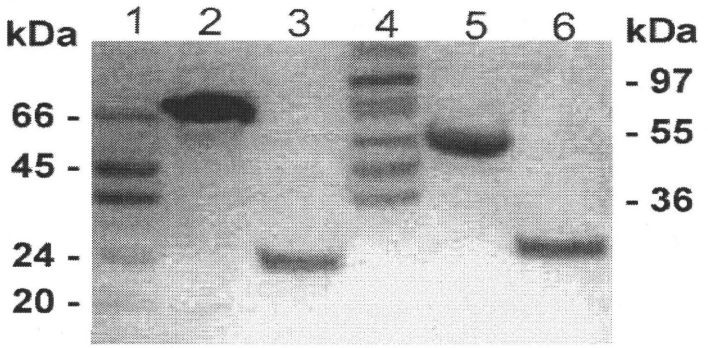

Figure 3-2. SDS-polyacrylamide gel electrophoretic analysis of the purified enzymes involved in the biosynthesis of ADP-D-*glycero*-β-*manno*-heptose. **Lane 1**- low molecular mass standards: bovine serum albumin (66 kDa), chicken egg ovalbumin (45 kDa), glyceraldehyde-3-phosphate dehydrogenase (36 kDa), carbonic anhydrase (29 kDa), trypsinogen (24 kDa), and trypsin inhibitor (20 kDa); **Lane 2** - purified transketolase (TktA) protein; **Lane 3 –** purified phosphoheptose isomerase (GmhA) protein; **Lane 4** - high molecular mass standards: myosin (205 kDa), β-galactosidase (116 kDa), phosphorylase b (97 kDa), fructose-6-phosphate kinase (84 kDa), bovine serum albumin (66 kDa), glutamic dehydrogenase (55 kDa), chicken egg ovalbumin (45 kDa), glyceraldehyde-3-phosphate dehydrogenase (36 kDa); **Lane 5** – purified bifunctional kinase/adenylyltransferase (HldE) protein; **Lane 6 –** purified phosphatase (GmhB) protein

Table 3-1. Summary of the TktA, GmhA, HldE and GmhB predicted and observed molecular weights (kD) as seen on the SDS-polyacrylamide gel, and the average yield of each protein in mg/mL culture.

Protein	TktA	GmhA	HldE	GmhB
Predicted Molecular Weight (kD)	72.2	20.8	51.1	21.3
Observed Molecular weight (kD) (SDS-PAGE)	~72	~23	~52	~24
Average yield (mg/mL)	20	100	45	200

3.3 Enzyme activity assays

3.3.1 High Performance Anion Exchange Chromatography coupled with Pulsed Amperometric Detection (HPAEC-PAD) enzyme activity assay

After the purification of the first three enzymes involved in the biosynthesis of ADP-heptose, the activity of each enzyme was studied using HPAEC-PAD. Figure 3-3 shows the chromatograms of four different reactions showing catalytic activities of the TktA, GmhA and HldE enzymes. In a 1.5 mL eppendorf reaction tube, the substrates and buffer mixture were incubated for 10 min at 37˚C without the presence of the enzymes.

A 20 µL reaction aliquot was taken from the reaction tube and diluted with 90 µL of reaction buffer. Another 20 µL was taken from the diluted sample to be injected into the CarboPac PA1 column via autosampler for the reaction at time zero. Chromatogram 1 shows the substrates fructose-6-phosphate and ribose-5-phosphate peaks with overlapping

retention time of 26.25 min. TktA at 500 ng was added into the reaction tube with the substrates and buffer mixture to initiate the reaction. After 1 hour of incubation at 37°C, 20 μL aliquot, as described earlier at reaction time zero, was collected and injected using the autosampler into the column. Chromatogram 2 showed the appearance of a small peak (28.00 min, Figure 3-3); however, there was no noticeable decrease in the substrate peaks.

Following this reaction, the activity of the next protein in the pathway, GmhA, was analyzed. In the same reaction tube, 500 ng of enzyme was added to initiate the next reaction, incubated at 37°C for 1 hour. An aliquot was injected into the HPLC as described above. No comparable change was observed between the substrates peak and intermediate peak (26.25 and 27.00 min respectively, Figure 3-3). This reaction was followed by the addition of the next enzyme in the pathway, the bifunctional HldE enzyme. The addition of HldE suggested the enzymes GmhA, TktA and HldE were active. In summary, a dramatic decrease in the substrates peak at 26.25 min, increase in the first intermediate peak at 27.00 min, and the appearance of the new peak at 24.35 min were observed on Chromatogram 4 (Figure 3-3). The method did not allow for direct detection of each reaction, but the addition of the HldE enzyme resulted in new peaks. The presence of the new peaks suggests that the enzymes were active, but further assay method development was needed to confirm activity of each enzyme.

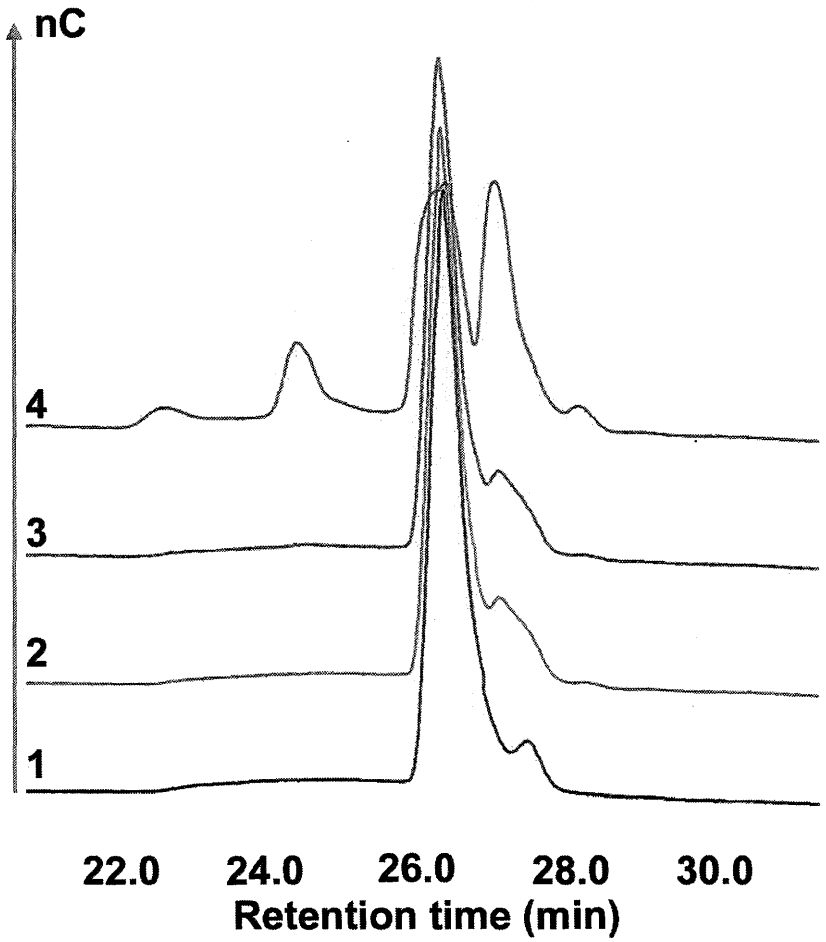

Figure 3-3. HPAEC-PAD analysis of sugar intermediates catalyzed by the TktA, GmhA and HldE enzymes of the ADP-heptose biosynthetic pathway. **1** - Reaction at time zero showing substrates ribose-5-phosphate and fructose-6-phosphate overlap at 26.25 min; **2** - Reaction after the addition of TktA observed a tiny peak at 27.80 min; **3** - Reaction after the addition of GmhA; **4** - Reaction after the addition of HldE showing two noticeable peaks at 24.35 and 27.8 min. All reactions were incubated at 37˚C for 1 hr after addition of each enzyme.

3.4 Pathway Reconstitution

To develop an assay that will help us identify inhibitors of the enzymes in the ADP-heptose pathway, the enzymes and reaction components were reconstituted *in vitro*. The activity of the enzymes in the pathway were observed by monitoring the amount of

inorganic phosphate released directly from the phosphatase enzyme, GmhB and indirectly from pyrophosphate, with the addition of inorganic pyrophosphatase, product of the adenylyltransferease reaction of the HldE enzyme (Figure 1-4). A simple, sensitive and non-radioactive end-point assay called phosphomolybdate/malachite green assay was used to quantify the amount of inorganic phosphate released. The Pi forms a colored complex with molybdate/malachite green, which can be quantified by measuring the absorbance at 660 nm. Because of the assay's simplicity and sensitivity, the ADP-heptose pathway was reconstituted, developed and optimized using this technique.

3.4.1 Optimal Temperature

After determining that the enzymes are active by HPAEC-PAD analysis, the effects of temperature was studied. A series of reactions in 1.5 mL eppendorf tubes containing 20 mM ribose-5-phosphate and fructose-6-phosphate, 100 mM ATP, 1 U pyrophosphatase, 10 mM TPP and 500 ng TktA, GmhA, HldE and GmhB in 20 mM HEPES pH 8.0 and 10 mM $MgCl_2$ were prepared to determined the activity at 25 ˚C and 37˚ C every 5 min. Both reactions at two different temperature gave similar results over the first 20 min as shown in Figure 3-4).

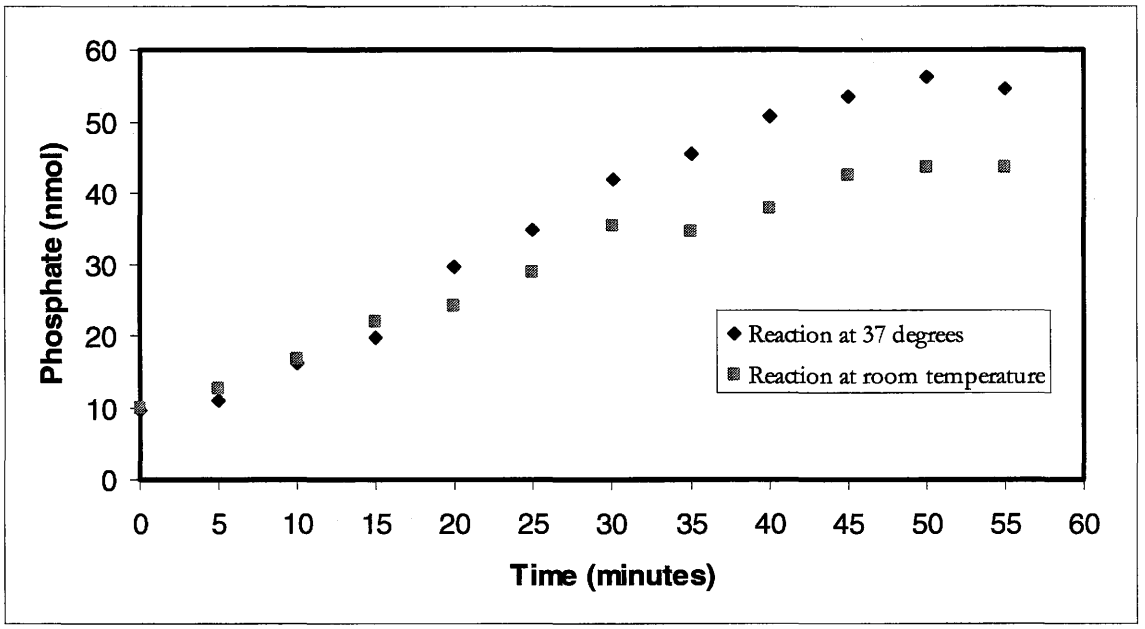

Figure 3-4. Effects of temperature on the reconstitution ADP-heptose *in-vitro* pathway assay. Two sets of identical assays were prepared in duplicate to compare the release of phosphate (Pi) in nmole of the reconstituted *in-vitro* assay at 25˚C and 37˚C. The assay consisted of 500 ng TktA, GmhA, HldE and GmhB to make a final 200 µL reaction volume. Samples were taken every 5 min to detect Pi release in nmole for 55 min.

3.4.2 ADP-heptose product validation

Six sets of reactions in duplicate were set-up to validate the production of the nucleotide sugar ADP-D-*glycero*-β-*manno*-heptose *in-vitro*. The presence of the nucleotide heptose sugar was detected at 254 nm by Paired Ion Chromatography – High Performance Liquid Chromatography (PIC-HPLC). The reactions in each tube were set-up so that the effects of each additional enzyme in a metabolically relevant direction could be observed. Hence, no new peaks should be observed at 254 nm unless all the

enzymes were present in the tube suggesting the transfer of the nucleotide from ATP by the adenylyltransferase activity of HldE. Reaction containing the assay components (described in section 2.9.2 of this report) without ATP and enzymes was used as the negative control. A peak with retention time of 14.0 min was observed, this peak was either from one of the substrates or assay components in the mixture. However, the identity of the peak was not pursued since it did not affect the detection of ATP, ADP and ADP-D-*glycero*-*β*-*manno*-heptose as shown in the following chromatograms. Chromatograms 2 to 5 show ATP and ADP peaks at 15.5 and 15.0 min respectively. Chromatogram 6 with the first four enzymes, TktA, GmhA, HldE and GmhB in the reaction tube, shows the presence of a new peak at 14.2 min, assumed to be the product ADP-D-*glycero*-β-*manno*-heptose.

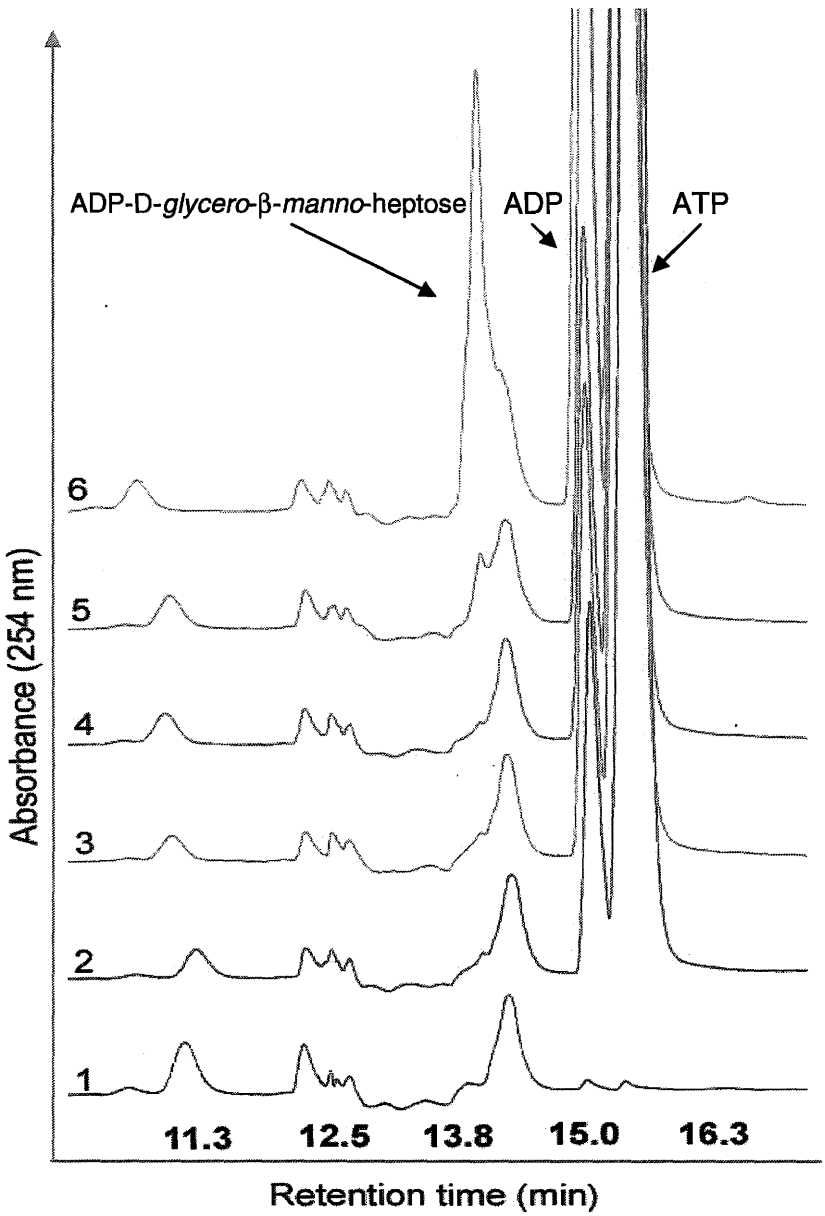

Figure 3-5. PIC-HPLC analysis of the nucleotide sugar ADP-D-*glycero*-β-*manno*-heptose. **1** - Blank, reaction without ATP and enzymes; **2** - Negative control, reaction without enzymes, showing peaks corresponding to background ADP and ATP at 15.0 and 15.5 min respectively; **3** - Reaction in the presence of the TktA enzyme; **4** - Reaction in the presence of TktA and GmhA; **5** - Reaction in the presence of TktA, GmhA and HldE;

6 - Reaction in the TktA, GmhA, HldE and GmhB all reactions were incubated for 30 min at 25°C showing new peak at 14.2 min.

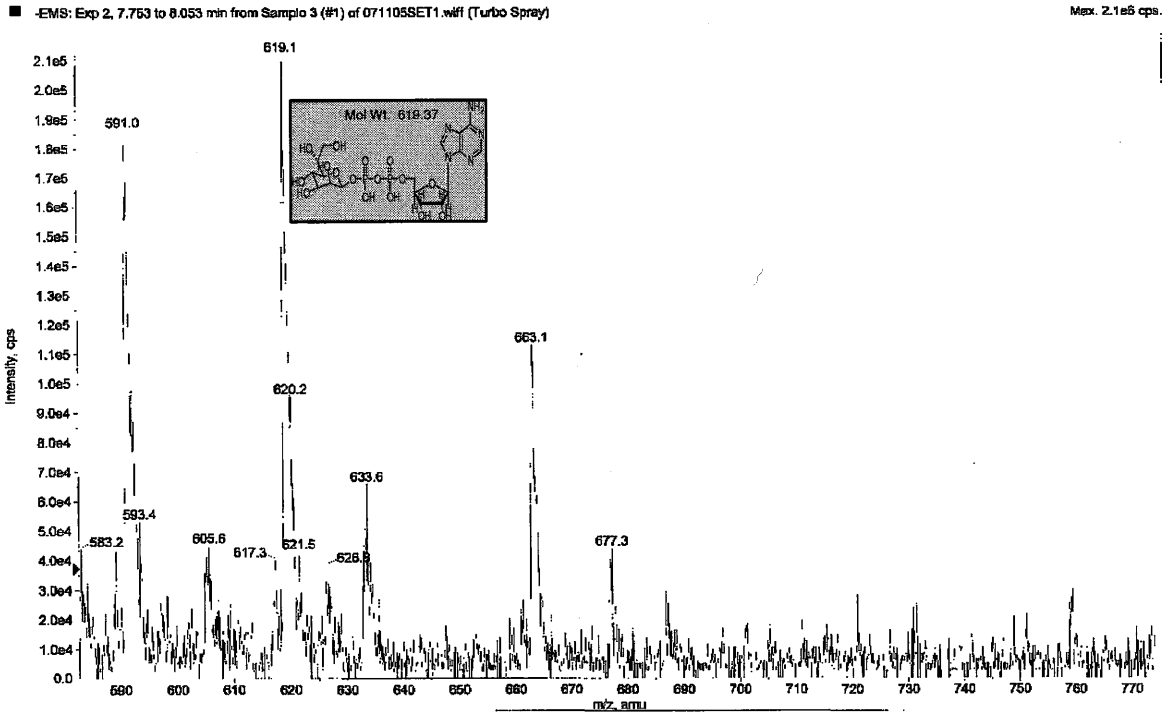

Figure 3-6 Liquid Chromatography/Mass spectroscopy (LC/MS) analysis of the nucleated sugar ADP-D-*glycero*-β-*manno*-heptose. The product of the ADP-heptose pathway, ADP-D-*glycero*-β-*manno*-heptose was confirmed by electrospray LC/MS analysis showing mass of 619.1 $[M + H]^-$.

The fraction of assumed to be the product ADP-D-*glycero*-β-*manno*-heptose from the previous HPLC analysis (Figure 3-5) was collected and analysed by LC/MS. The electrospray LC/MS analysis was performed by Dr. Kalinka Koteva in the Department of Biochemistry and Biomedical Sciences at McMaster University on the sugar product. The calculated molecular weight for the compound with molecular formula of $C_{17}H_{27}N_5O_{16}P_2$ was 619.35 Daltons and the analysis showed a molecular weight of 619.1 $[M + H]^-$. Therefore, the reconstituted pathway catalyzed the sugar product ADP-D-

glycero-β-*manno*-heptose in a metabolically relevant direction as confirmed by HPLC and LC/MS analyses.

3.5 Assay Development

3.5.1 Assay Linerity

An important factor to consider in assay development is the linearity of the assay over a certain period of time. During this time period, the velocity of the enzyme is constant and can be used as a convenient measure of reaction rate (8, 57). For convenience purposes, we need to rely on a single time point as a reflection of the initial velocity phase of the enzymatic reactions instead of taking multiple time points.

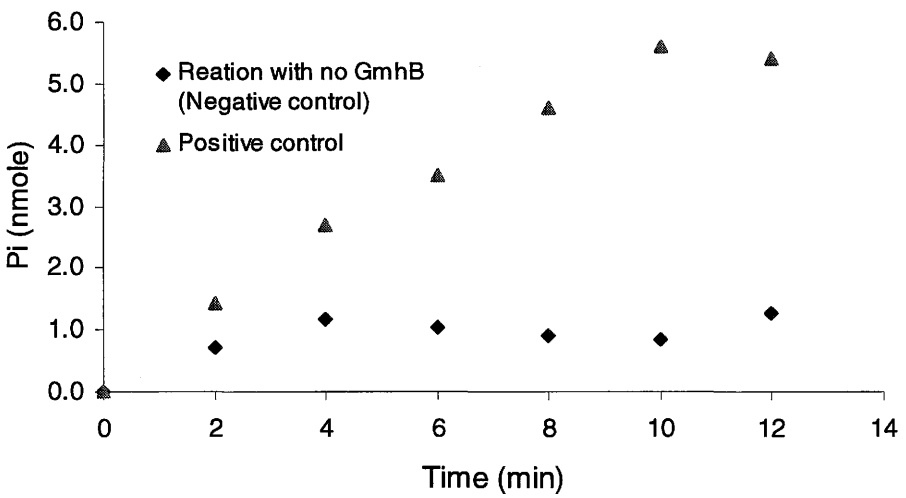

Figure 3-7 ADP-heptose pathway assay linearity. The initial rate of the enzymes in the ADP-heptose pathway was analyzed by Phosphomolybdate/malachite green assay. The ADP-heptose pathway assay was found to be linear for at least 10 min (R^2 = 0.9934) using 4.63 nmole GmhA, 0.32 nmole TktA, 4.77 nmole GmhB and 1 nmole HldE. The negative control was the reaction without the addition of the GmhB protein.

3.5.2 Steady state kinetics of fructose-6-phosphate

After establishing a single time point that reflects the initial velocity phase, the kinetic parameters for fructose-6-phosphate and ribose-5-phosphate were analyzed to get a better idea of the starting substrate concentration for assay development.

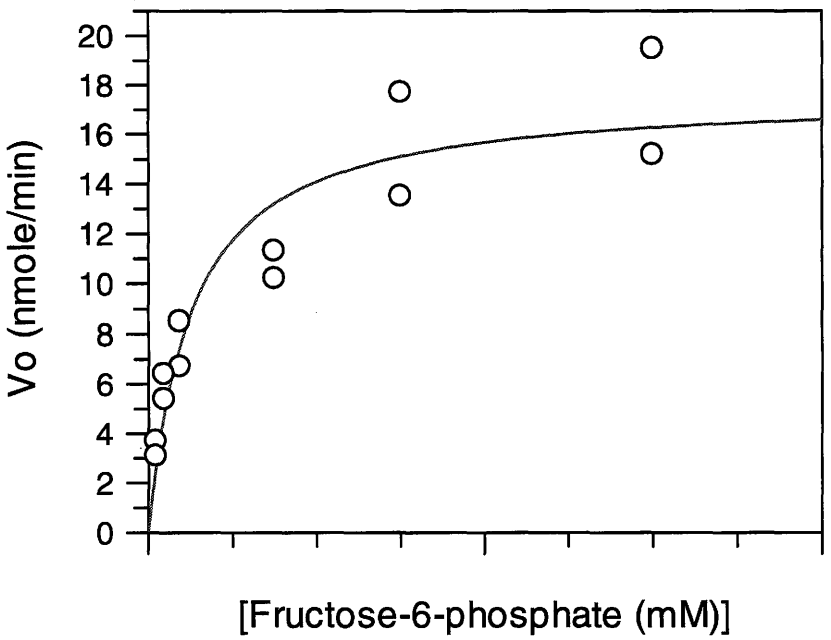

Figure 3-8. Steady state kinetics data of fructose-6-phosphate for the ADP-heptose biosynthetic pathway. The reaction was set-up by varying the concentration of fructose-6-phosphate from 0.0 to 3.0 mM with 3 mM ribose-5-phosphate, 1.0 mM ATP, 0.10 mM TPP with 4.63 nmole GmhA, 4.77 nmole GmhB, 0.31 nmole TktA, 1.0 nmole HldE and 1 U pyrophosphatase in 20 mM HEPES pH 8.0, 10 mM $MgCl_2$ and 10 mM KCl. The K_m value was determined to be 250 ± 72 μM.

Since there is no direct assay to measure the kinetic parameters of each enzyme, the kinetic parameters for the whole pathway were determined using the

phosphomolybdate assay. Using a total of eight concentrations in duplicate, the results reported a K_m value of 250 ± 72 μM, k_{cat} of 0.94 ± 0.07 s^{-1} and k_{cat}/K_m of 3.8 x 10^3 M^{-1} s^{-1}.

3.5.3 Steady state kinetics of ribose-5-phosphate

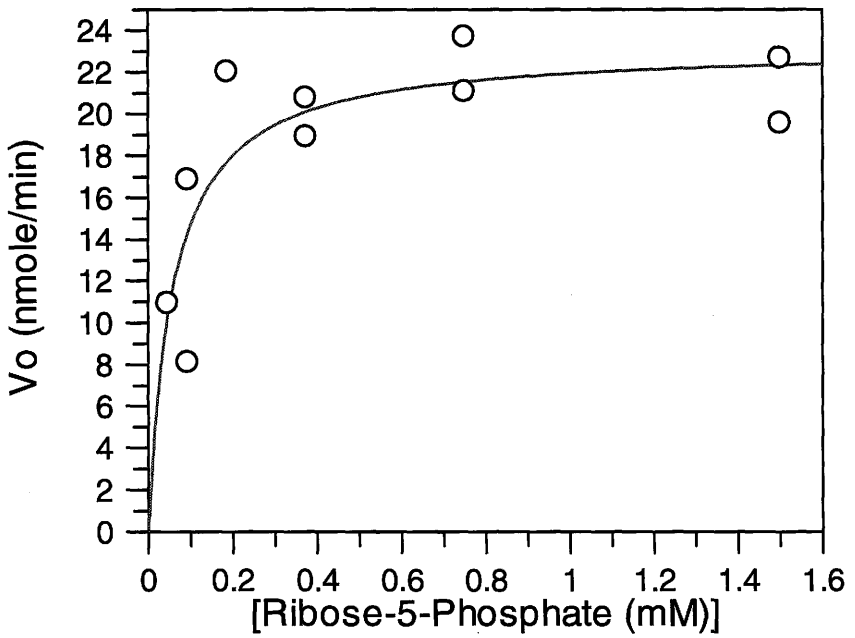

Figure 3-9. Steady state kinetics of ribose-5-phosphate for the ADP-heptose biosynthetic pathway. The reactions were set-up by varying the concentrations of ribose-5-phosphate from 0.0 to 3.0 mM with 3 mM fructose-6-phosphate, 1.0 mM ATP, 0.10 mM TPP with 4.63 nmole GmhA, 4.77 nmole GmhB, 0.31 nmole TktA, 1.0 nmole HldE and 1 U pyrophosphatase in 20 mM HEPES pH 8.0, 10 mM $MgCl_2$ and 10 mM KCl reaction buffer. The K_m value was determined to be 58 ± 23 μM.

The kinetic data of the whole ADP-heptose biosynthetic pathway was determined for the substrate ribose-5-phosphate. A total of eight ribose-5-phosphate concentrations in duplicate were used to determine the kinetic parameters of the substrate. The K_m value was calculated to be 58 ± 23 μM, k_{cat} is 1.2 ± 0.09 s^{-1} and k_{cat}/K_m is 2.1 x 10^4 M^{-1} s^{-1}.

3.5.4 Effects of DMSO

Before any further assay optimization, the amount of DMSO to be included into the *in vitro* assay was taken into consideration. For high throughput screening, it is important to determine the DMSO concentration that will allow for sufficient compound to be added into the assay while maintaining an accepted level of enzyme activity (16). The McMaster HTS lab compound library is dissolved in DMSO, hence the effect of DMSO on the biosynthetic pathway was considered and the effects were determined by the phosphomolybdate assay. In Figure 3-10, the graph shows that even at 10% DMSO, the enzymes in the *in vitro* pathway assay maintained activity and linearity for 10 min.

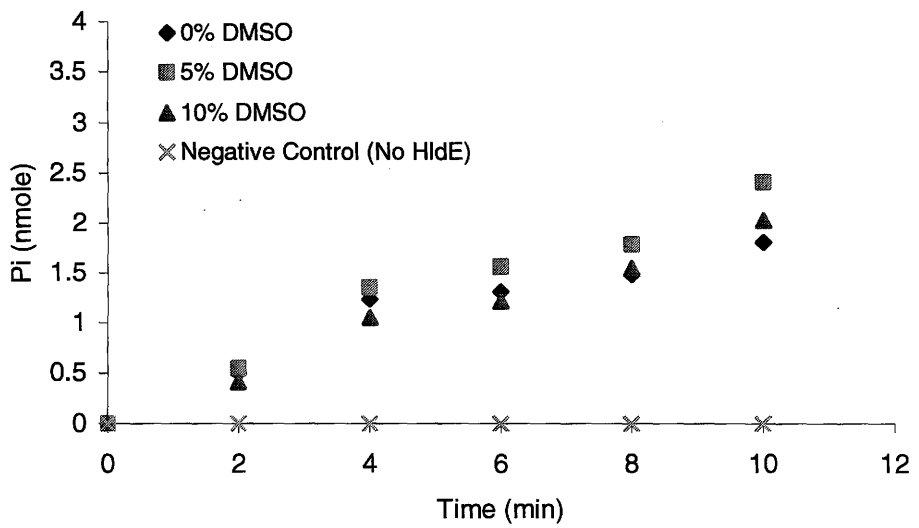

Figure 3-10. Enzyme activity in the presence of DMSO. The catalytic activity of the enzymes in the pathway were analyzed in 0% (◆), 5% (▩) and 10 % (▲) DMSO using the phosphomolybdate assay. Three DMSO concentrations were compared every 2 min and showed only a slight change in signal at 660 nm. Negative control was set-up without the presence of HldE (X).

3.5.5 Optimizing TktA condition for high throughput screening

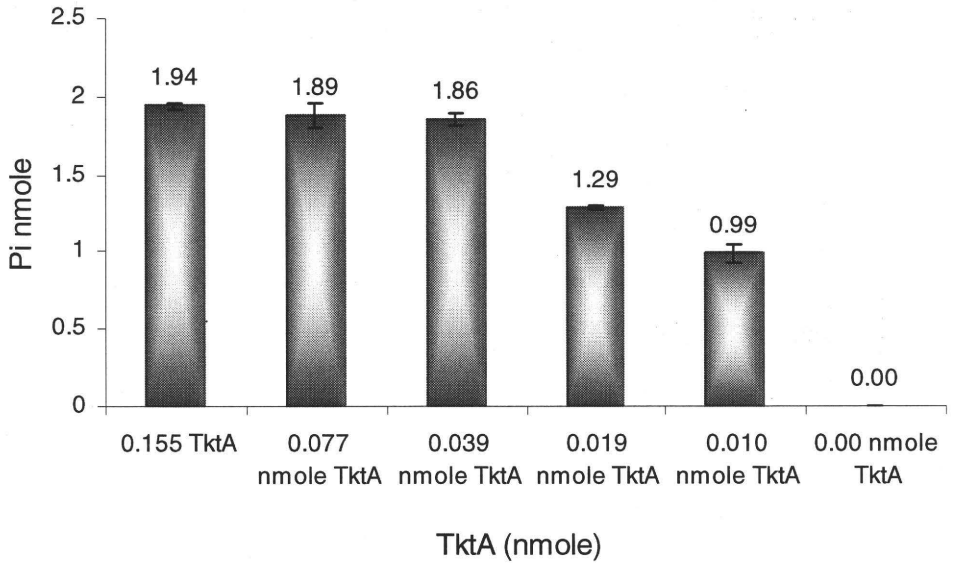

Figure 3-11. Determining the optimal TktA condition for HTS. Six sets of reactions in duplicate were set-up with varying TktA concentrations of 0.00, 0.010, 0.019, 0.039, 0.077 and 0.155 nmole. Using the phosphomolybdate assay, the amount of Pi was observed to decrease at 0.039 nmole TktA.

To establish an assay suitable for HTS, the amount of TktA in the reaction mixture that gives a linear response for at least 10 min. and shows a decrease in activity when inhibited even at low inhibitor concentration was determined. The amounts of TktA were varied from 0 to 0.155 nmole while keeping the other enzymes, GmhA, HldE and GmhB at constant amounts. Figure 3-11 shows very similar responses at 0.155, 0.077 and 0.039 nmole TktA, corresponding to the production of 1.94, 1.89 and 1.86 nmole Pi respectively. However, at 0.019 nmole TktA, the Pi decreased from 1.86 to 1.29 nmole Pi. Hence, the amount of 0.039 nmole was used as the TktA condition to further optimize the proceeding enzymes in the pathway.

3.5.6 Optimizing GmhA condition for high throughput screening

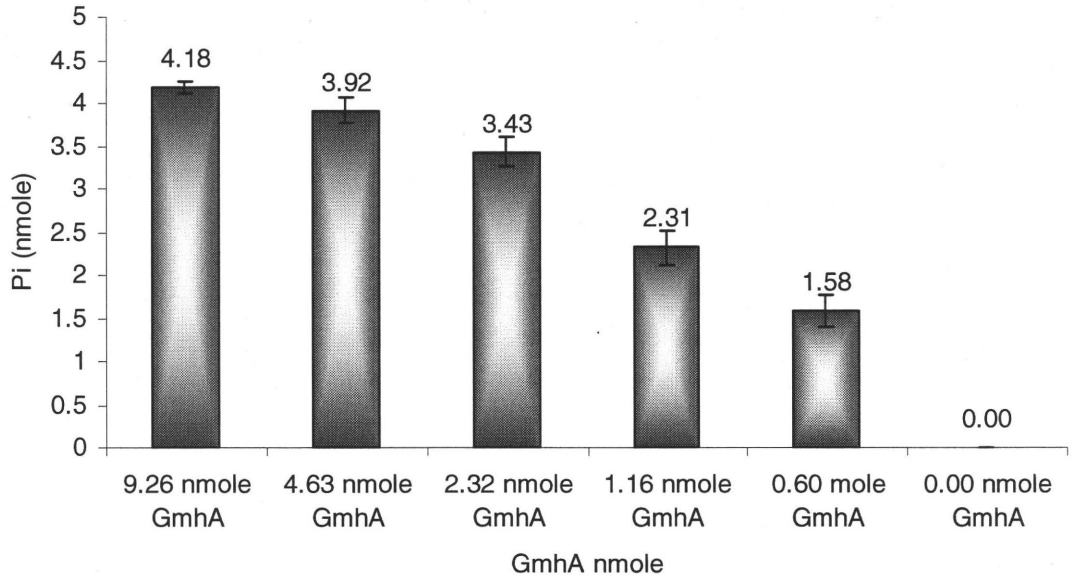

Figure 3-12. Determining of the optimal GmhA condition for HTS. Six sets of reactions in duplicate were prepared using 0.00, 0.60, 1.16, 2.32, 4.63 and 9.26 nmole GmhA to determine the amount of GmhA that will be suitable for HTS. Decrease in phosphate response in nmole was observed between 2.32 and 1.16 nmole GmhA.

Following the optimization of TktA, the next enzyme in the reconstituted pathway assay, GmhA, was studied using the phosphomolybdate assay. Six different GmhA amounts from 0.00 to 9.26 nmole were used while keeping the concentration of the other enzymes constant to determine the optimal GmhA condition suitable for HTS. Figure 3-12 shows that the amount of Pi generated decreased from 0.34 to 0.23 nmole as the amount of GmhA was decreased from 2.32 to 1.16 nmole GmhA. Thus, an amount of 2.32 nmole was selected as the optimal GmhA condition for the pathway assay, and subsequently used to further optimize HldE and GmhB conditions suitable for HTS.

3.5.7 Optimizing HldE condition for high throughput screening

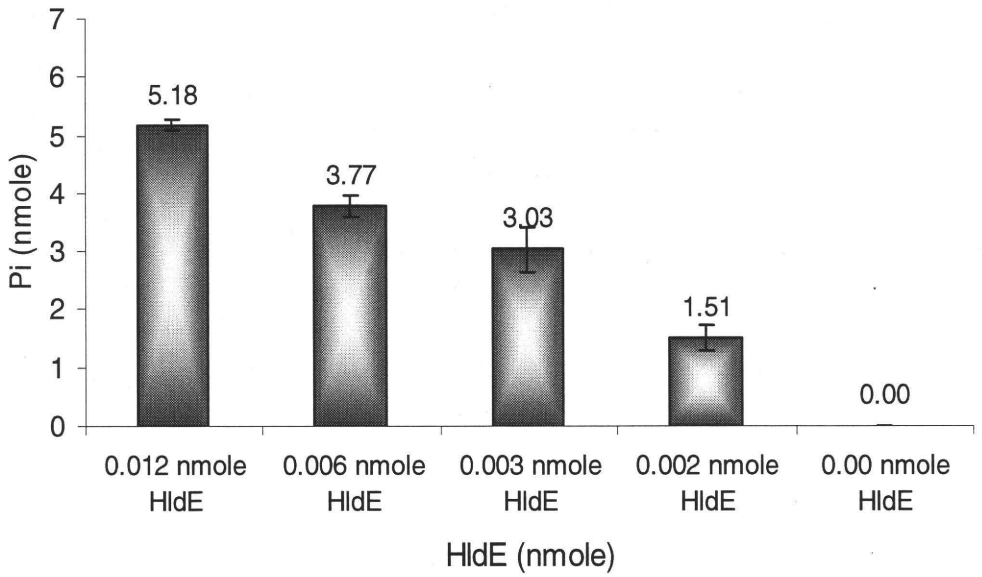

Figure 3-13. Determining the optimal HldE condition for HTS. Five sets of reactions containing 0.00, 0.002, 0.003, 0.006 and 0.012 nmole of HldE were set-up in duplicate to determine the optimum HldE condition suitable for HTS. The amount of phosphate decreases as the amount of HldE decreased from 0.012 to 0.006 nmole.

After establishing the optimum conditions for TktA and GmhA, the next enzyme in the pathway, HldE, was examined. The amounts of HldE were varied from 0.00 to 0.012 nmole while keeping the other enzymes in the pathway at constant amounts. The production of phosphate was monitored at 660 nm using the phosphomolybdate assay. The amount of Pi produced decreased from 5.18 nmole to 3.77 nmole as the amount of HldE was decreased from 0.012 to 0.006 nmole. The amount of 0.012 nmole was used as the optimal HldE condition for HTS and to further optimize the last enzyme in the pathway, GmhB.

3.5.8 Optimizing GmhB condition for high throughput screening

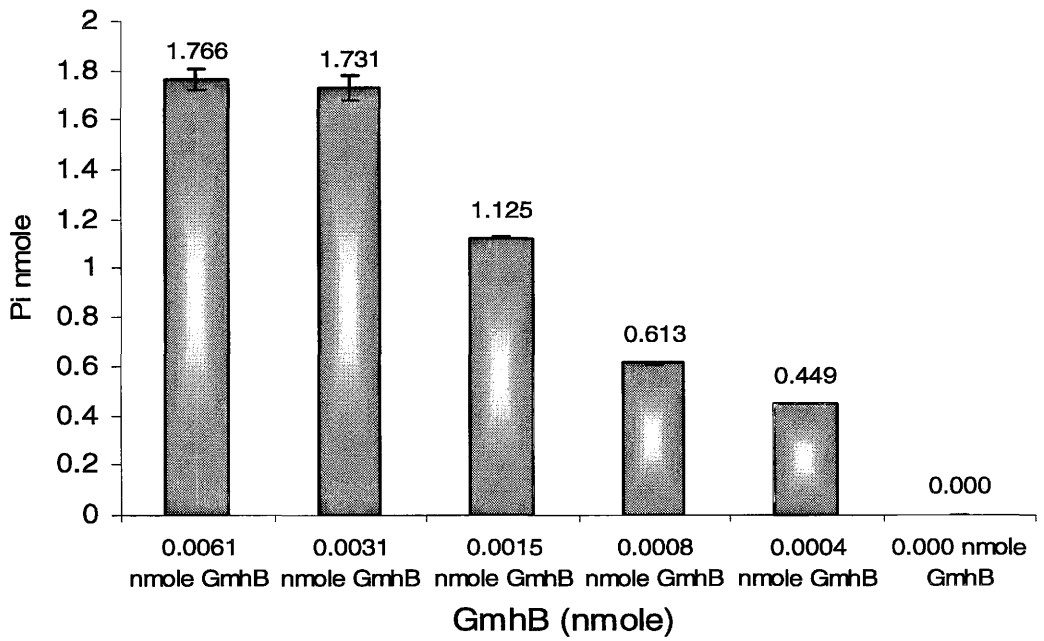

Figure 3-14. Determining the optimal GmhB condition for HTS. Six sets of reactions in duplicate containing 0.000, 0.0004, 0.0015, 0.0031 and 0.0061 nmole GmhB were set-up to determine the optimum GmhB condition suitable for HTS. The amount of phosphate detected at 660 nm decreases as the amount of GmhB decreases from 0.0031 nmole to 0.0015 nmole.

After establishing the optimum conditions for TktA, GmhA and HldE, the optimum condition for the last enzyme in the reconstituted pathway assay, GmhB, was determined. The amounts of GmhB were varied from 0.00 to 0.0061 nmole while keeping the amount of the other enzymes constant. The production of Pi was monitored at 660 nm using the phosphomolybdate assay and a decrease of phosphate production from 1.73 to 1.12 nmole was observed as the amount of GmhB was decreased from 0.0031 to 0.0025 nmole (Figure 3-14). The amount of 0.0031 nmole GmhB was used to validate the ADP-heptose pathway assay.

3.6 ADP-heptose assay validation

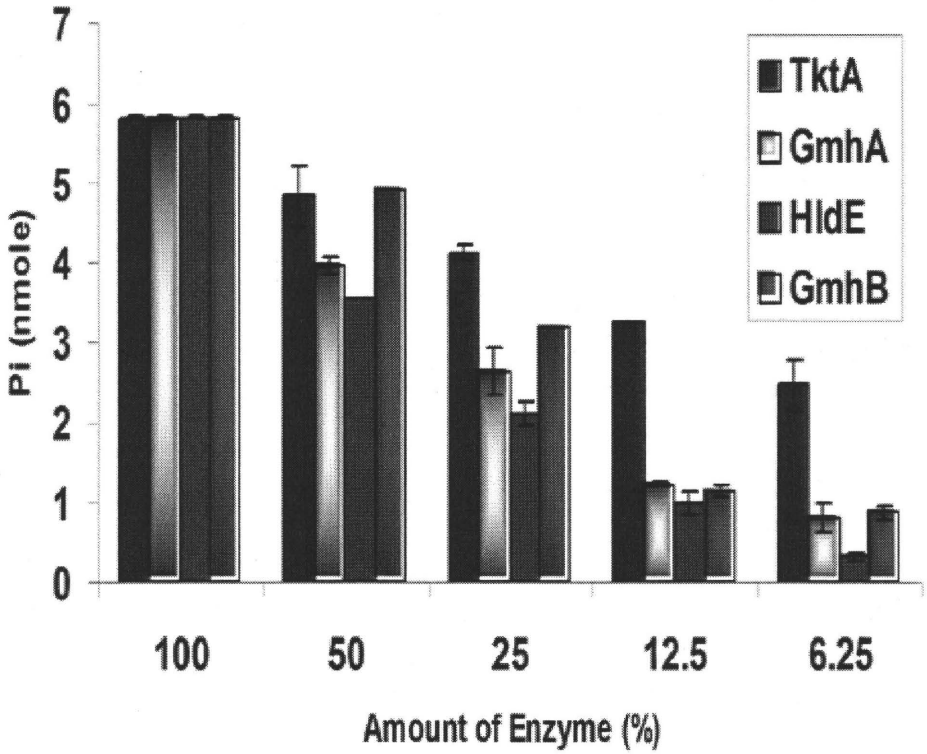

Figure 3-15. Assay validation: Effects of lowering the amount of each enzyme in the ADP-heptose biosynthetic pathway. Reactions were performed in duplicate in which TktA■ , GmhA □, HldE ■, and GmhB ■ were present at 32 pmole, 2.1 nmole, 12 pmole, and 2.5 pmole respectively as 100% enzymatic amount. Each enzyme was analyzed by lowering the amount of one enzyme while keeping the other three at constant amounts.

It is essential to know whether the optimum enzymatic conditions have an overall effect on the pathway before screening against small compound library. Thus, a decrease in any of the enzyme's activity should show lowered Pi signal suggesting decrease of the production of ADP-D-*glycero*-β-*manno*-heptose. The effects of lowering the enzymatic amounts were analyzed for each enzyme separately. In the analysis of the effects of TktA, Figure 3-15 shows that as the enzymatic amounts of TktA were decreased by 50%,

25%, 12.5 % and 6.25% (16, 8, 4 and 2 pmole respectively) while keeping GmhA, HldE and GmhB constant at 100%, the overall phosphate production decreased as well.

The same method was applied for the GmhA, HldE and GmhB enzyme to show Pi decrease as illustrated in Figure 3-15.

3.7 Steady-state kinetics of ATP

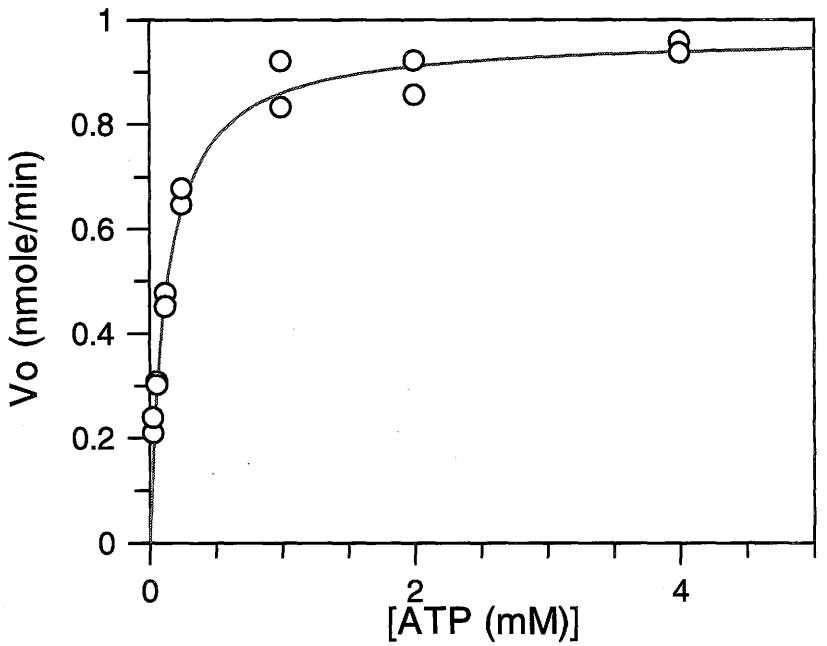

Figure 3-16 Kinetic parameters of ATP for the ADP-heptose biosynthetic pathway. The kinetic parameters were determined by the phosphopmolybdate assay by varying the concentrations of ATP from 0.0 to 4.0 mM. The ATP at varying concentrations was mixed with 1 mM ribose-5-phosphate and fructose-6-phosphate in 0.1% TWEEN-20, 5% DMSO with 2.1 nmole GmhA, 2.5 pmole GmhB, 32 pmole TktA, 12 pmole HldE, 0.1 U pyrophosphatase, 0.10 mM TPP in 20 mM HEPES pH 8.0, 10 mM $MgCl_2$ and KCl reaction buffer to study the kinetics of ATP. The K_m value was determined to be 130 ± 10 μM.

The kinetic data of the whole ADP-heptose biosynthetic pathway after establishing the optimized conditions was determined using seven concentrations of ATP from 0.0 to 4.0 mM in duplicate. The K_m, k_{cat} and k_{cat}/K_m values were calculated to be 130 ± 10 μM, 1.34 ± 0.02 s^{-1} and 1.1 x 10^4 M^{-1} s^{-1} respectively.

Table 3-2: Summary of the K_m, k_{cat} and k_{cat}/K_m values of the HldE-PK-LDH and TktA-GmhA-HldE-GmhB-pyrophosphatase linked enzymes.

	ATP			Ribose-5-phosphate			Fructose-6-phosphate		
Linked Enzymes	K_m (mM)	k_{cat} (s^{-1})	k_{cat}/K_m (M^{-1} s^{-1})	K_m (mM)	k_{cat} (s^{-1})	k_{cat}/K_m (M^{-1} s^{-1})	K_m (mM)	k_{cat} (s^{-1})	k_{cat}/K_m (M^{-1} s^{-1})
HldE-PK-LDH	0.3 ± 0.06	3.35 ± 0.19	1.13 x 10^4						
TktA-GmhA-HldE-GmhB-PPtase[1]	0.13 ± 0.01	1.34 ± 0.02	1.06 x 10^4	0.06 ± 0.02	1.20 ± 0.09	2.14 x 10^4	0.25 ± 0.07	0.94 ± 0.07	3.80 x 10^3

[1] PPtase-inorganic pyrophosphatase

3.8 Z' – factor determination

After the optimization of the reconstituted ADP-heptose pathway, the Z'-factor for the assay was determined. The calculated Z'-factor value provides a statistical evaluation of whether or not the developed assay is suitable for HTS. The Z'-factor is considered to be an improvement over a standard signal to noise measurement and provides an indication of the quality of an assay (61). Duplicate plates containing only low (no HldE) and high controls (with HldE) were prepared to evaluate the Z'-factor. A Z'-factor of around 1 is an ideal assay, <1-0.5 is a good assay, <0.5-0.9 is a mediocre

assay that may benefit from further development, and <0.1 is a poor assay that will not be useful for HTS (61). In this experiment, the Z'-factor was determined to be 0.70, suggesting that the assay is suitable for HTS and the screening window is reliable to identify any enzyme inhibitors (Figure 3-17).

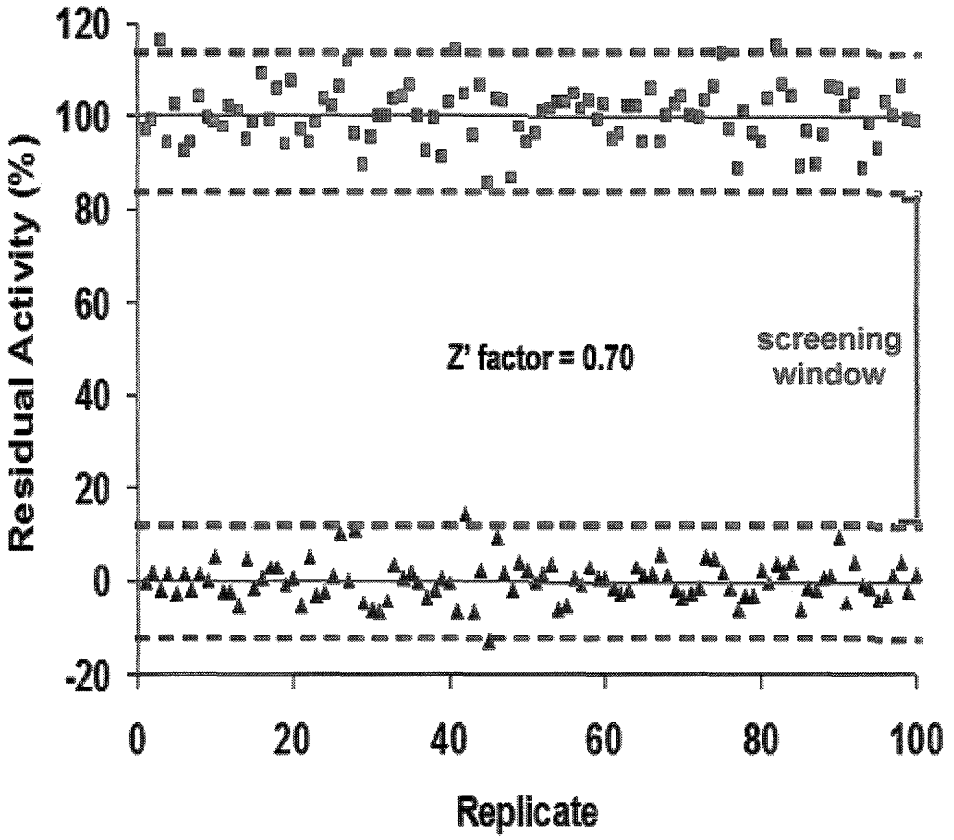

Figure 3-17. Evaluation of the *in vitro* ADP-heptose biosynthetic pathway screen. The residual activity of the high (■) (reaction with HldE) and low (▲) (reactions without HldE) controls were plotted for each replicate. The solid line (-) indicates the average for the controls and the heavy dashed lines (---) indicate three standard deviations. The screening window is located between the inner three standard deviation lines for the low and high controls at approximately 12 and 82 % residual activity, respectively. The statistical parameter Z' was calculated to assess the quality of the screen and determined to be 0.70 shown in the data above.

3.9 IC_{50} of AMP-PCP

The concentration of inhibitor that yields 50% inhibition was determined using the phosphomolybdate assay. A known kinase inhibitor, AMP-PCP was employed to show inhibition of the HldE kinase domain. Eight AMP-PCP concentrations in duplicate ranging from 0.0 to 40.0 mM were used against the optimized ADP-heptose pathway assay with 140 μM ATP. AMP-PCP is a non-hydrolyzable ATP analogue that replaces the β-γ oxygen bridging with a carbon atom (Figure 3-18). Since AMP-PCP and ATP are structurally similar, the inhibition of AMP-PCP is predicted to be competitive with ATP. Figure 3-19 below shows that AMP-PCP decreases the enzymatic activity of HldE with IC_{50} value of 5.1 ± 1.2 mM.

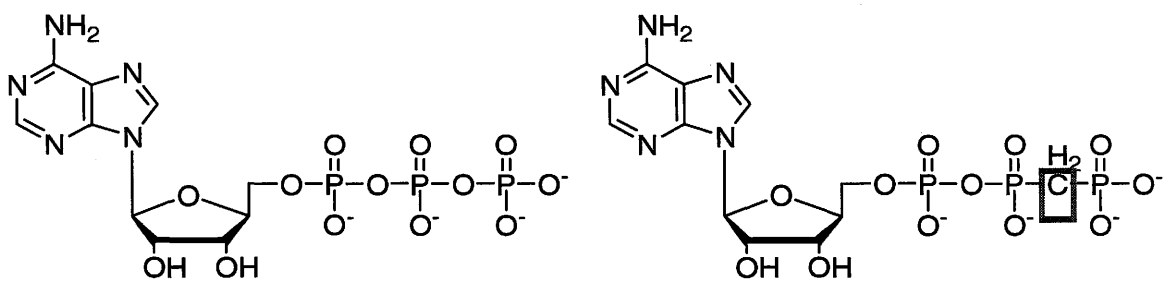

Figure 3-18. Chemical structures of adenosine triphosphate (ATP) on the left and its analogue β-γ-Methyleneadenosine 5'-triphosphate (AMP-PCP) on the right. AMP-PCP, a non-hydrolyzable ATP analogue that replaces the β-γ oxygen bridging with a carbon atom (red box), was used to determine the IC_{50} value of the ADP-heptose reconstituted pathway.

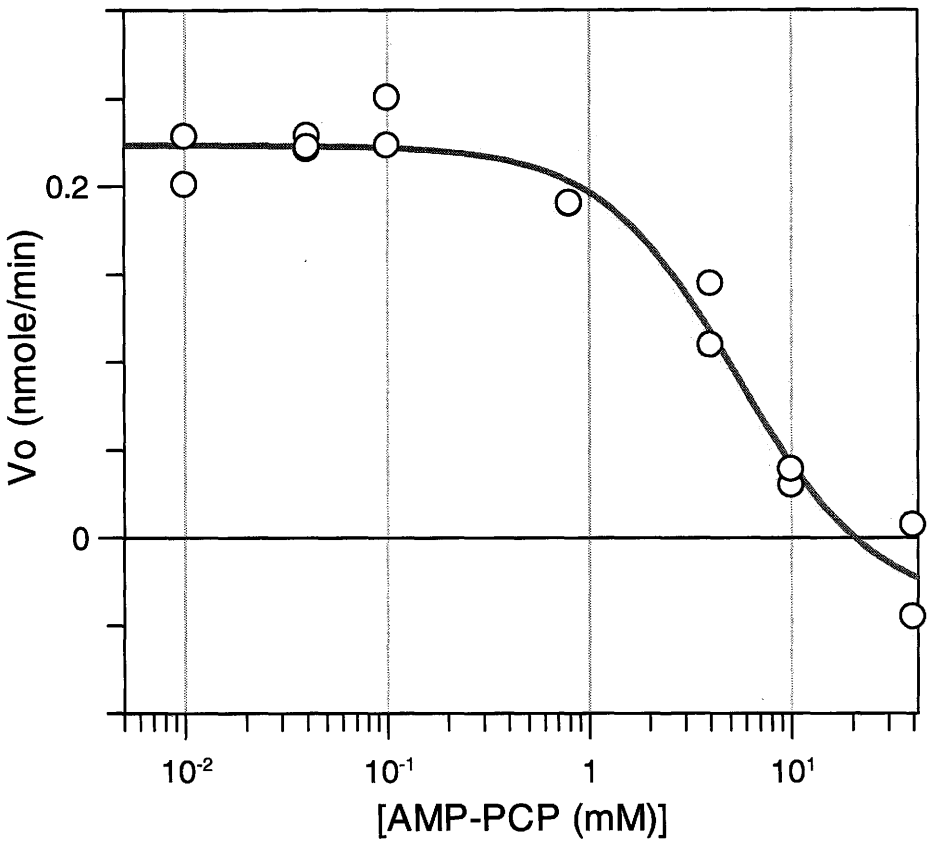

Figure 3-19. IC_{50} of AMP-PCP for the ADP-heptose pathway. The concentration of AMP-PCP was varied from 0.00, 0.01, 0.04, 0.10, 0.80, 4.0, 10.0 and 40.0 mM in order to determine the IC_{50} value. The condition for the reaction was adopted from the HTS primary screen as featured in Section 3.9.1. The IC_{50} value was determined to be 5.4 ± 1.2 mM AMP-PCP.

3.10 Primary screen against 1,000 small compounds

After assay optimization and determining that the quality of the assay was excellent with a Z'-factor of 0.70 as shown in Figure 3-17 (61), the pathway was screened against 1000 small molecules in 96-well microtitre plate format in duplicate at the McMaster HTS lab. The compounds obtained from ChemDiv Inc were dissolved at ~1 mM DMSO and a final concentration of 50 μM was added into the reaction. Using the

phosphomolybdate assay, the release of Pi was measured at 660 nm for each reaction plate. The results were reported as residual activity (%) and plotted on opposite axes (Figure 3-20). Duplicates are considered to be in agreement if they fall on a line through the origin with a slope of 1 (red dashed line). Hits were defined as compounds that exhibited an activity of less than or equal to 60% of the high controls.

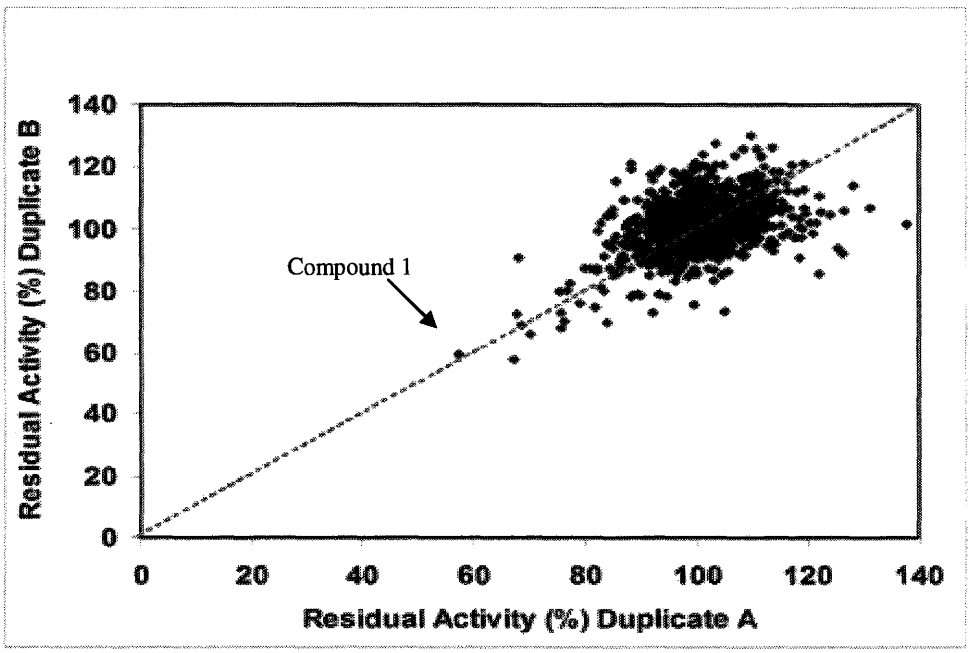

Figure 3-20. Residual activity plot: High throughput screening of kinase library of 1000 small molecules against the ADP- heptose biosynthetic pathway using the phosphomolybdate assay. Residual activity (%) duplicate values (A and B) for each compound are plotted on opposite axes. In the assay, 32 pmole TktA, 2.1 nmole GmhA, 12 pmole HldE, and 2.5 pmole GmhB per reaction were present in a master mix containing 1mM fructose-6-phosphate, 140 uM ATP, 0.1% TWEEN-20 and 0.1 U pyrophosphatase in 20 mM HEPES pH 8.0, 10 mM $MgCl_2$, 10 mM KCl reaction buffer. The compounds, dissolved in DMSO, were added to the reaction wells and pre-incubated for 8 min at 25°C. The reaction was initiated with the addition of 1 mM ribose-5-

phosphate. The reaction was quenched after 12 min incubation at 25˚C with 5% TCA at 4 ˚C.

3.10.1 Structure of Compound 1

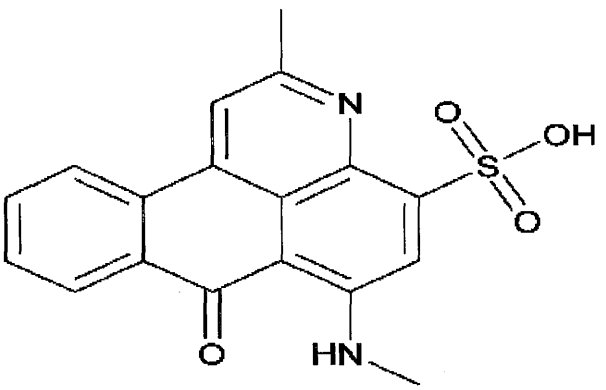

Figure 3-21. Chemical structure of Compound 1. The chemical structure of the inhibitor Compound 1 from ChemDiv lab showed 57.25% and 59.75% residual activity in replicates 1 and 2 respectively.

The primary screen of 1,000 small chemical compounds against the ADP-heptose pathway showed the compound in Figure 3-19 to inhibit the enzymatic activity by decreasing the phosphate production. With a final concentration of 50 μM MAC-151130, the residual activities in replicates 1 and 2 were determined to be 57.25% and 59.75% respectively.

3.11 Hit follow-up

3.11.1 IC_{50} of Compound 1

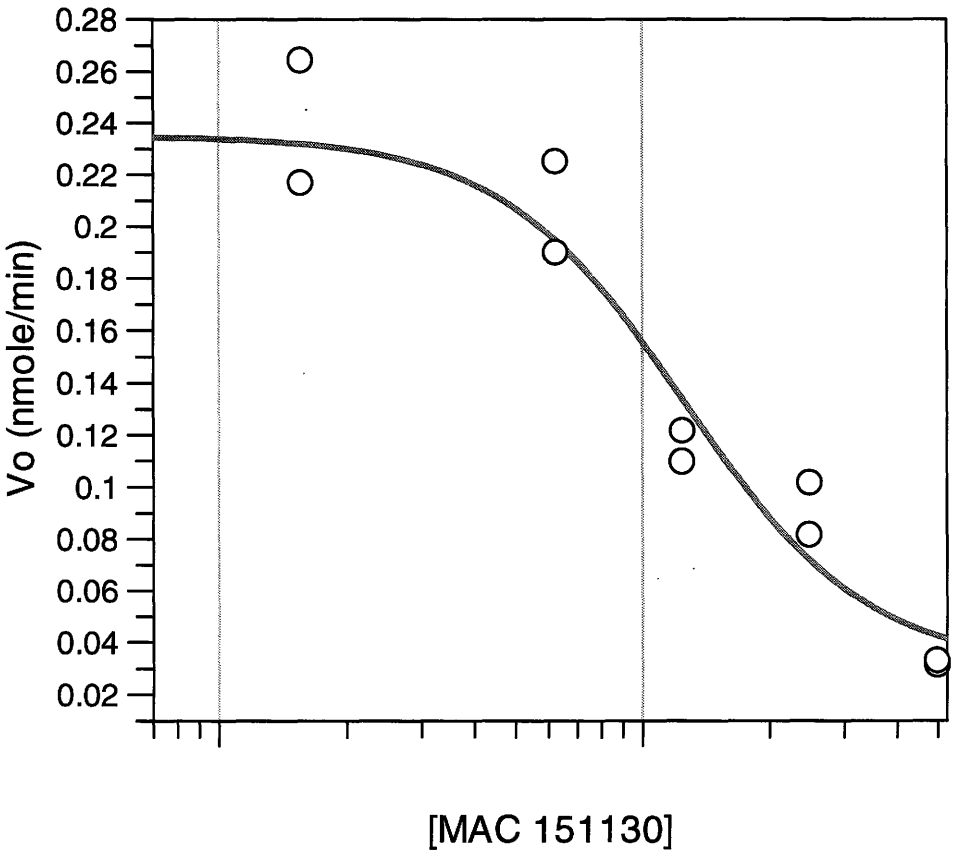

Figure 3-22. IC_{50} of the ADP-heptose pathway for Compund 1. Six concentrations of COMPOUND 1 (0.00, 15.6, 62.5, 125, 250 and 500 μM) were used in duplicate against the optimized ADP-heptose pathway assay featured in Section 3.9.1 with 140 μM ATP. The IC_{50} value was determined to be 130 ± 30 μM using the phosphomolybdate assay measured at 660 nm.

Compound 1 showed a residual activity of less than 60% in both replicates from the primary HTS acquisition (Section 3.10 and 3.10.1); the compound was further

analyzed to make sure that the result is not a false-positive result. Six sets of reactions in duplicate were prepared in a 96-well microtitre plate. The concentration of Compound 1 was varied from 0 to 500 μM and screened against the optimized HTS pathway assay with 140 μM ATP. The compound was incubated for 8 min at 25°C prior to the initiation of the reaction with ribose-5-phosphate. The enzymatic activity was determined by the phosphomolybdate assay by measuring the phosphate production at 660 nm. A concentration of 125 ± 25 μM Compound 1 showed a 50% decrease in the enzyme activity, proving that the compound does inhibit the pathway and is not a false-positive result.

3.12 HPLC secondary screen

Since the reconstituted ADP-heptose pathway consists of four enzymes, we need to evaluate which enzyme is being inhibited by compound 1. A new HPLC method was developed to detect the production of ADP-heptose using the exact conditions used for HTS and IC_{50} experiments. The method employed a VYDAC protein and peptide C18 column using a methanol gradient (5-90%) in 10 mM KH_2PO_4 pH 4.2 and 1 mM TBAHS to separate ATP, ADP and ADP-heptose.

Three sets of reactions were prepared in duplicate: one which was analyzed at time zero (negative control), another without the inhibitor (positive control) and finally, the reaction with 500 μM compound 1 with 10 min pre-incubation. Unless otherwise indicated, reactions were initiated with the addition of ribose-5-phosphate. Chromatogram A, Figure 3-23, shows ATP with a retention time of 18.8 min.

Chromatogram B is a complete reaction showing three peaks corresponding to ADP-heptose, ADP, and ATP, with retention times of 16.8, 17.4 and 18.8 min respectively. The chromatogram shows that the enzymes in the pathway are consuming ATP as the peak decreased while ADP and ADP-heptose peaks increases (Figure 3-23). Finally, the reaction with 500 μM Compound 1 showed inhibition of the HldE kinase domain (Chromatogram C), since only a small decrease in the ATP peak was observed and the peaks for ADP and ADP-heptose have areas smaller to those observed in chromatogram B.

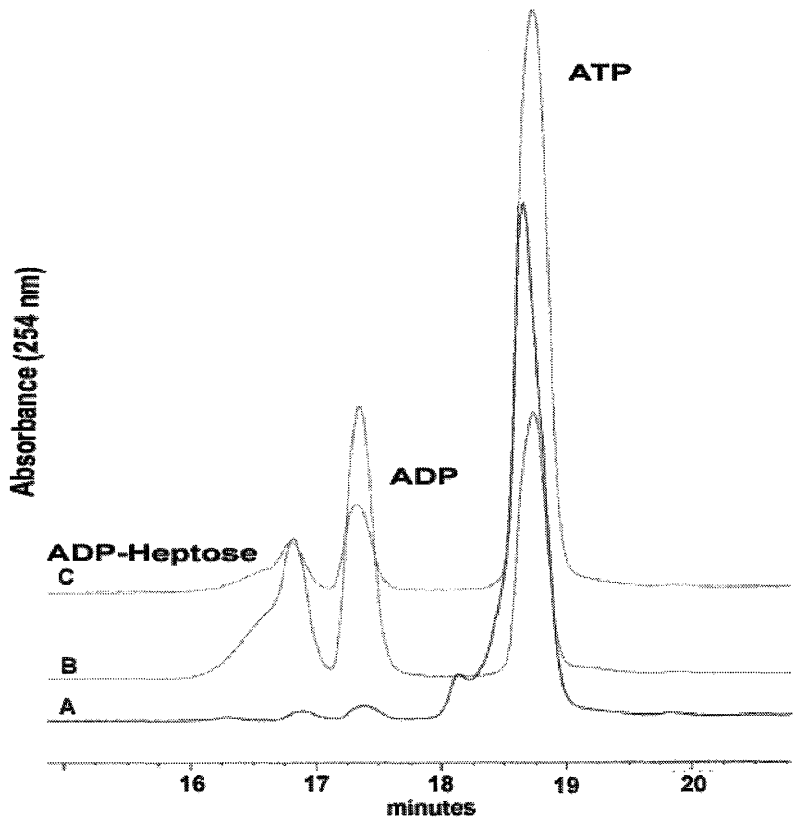

Figure 3-23. Paired-Ion Chromatographic analysis of the effects of Compound 1 on the production of ADP-D-*glycero*-β-*manno*-heptose. A 50 uL sample was injected into a VYDAC protein and peptide C18 column using a methanol gradient (5-90%) in 10 mM KH_2PO_4 pH 4.2 and 1mM TBAHS. **A**- Negative control: ATP with retention time of 18.8 min from the reaction without the bifunctional kinase/adenylyl transferase HldE incubated for 10 min at 25˚C. **B** – Positive Control: ATP, ADP (17.35 min) and ADP-D-*glycero*-β-*manno*-heptose (16.8 min) peaks from the reaction in the absence of inhibitor. **C** - ATP, ADP and ADP-D-*glycero*-β-*manno*-heptose from the reaction with 500 uM inhibitor (Compound 1 with MAC id MAC 151130). Note that reactions **A** and **B** were incubated for 10 min at 25˚C, and **C** was pre-incubated for 10 min prior to addition of 1.0 mM ribose-5-phosphate to initiate the reaction. The separation of ATP, ADP and ADP-L-glycero-D-manno-heptose was established earlier using standard ATP and ADP, and the fraction of the peak believed to be ADP-heptose was collected and submitted for MS analysis to confirm the product, ADP-D-*glycero*-β-*manno*-heptose

3.13 Hit Characterization

After determining that the compound Compound 1 was inhibiting the HldE kinase domain activity, an ADP-coupled assay was employed to measure the apparent K_m for ATP, IC_{50} and K_i values for Compound 1.

3.13.1 Apparent Km of ATP for HldE

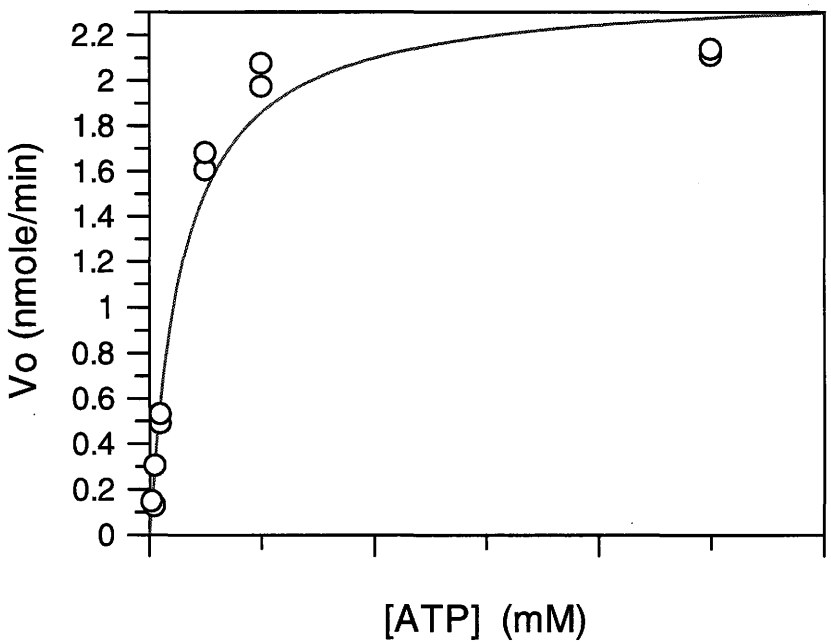

Figure 3-24. Apparent K_m of HldE for ATP using ADP-coupled assay. Seven ATP concentrations varying from 0.00 to 5.0 mM were mixed in duplicate with 0.30 mM NADH, 3 mM PEP, 2.5 U pyruvate kinase, 2.8 U lactate dehydrogenase, 1 mM fructose-6-phosphate and ribose-5-phosphate, 5 nmole GmhA, 0.125 nmole TktA in 20 mM HEPES pH 8.0, 10 mM MgCl and 40 mM KCl to make a 100 µL final volume in a 96-well microtitre plate. The reaction was initiated by the addition of ATP at varying concentrations. The ADP production was monitored at 340 nm for 20 minutes to determine the apparent K_m of HldE kinase domain (300 ± 63 µM).

The apparent K_m for ATP was determined by using excess TktA and GmhA to produce the HldE kinase substrate D-*glycero*-D-*manno*-heptose-7-phospate *in situ* and the pyruvate kinase/lactate dehydrogenase coupled to measure ADP production at 340 nm. The concentrations of ATP were varied using concentrations of 0.00, 0.025, 0.05, 0.10, 0.50, 1.00 and 5.00 mM to study the K_m of the HldE kinase domain. The K_m, k_{cat}, and k_{cat}/K_m values were calculated to be 300 ± 63 μM, 3.35 ± 0.19 s^{-1} and 1.1 x 10^4 M^{-1} s^{-1} respectively. The apparent K_m value of 300 μM was used as the ATP concentration to determine the IC_{50} and K_i values of MAC-151130 for HldE.

3.13.2 HldE IC_{50} of Compound 1

Excess of TktA and GmhA enzymes were used to produce the HldE kinase substrate D-*glycero*-D-*manno*-heptose-7-phospate *in situ* and mixed with pyruvate kinase/lactate dehydrogenase coupled to measure ADP production at 340 nm. The concentrations of Compound 1 used were varied using 0.00, 0.004, 0.008, 0.016, 0.031, 0.063, 0.125, 0.250, 0.500, 1.00 and 1.50 mM for the determination of the IC_{50} of Compound 1 for the HldE kinase domain. The IC_{50} value was calculated to be 160 ± 10 μM with a slope factor of 1.12 ± 0.12. The IC_{50} value obtained from this experiment was very close to the IC_{50} value of 130 ± 30 μM determined with the phosphomolybdate assay for the entire pathway (Figure 3-25).

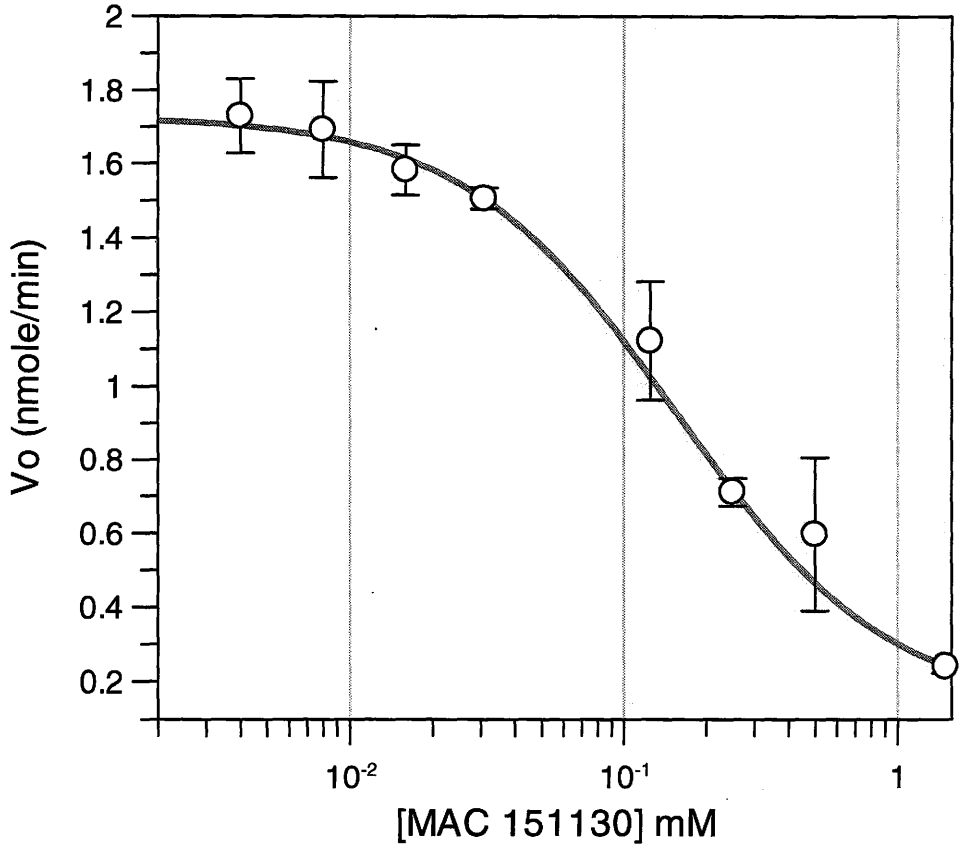

Figure 3-25. IC_{50} of Compound 1(MAC 151130) for HldE using the ADP-coupled assay. Eleven compound 1 (MAC 151130) concentrations varying from 0.00 to 1.5 mM in duplicate were mixed with 0.30 mM NADH, 3 mM PEP, 2.5 U pyruvate kinase, 2.8 U lactate dehydrogenase, 1 mM fructose-6-phosphate and ribose-5-phosphate, 5 nmole GmhA, 0.125 nmole TktA in 20 mM HEPES pH 8.0, 10 mM MgCl and 40 mM KCl to make a 100 µL final volume in a 96-well microtitre plates. The reaction was initiated by the addition of ATP at 300 µM concentration. NADH oxidation was monitored at 340 nm for 20 minutes. The IC_{50} value of 160 ± 10 µM was determined using the software GraFit.

3.13.3 K_i value of Compound 1

The mode of inhibition was assessed by generating a double reciprocal Lineweaver-Burke plot with individual lines to fit a simple double reciprocal model using the equation: $1/v_o = (\alpha\ K_m/V_{max})\ 1/[S] + 1/V_{max}$. Figure 3-26 shows a series of lines intersecting on the y-axis, and the value of V_{max} or $1/V_{max}$ that is not changed in the presence of the inhibition. The x-intercept becomes smaller as [I] increases, suggesting an increase in K_m (decrease in $-1/K_m$).

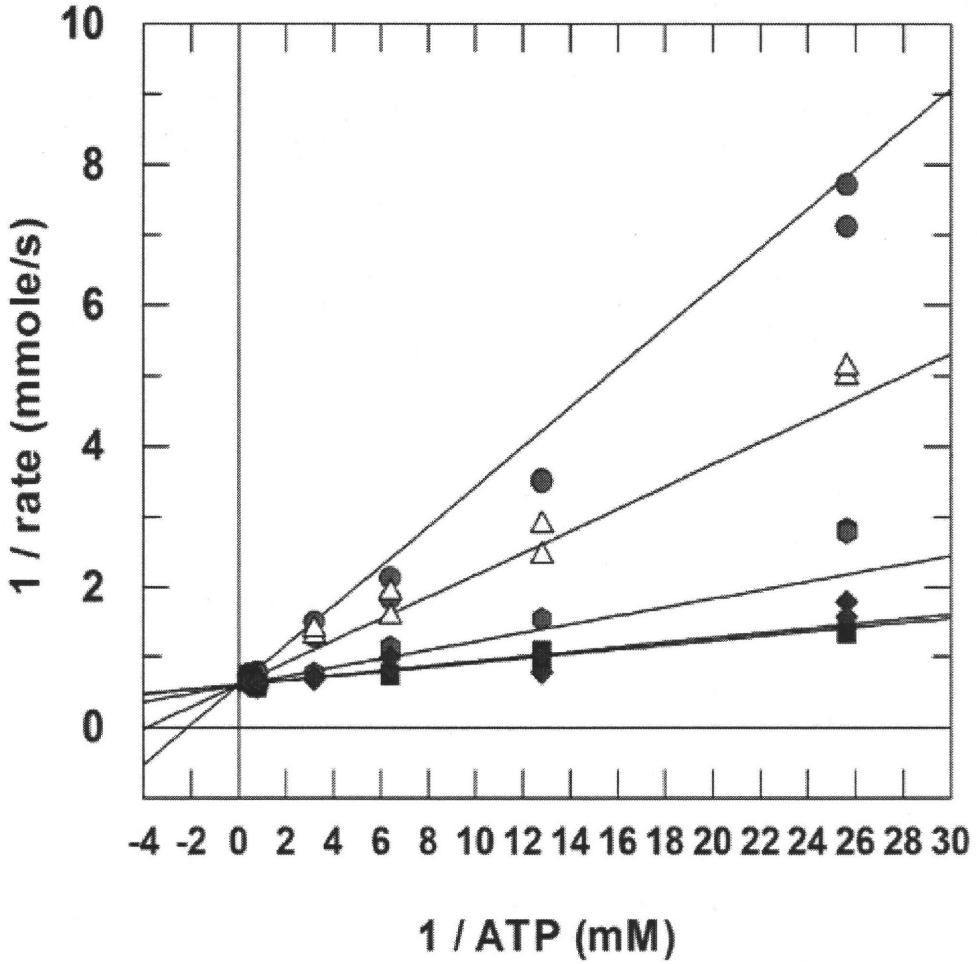

Figure 3-26. Characterization of HldE inhibitor Compound 1. The pathway assay was modified such that the substrate D-*glycero*-D-*manno*-heptose-7-phosphate was readily accessible to HldE in the presence of ATP. Five times the amount of TktA (162 pmole) and GmhA (10.5 nmole) were used for this assay with 12 pmole HldE. Both substrates, fructose-6-phosphate and ribose-5-phosphate, were present at 1 mM while the concentration of ATP was varied (0.04 mM, 0.08 mM, 0.16 mM, 0.32 mM, 1.25mM and 2.5 mM) against four Compound concentrations of 0.004 mM(◆), 0.06 mM (●), 0.25 mM (△) and 0.5 mM (●) and 0 mM (■) for the negative control. The mixture was pre-incubated for 10 min and initiated by the addition of ATP. ADP production from the kinase activity of HldE was monitored at 340 nm for 20 minutes. The K_i for Compound 1 was 63 ± 8 μM and the mode of inhibition was determined to be competitive with ATP as indicated by the reciprocal-plot.

3.14 Antibiotic minimal inhibitory concentrations – MICs K_i value of Compound 1

The MICs for the wild type and *hldE* gene mutant *E. coli* BW25113 were performed in a 96-well microtitre plate in duplicate. Figure 3-26 shows that the MIC of novobiocin for the wild type is 128 μg/mL and 32 μg/mL for the mutant *hldE*.

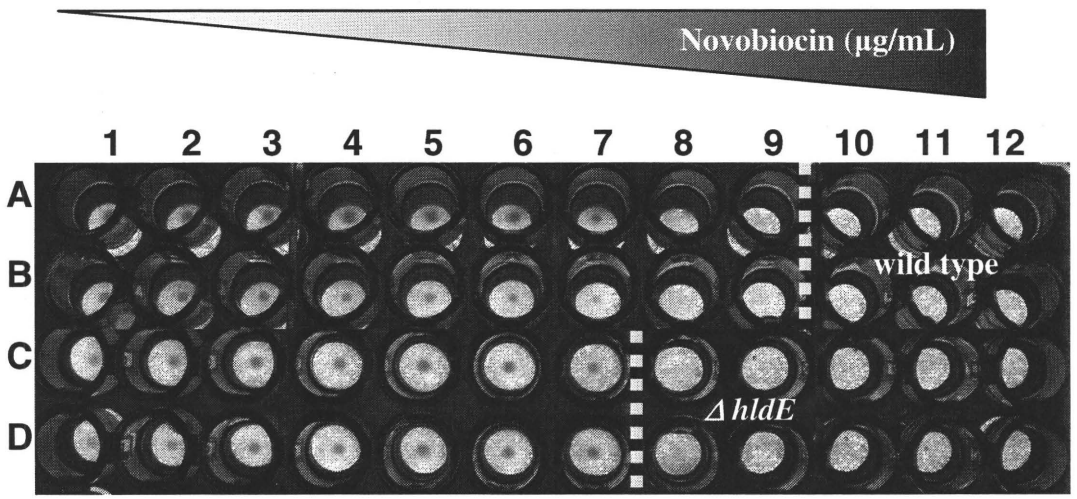

Figure 3-27. MIC of novobiocin for the wild type and *hldE* gene deletion *E. coli* BW 25113. The concentration of novobiocin increases across the 96-well microtitre plate (1 to 11) by two-folds starting from 0.5 to 256 μg/mL. The concentrations of novobiocin in each column are as follows: **1**- 0.0 μg/mL; **2**- 0.5 ug/mL; **3**- 1.0 μg /mL; **4** - 2.0 μg /mL; **5** - 4.0 μg /mL; **6** - 8.0 μg /mL; **7** - 16.0 μg /mL; **8**- 32 μg /mL; **9** - 64 μg /mL; **10** - 128 μg /mL; **11** - 256 μg /mL and **12** - sterility control (no bacterial suspension, only media). The wild type *E. coli* BW 25113 bacterial suspension was dispensed in rows A and B (negative control), while the *hldE* gene deletion *E. coli* BW 25113 suspension was dispensed in rows C and D (positive control). The MIC of novobiocin for the wild type and mutant *E.coli* BW 25113 were determined to be 128 μg /mL and 32 μg /mL respectively.

The biological activity of the inhibitor Compound 1 was observed in the presence of the antibiotic novobiocin on a 96-well microtitre plate. The concentrations of novobiocin and Compound 1 in each well were varied to set-up a check board MIC. Figure 3-27 shows that the presence of Compound 1 does not influence the activity of

novobiocin on the growth of *E. coli*. The novobiocin produced a tailing effect in the bacterial growth similar to those observed in the negative control on Figure 3-27. The MIC for novobiocin according to the OD_{600} readings was observed to be 128 μg/mL whether or not Compound 1 is present in the wells.

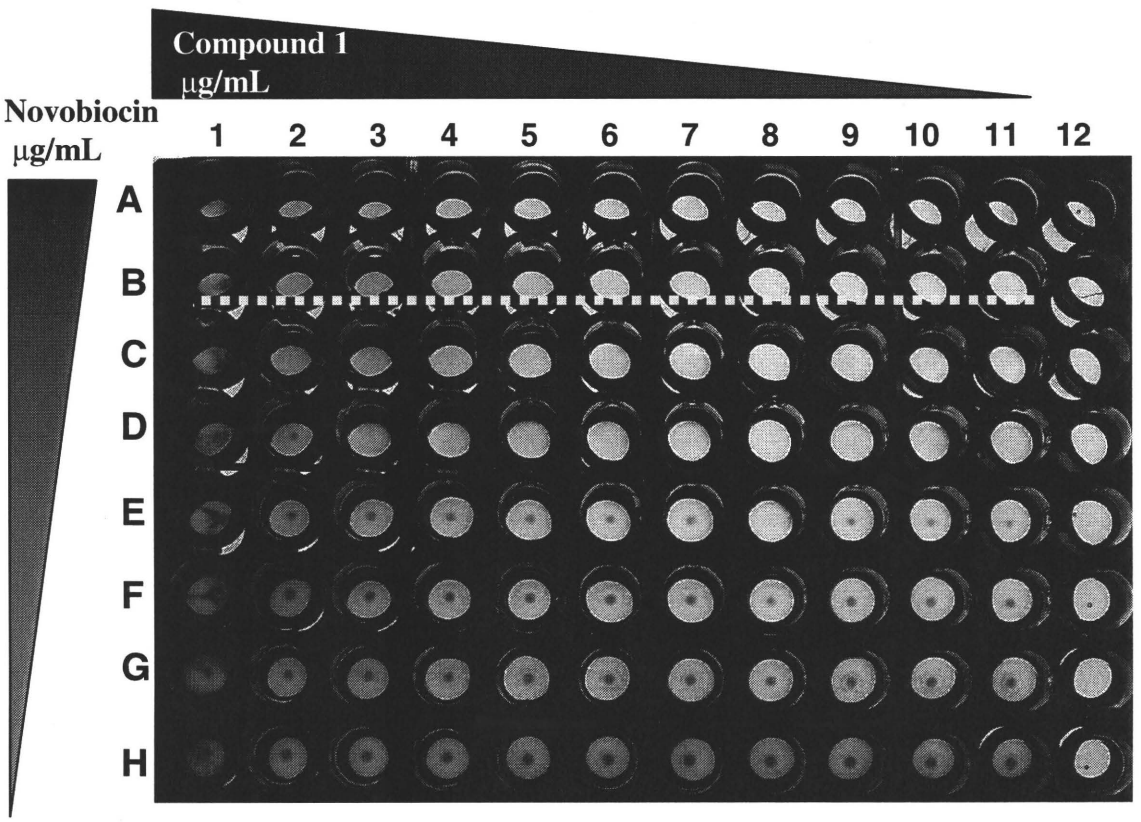

Figure 3-28. MIC of novobiocin with MAC-151130 for wild type *E. coli* BW 25113. The concentration of novobiocin increases across the 96-well microtitre plate (A to H) by two-folds starting from 4.0 to 256 μg /mL. The concentration of novobiocin in each row are **A** – 256 μg /mL; **B** - 128 μg /mL; **C** – 64 μg /mL; **D** – 32 μg /mL; **E** – 16 μg /mL, **F** – 8.0 ug/mL; **G** – 4.0 μg /mL and **H** – 0.0 μg /mL. The concentration of Compound 1 increases across the 96-well microtitre plate (1 to 11) by two-folds starting from 0.5 to 256 μg /mL. The concentration of compound 1 in each column are **1**- 0.0 μg /mL; **2**- 0.5 μg /mL; **3**- 1.0 μg /mL; **4** - 2.0 μg /mL; **5** - 4.0 μg /mL; **6** - 8.0 μg /mL; **7** - 16.0 μg /mL; **8**- 32 μg /mL; **9** - 64 μg /mL; **10** - 128 μg /mL; **11** - 256 μg /mL and **12** - sterility control (no bacterial suspension, only media). The MIC of novobiocin with or without Compound 1 was 128 μg /mL.

4. Discussion

4.1 ADP-heptose assay development

The biosynthesis of the highly conserved heptose component of the LPS inner core was recently elucidated biochemically and genetically. Mutational studies of the genes responsible for the biosynthesis of the heptose region of the LPS molecules in *E. coli* resulted in mutants with a 'deep-rough' phenotype (4, 5,9,12, 19 and 20). As mentioned previously in Chapter 1, although 'deep-rough' mutants are viable, they were found to be sensitive to the antibiotic novobiocin (6, 9, 10, 19, 20 and 21). Presently, there has been no reported inhibitor that targets any of the enzymes involved in the ADP-heptose biosynthetic pathway. By developing an *in vitro* pathway assay suitable for HTS, we were able to screen the ADP-heptose pathway against a 1000 compound chemical library, and found one molecule that showed inhibition of one of the enzymes in the pathway.

To further understand the enzymes at a chemical and catalytic level, each gene in the ADP-heptose pathway, namely *tktA*, *gmhA*, *hldE* and *gmhB,* was successfully cloned and overexpressed as a hexa-His tagged construct in *E. coli* to obtain purified proteins (Figure 3-1a, 3-1b and 3-1c). The purifications of TktA, GmhA, HldE and GmhB, gave good yields sufficient for assay development and kinetic studies (summarized on Table 3-1).

To determine whether the enzymes in the biosynthetic pathway were active after separation from their physiological neighbours, a series of small scale *in vitro* reactions were set-up and analyzed using the HPAEC-PAD technique. This method requires the use of a non-porous pellicur resin, such as the CarboPac PA1, for the separation of oligosaccharides by high pH anion-exchange chromatography, coupled with PAD. This technique has been demonstrated to be effective in the separation and detection of carbohydrates ranging from small monosaccharides to branched oligosaccharides and large linear polysaccharides (20) .

Since the sugar intermediates of the ADP-heptose pathway are not available commercially, we were unable to establish reference compounds for peak comparison. Hence, in order to perform this assay, we observed the appearance of new peaks and any changes in peak separation, and used the information as an indication of enzymatic activity. As illustrated in Figure 3-3, the appearance of a new peak was observed in the presence of the HldE in the reaction mixture. The new peak was assumed to correspond to a sugar intermediate catalyzed by the kinase reaction of HldE. However, a better method is required to further analyze the enzymes.

Since the HPAEC-PAD gave poor resolution, another method to study the enzymes in the pathway was developed. The biosynthetic pathway was reconstituted *in vitro*, where equimolar amounts of TktA, GmhA, HldE and GmhB were incorporated with two commercially available substrates to confirm substrate-dependent Pi formation

using phosphomolybdate/malachite green detection at 660 nm (7). The phosphomolybdate/malachite green assay, a simple, sensitive and non-radioactive end-point assay, was used to quantify the amount of inorganic phosphate in the reaction solution. Inorganic phosphate is released directly from the phosphatase reaction of GmhB and indirectly from the pyrophosphate product of the adenylyltransferease reaction by the bifunctional HldE enzyme with the addition of the enzyme and inorganic pyrophosphatase in the mixture (Figure 4-1). Liberated phosphate forms a coloured complex with molybdate/malachite green, which can be quantified by measuring the absorbance at 660 nm. At this point, the *in vitro* assay was at its very early stage and assay conditions needed to be optimized.

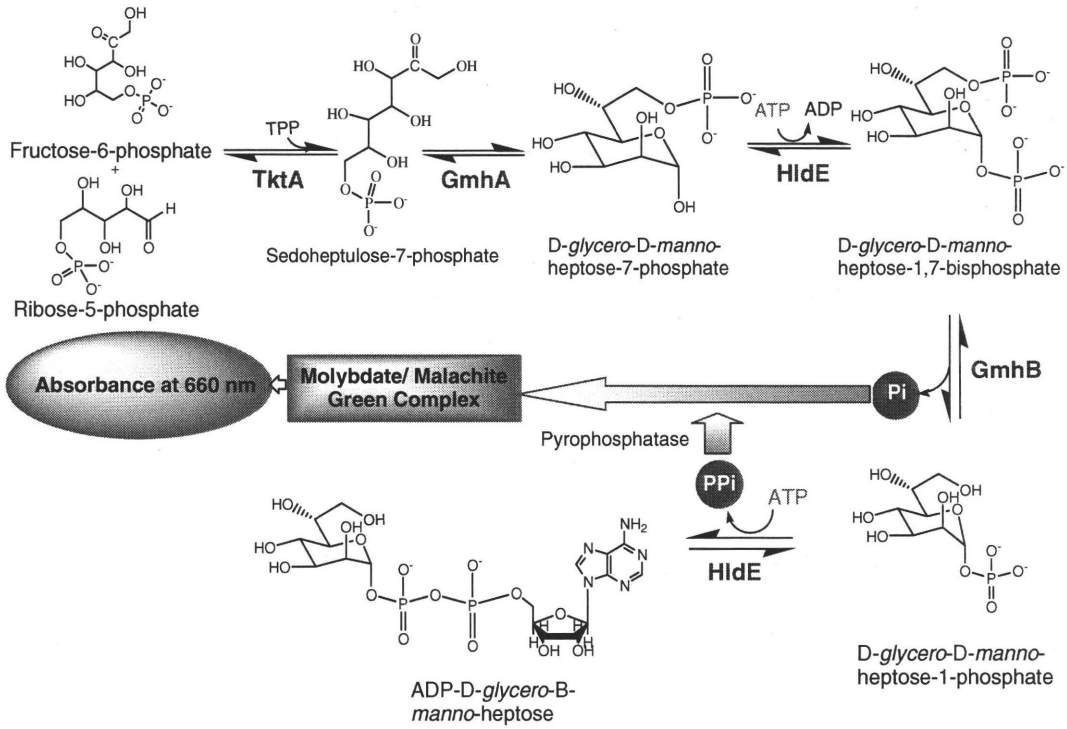

Figure 4-1. Schematic diagram of the phosphomolybdate/malachite green assay used to detect Pi released in the ADP-heptose pathway. Inorganic phosphate (circled in red) is released from GmhB and indirectly from the pyrophosphate product of the HldE adenylyltransferease reaction with the addition of the inorganic pyrophosphatase in the mixture. The liberated phosphate reacts with the molybdate/Malachite green complex which to make a coloured complex with an absorbance at 660 nm.

The stability of both enzymes and substrates at room temperature is an important factor to be considered when developing an assay suitable for HTS, since screening will take place at ambient temperature and the liquid handler can only accommodate one reagent reservoir at non-ambient temperature. The results in Figure 3-4 indicated that the reactions incubated at 25˚C and at 37 ˚C were comparable for at least 20 min, suggesting that the assay can accommodate HTS conditions at ambient temperature.

To ensure that the Pi formation detected by the phosphomolybdate/malachite green assay was from the GmhB and HldE adenylytransferase activities and not from other sources, the formation of the product, ADP-D-*glycero*-β-*manno*-heptose at the end of the pathway was confirmed by reverse-phase HPLC and LC/MS analyses. The catalysis of the product, ADP-D-*glycero*-β-*manno*-heptose was observed through the appearance of the new peak (Figure 3-5, chromatogram 6), whose identity was confirmed by LC/MS. In addition, this experiment also showed a decrease in ATP concentration, as the concentration of ADP increased in the presence of the HldE enzyme (Chromatograms 5 and 6, Figure 3-5). Furthermore, although the adenylyltransferase of the bifunctional HldE was included *in vitro*, no sugar intermediate was observed until the phosphate cleavage reaction by the GmhB enzyme occurred at the carbon atom at position 7. This finding reinforces importance of the role of GmhB in the ADP-heptose biosynthetic pathway. In conclusion, the HPLC and LC/MS results confirmed that the enzymes TktA, GmhA, HldE and GmhB in the ADP-heptose pathway of the LPS inner core catalyze the formation of the nucleated sugar ADP-D-*glycero*-β-*manno*-heptose in a metabolically relevant direction starting from two commercially available substrates.

It is important to realize that assays are set-up so that one is measuring the initial velocity of the enzyme reaction. The initial velocity is the initial portion or the linear phase of an enzyme progress curve that typically lasts until about 10-20% of the initial substrate concentration is converted to product (8). The initial velocity of an enzymatic

reaction is considered to be the best measure of enzymatic reaction rate. Using this parameter makes subsequent analysis of reaction mechanism and mechanism of inhibition more straightforward (8). In addition, the initial velocity phase of the reaction is most sensitive to inhibition, therefore making detection of inhibitors during library screening more effective. The reconstituted ADP-heptose pathway assay was found to be linear for at least 10 min with an R^2 value of 0.9934 after adjusting the level of each enzyme to achieve assay linearity (Figure 3-7). By analyzing Pi release every two min, the 10 min time point was established as the point reflecting the initial velocity phase. Therefore, for purposes of convenience and screening efficiency, we used 10 min as a single time point measurement for kinetic studies and screening unless otherwise noted.

Dimethyl sulfoxide (DMSO) is a common solvent used to dissolve a variety of molecules. It is highly miscible in water and all the McMaster HTS lab compound libraries are dissolved in DMSO. Although DMSO is a very versatile solvent, it could pose a negative effect to the enzyme activity at higher concentrations. Figure 3-10 illustrates comparable results in reactions containing 0, 5 and 10% DMSO. The enzymatic activity of the pathway assay did not show any negative effects even at 10% DMSO. Hence, the reconstituted *in vitro* assay was determined to be suitable for screening of a small compound library dissolved in DMSO as high as 10% concentration.

The next step in assay development was to optimize enzymatic levels of each enzyme in the pathway for HTS. The substrates, ribose-5-phosphate and fructose-6-

phosphate at 1 mM concentrations were used to initiate the reactions in the pathway. The levels of enzymes were lowered in a step-wise fashion to a condition that would show a decrease in Pi release while maintaining a linear dependence over 10 min (Figure 3-11 to Figure 3 -14). In quantitative screenings of compound libraries, it is important to know that the observed diminutions in enzymatic activity are well correlated with formation of an enzyme-inhibitor complex. Hence, if 50% of the enzyme is bound to an inhibitor, then a 50% reduction in the reaction velocity should be observed (8). After establishing the levels of enzymes individually, the assay was further examined to determine whether or not the established enzymatic levels would still show decrease Pi amounts by lowering each enzymatic amount by 50%, 25%, 12.5% and 6.25%. Further assay development took place until the levels of TktA, GmhA and GmhB were lowered from 3.9 to 3.2 pmol, 2.3 to 2.1 pmole and 3.1 to 2.5 pmole respectively to achieve this goal (Figure 3-15).

The kinetic parameters for the ADP-heptose pathway at optimized conditions were determined for the substrate ATP. ATP is consumed by the bifunctional kinase/adenylyl transferase enzyme HldE. For many enzymes, the K_m value is considered to be a reasonable estimate of the substrate concentration encountered by the enzyme *in vivo* (8). Thus, the kinetic parameters for ATP were determined with optimized assay conditions to characterize the HldE enzyme and to have an idea of an appropriate starting substrate concentration for HTS. By using a substrate concentration equal to or close to the K_m value, the system would provide a balanced population of enzyme and enzyme-substrate complex available for inhibitor interactions. The K_m value for ATP would also

be useful for the IC_{50} determination for initial characterization. Finally, assays run under this condition provide the best opportunity to identify the full constellation of inhibitory molecules from a collection of diverse small synthetic molecules (8).

The criteria for evaluating the suitability of an HTS assay for hit identification was determined by calculating the Z'-factor. The Z'-factor is a screening window coefficient that is reflective of both the assay signal dynamic range and the data variation associated with the signal measurement, providing a simple statistical assessment of assay quality (61). The hit threshold or hit limit is commonly set at 3 standard deviations (SD) from the mean of the sample data with 99.73% confidence limit. Screening involved assaying each data point multiple times to increase the confidence of each data point in order to minimize the number of false-positive and false-negative hits (61). The dynamic range of the assay signal can be defined by the difference between the mean of the high controls and the mean of the low controls. The optimized reconstituted pathway assay showed a large separation band and has the potential to be an excellent assay for HTS (Figure 3-17) (61).

Prior to screening, it is critical to recognize the potential influence of the enzyme concentration on apparent inhibitor affinity. Hence, the ability of this optimized reconstituted assay to identify inhibitors of a component enzyme was also validated using the non-hydrolysable ATP-analogue AMP-PCP which we predicted would inhibit the kinase activity of HldE enzyme (Figure 3-19). After assay optimization and establishing

a screening method, the reconstituted pathway was screened in duplicate against 1000 synthetic small molecules that exhibit broad spectrums of inhibition against protein kinases at 50 μM. The screen identifies one molecule that decreased the residual activity by ~40% (Figure 3-20 and 3-21).

The IC_{50} value of Compound 1 for the reconstituted pathway was determined to be 130 ± 30 μM following the primary HTS screen (Figure 3-22). Further hit characterizations were performed to identify the enzyme being inhibited by Compound 1 as well the mode of inhibition.

The activities of the enzymes in the pathway were established in the presence and absence of Compound 1. Reaction progress was observed by reverse-phase HPLC, while monitoring absorbance at 254 nm. The reaction without the inhibitor reports residual substrate ATP, the product ADP from the kinase activity, and the HldE transferase product ADP-D-*glycero*-β-*manno*-heptose as shown in Figure 3-23. The peak area ratio of ATP: ADP: ADP-D-*glycero*-β-*manno*-heptose without the inhibitor was 4:3:3. Since ATP, ADP and ADP-D-*glycero*-β-*manno*-heptose levels can be monitored, we can narrow our possibilities to establish which enzyme is being inhibited. For instance, if the compound inhibits either the GmhB or the HldE adenylyltransferase activity, the peak area of ATP: ADP should be approximately that observed in the absence of the inhibitor. However, if the compound inhibits whether TktA, GmhA or HldE kinase activity, then the levels of ATP should be much more significant and the ADP levels should be less

than those observed in the reaction without the inhibitor. In Figure 3-23 C, the ratio of ATP: ADP: ADP-D-*glycero*-β-*manno*-heptose is 8:1:1 suggesting that either TktA, GmhA or the kinase activity of HldE are the possible targets.

To further characterize the inhibitor, ADP production by the HldE kinase activity was coupled with pyruvate kinase/lactate dehydrogenase to monitor the NADH oxidation which can be measured at 340 nm (Figure 4-1). Since HPLC analysis has indicated that the HldE kinase activity is one of the possible targets, the apparent K_m of the HldE kinase domain for ATP of 300 ± 63 μM was determined using the ADP-coupled assay. Since the sugar substrate D-*glycero*-D-*manno*-heptose-7-phosphate was not available commercially, excess amounts of the TktA and GmhA enzymes were added into the reaction mixture to synthesize the substrate *in situ* (Figure 3-24).

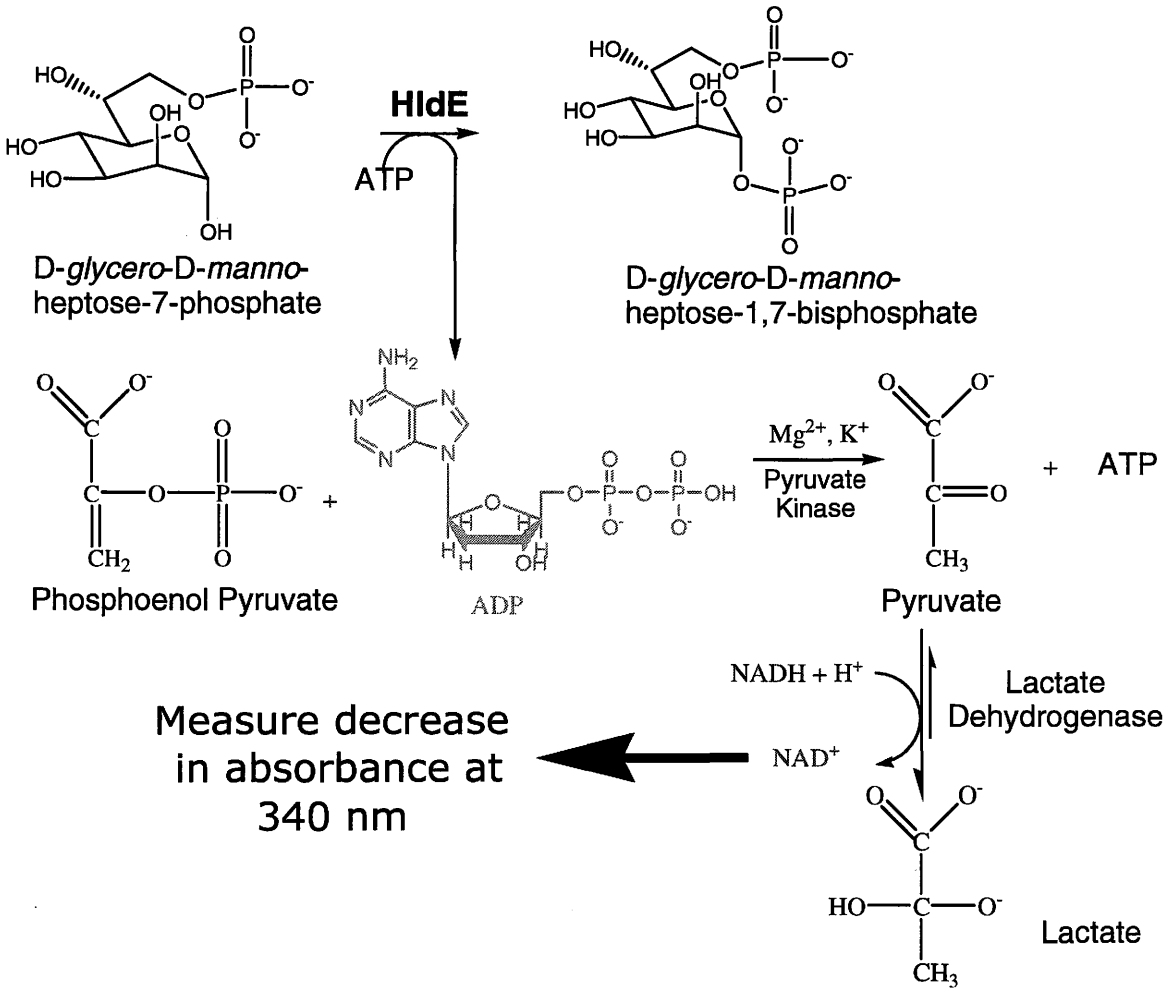

Figure 4-2. ADP-coupled with pyruvate kinase/lactate dehydrogenase assay. The ADP product (purple) of the HldE kinase activity was monitored with the lactate dehydrogenase dependent oxidation of reduced NADH + H^+ in the presence of phosphoenol pyruvate and pyruvate kinase. The oxidation of NADH + H^+ can be monitored as it shows decrease in absorbance at 340 nm.

The IC_{50} for the compound Compound 1 was determined using the same ADP-coupled assay. The concentration of ATP used for this assay was equivalent to the K_m value of 300 μM as determined previously (Figure 3-24). The IC_{50} of Compound 1 was determined to be 160 ± 10 μM (Figure 3-25) which, value is very close to the IC_{50} of 130 ± 30 μM determined earlier for the whole pathway using phosphomolybdate/malachite

green (Figure 3-22). The measured IC_{50} values only differ slightly even at excess amounts of TktA and GmhA, suggesting that the effect of the inhibitor in the pathway is still measurable and only affecting the activity of the HldE enzyme. Hence, the two enzymes, TktA and GmhA were eliminated as possible targets.

We further characterized the mode of enzyme inhibition by generating a double reciprocal plot. The synthetic compound was found to be a competitive inhibitor of the ATP substrate for the kinase domain of HldE, with a K_i value of 63 ± 8 μM (Figure 3-26). This conclusion was deduced from the series of intersecting lines on the y-intercept, showing equal V_{max} ($1/V_{max}$) values even in the presence of the inhibitor. In addition, the K_m value increases as the concentration of the inhibitor increases, suggesting a decrease enzyme affinity to ATP due to competitive inhibition with Compound 1 (8).

Compound 1 from the primary screen of the 1000 kinase compound library is the first reported compound to show inhibition of the ADP-heptose biosynthetic pathway. The biological activity of the inhibitor was assessed in the presence of increasing novobiocin on a 96-microtitre plate. The result showed no synergistic effect between Compound 1 and novobiocin (Figure 3-28). Therefore, more efforts are required to improve the biological activity of inhibitor. For instance, the structure modification could increase enzyme inhibition.

In order to improve the activity of Compound 1, the chemical structure must be analyzed in comparison to the other compounds in the library that are analogous in

structures but different activity. From the primary screen, Compound 1 showed reduced pathway activity by ~40%, while Compound 2, analogous to the structure of Compound 1 manifested only ~20% inhibition. In contrast, Compound 3 was not an inhibitor, suggesting that the sulfonic acid was likely important for activity.

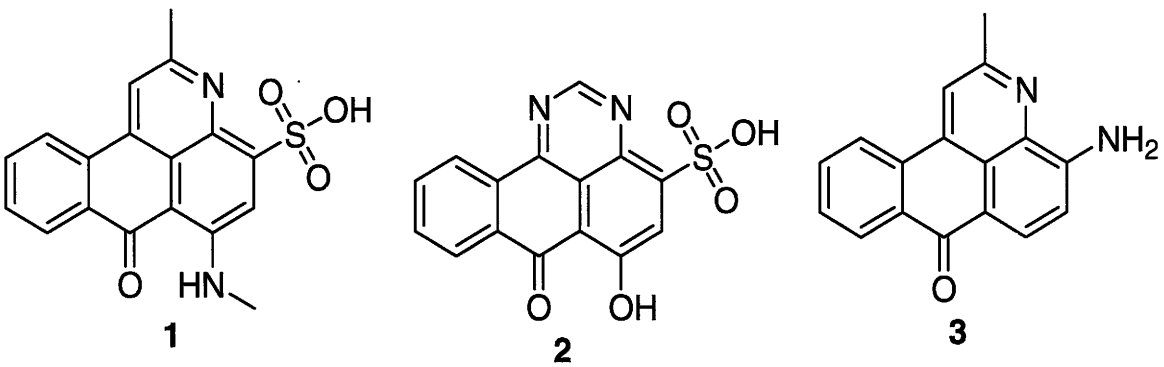

Figure 4-3. Comparison of the chemical structures of compounds 1, 2 and 3 from the primary screen against 1000 kinase library. **1** – (Compound 1) Structure of the inhibitor which showed ~40% decrease in pathway activity. **2** - Structure of compound 2 which showed ~20% decrease in pathway activity. **3** – Structure of compound 3 which showed no inhibition to the pathway activity.

4.2 Concluding remarks

This study showed that the optimized reconstituted ADP-heptose biosynthetic pathway is suitable for high-throughput screening by empirically linking the enzymes in the pathway to establish an assay in a metabolically relevant direction. By screening the enzymes in tandem, it avoided problems with substrate availability and stability. This pathway enabled the identification of the first reported inhibitor of ADP-heptose pathway in bacterial LPS. This simultaneous *in vitro* assay allows for the detection of the novel LPS inhibitor that could potentially lead into novel therapeutic agents against Gram-negative infections. Finally, this assay opens up a new opportunity in antibacterial drug development and for enzyme characterization of the mutants constructs dedicated to understand the enzymatic activity involved in the pathway.

In the efforts to improve drug development, the crystal conditions for the GmhA, GmhB and HldE proteins were set-up for structure-based drug design (See Appendix 1). Here, we were able to report the first protein structure of GmhA bound with the substrate, sedoheptulose-7-phosphate in collaboration with Dr. Murray Junop at McMaster University. In addition, the data for the GmhB protein crystal was collected recently with a resolution of 1.5Å. The structure of the GmhB protein, once solved, will contribute to further understand this enzymatic step in the pathway. Finally, no conditions have yet been identified for the HldE protein and are still being conducted in the Junop lab in the hopes to solve the tertiary structure of this protein. However, the reconstituted pathway assay and the tertiary protein structures are steps ahead to fully understand the ADP-heptose pathway biochemically.

Appendix 1

5.1 Crystallization of apoprotein GmhA and in complex with the substrate

5.1.1 Materials and Methods

All chemicals used in crystallization solutions were acquired from BioShop Canada, Ltd. (Burlington, ON) excluding polyethylene glycol (PEG) 8000, which was purchased from Calbiochem, VWR (Mississauga, ON). VDX 24-well plates and siliconized cover slides were obtained from Hampton Research (Laguna Niguel, CA) and high vacuum grease was purchased from Corning, VWR (Mississauga, ON). The crystallization trial kits Wizard I and Wizard II were acquired from Emerald Biostructures, DeCode Genetics (BainBridge Island, WA). The crystallization screens Crystal Screen, Crystal Screen II, Crystal Screen Cryo, Crystal Screen Natrix and Additive Screen I, II and III were all purchased from Hampton Research (Laguna Niguel, CA).

The purification scheme of native GmhA is described previously of this report. Two-step purification was performed to obtain ~98% pure protein samples as analyzed by 13% SDS-polyacrylamide gel. The pooled fractions were dialyzed overnight as described in the previous section (Table 2-3) and the buffer was exchanged by concentration to 1 mL in a 10,000 MWCO Millipore ultra-15 centrifugation filter followed by dilution with 20 mM HEPES pH 8.0, repeating a total of three times. The protein was then concentrated to 10 mg/ml (0.48 mM GmhA) and stored at 4°C.

5.1.2 General Crystallization Protocol

All protein-substrate and apoprotein crystals were grown using the standard hanging drop/vapour diffusion method using VDX 24-well plates with siliconized cover slides sealed with high vacuum grease. Reservoirs contained 500 µl of solution and drop size varied from 1-3 µl with different ratios of protein solution. The substrate sedoheptulose-7-phosphate was synthesized in our lab and 20 mM stock solution was prepared for crystallization. One microlitre of substrate was mixed with 9 uL protein to use for crystallization trials with commercially available kits: Wizard I and Wizard II, Crystal Screen, Crystal Screen II, Crystal Screen Cryo and Crystal Screen Natrix. Each screen contained 48 different crystallization conditions and the protein drops were prepared in duplicate.

5.1.3 Crystal Optimization

Once conditions were identified to support the crystallization of the protein, the fine screening technique was employed to improve crystal size and quality. Optimization entails changing one or more components of the crystallization solution to a controlled condition in an attempt to find the optimal conditions. Components that were altered in this case included the pH of the buffer (29) and the concentration of precipitant (18). Briefly, the buffer pH was screened ± 0.5 pH unit, the buffer concentration by ± 10 mM and precipitant concentration by ± 1%. Within the realm of fine screening, the concentration of protein and the ratio of protein to crystallization solution within the drop

were altered, in addition to the drop size. The crystallization temperature was varied from 20˚C to 4˚C in the attempt to improve crystal quality (4).

5.1.4 Crystal Optimization: Additives

The addition of additives was also employed in an attempt to optimize the quality of crystals. Additives, such as salts, ions, organics and detergents, may aid in crystallization through stabilizing intra- and intermolecular interactions, as well as protein-solvent interactions. The Hampton Research kits Additive Screen I, II and III were used for optimization of crystals.

5.1.5 Cryo Protectant

Protein crystals were soaked into a cryo protectant solution prior to X-ray exposure. This was performed in an attempt to stabilize the protein crystal when exposed to the outside environment upon release from the closed environment of the VDX 24-well plates.

Table 5-1. Summary of the cryo solutions and their components used for protein crystal protection.

Cryo protectant 1	Cryo protectant 2	Cryo protectant 3
15.45 mM Hepes pH 7.3 3.1 mM DTT 2.31% PEG-8000 77.27 mM Imidazole 4.67% 1,6-Hexendiol 30% Glycerol	10.0 mM Hepes pH 7.3 2.0 mM DTT 1.5% PEG-8000 50 mM Imidazole 3% Ethyleneglycol 30% Glycerol	10.0 mM Hepes pH 7.3 2.0 mM DTT 1.5% PEG-8000 50 mM Imidazole 30% Glycerol

5.1.6 Data Collection

X-ray diffraction data for the apoprotein and protein with substrate complex were collected using a Rigaku/MSC. RU-H#R system equipped with a RU300 rotating copper anode (λ = 1.5418) and an R-axis IV ++ area detector (all Rigaku/MSC Ltd., La Jolla, CA). Crystals were kept frozen in a continuous stream of liquid nitrogen using a CryoJet (Oxford Instrumentation, Abingdon, England). Data were collected using CrystalClear software (Rigaku/MSC Ltd., La Jolla, CA) on a Dell Precision 330.

5.1.7 Data Processing

A single crystal was transferred to a small amount of cryoprotectant buffer using 0.4-0.5 mm loop. The loop containing the crystal was mounted on the goniometer head and flash frozen in the liquid nitrogen stream at 100° K.

Diffraction data were collected at 100 K and each image was exposed for 45 min, employing a 1° oscillation. Following collection of the diffraction images, the patterns were indexed to identify the space group and unit cell dimensions of the crystal using CrystalClear. Upon refinement of the unit cell parameters the reflections on each diffraction image were integrated to yield a list of the reflections measured. Finally, the reflections that were measured were scaled and average together to yield and final reflection list.

5.2 Results

The crystallization condition consisted of 3% Polyethylene glycol (PEG)-8000, 100 mM imidazole pH 7.3, and 3% of either glycerol, ethylene glycol or 1,6-Hexandiol. The model building and refinement of the crystal structures of GmhA with and without the substrate, sedoheptulose-7-phosphate, was performed by Dr. Murray Junop at McMaster University. The reflection list was converted to a format compatible with the CNS (define) by using the CCP4 software. Following generation of an initial model alternating rounds of manual rebuilding and model refinement were performed. To solve the structure of the GmhA protein crystal, molecular refinement technique was employed for phase determination since the protein of interest is reasonably similar to the search model GmhA from *V. cholerae* with 78.9% sequence identity 49% structural identity (PDB accession # 1x94) (44). The search model from *V. cholerae* is the same protein but in different form, such as without a mutation or without a ligand bound. This search model was used to search the unit cell for the location of the protein, once the search model is oriented correctly in the unit cell; it generates the asymmetric unit that can be used as initial estimates for the structure of interest. Dr. Junop collected a complete data set to 1.95 Å resolution for the GmhA crystal and in the tetramer space group $P2_12_12_1$, in contrast to the dimmer space group P 2_1 2_1 2 search model in *V. cholera* (Figure 5-1). Final model refinement gave R value of 21.36% and Rfree of 23.2%.

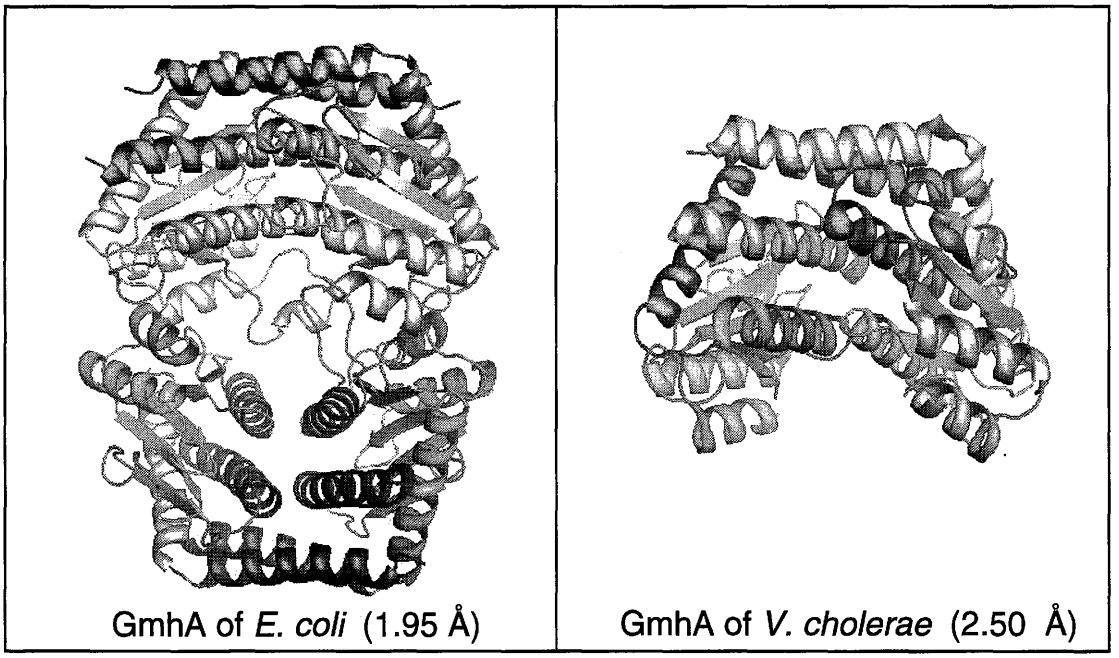

Figure 5-1. Tertiary structure of the GmhA protein in E.coli (left) and in V. cholera (right). Protein structure of GmhA with 1.95 Å resolution with a tetramer space group of $P2_12_12_1$, and the GmhA with the dimmer space group P 2_1 2_1 2 search model in *V. cholera*. The tertiary structure of *E. coli* GmhA showed a tetramer consists of four chains A, B, C and D. The structure was solved using molecular replacement using the program CCP4 with a search model dimer from the *Vibrio cholerae* GmhA structure with PDB accession number of 1X94. The structures are shown in cartoons using Pymol.

Table 5-2. Data collection statistics for *E. coli* GmhA without the substrate sedoheptulose-7-phosphate.

Information	**Statistics**
Space group	$P2_12_12_1$
Unit cell dimensions (Å)	a = 83.93 b = 89.61 c = 106.91 α = 90° β = 90° γ = 90°
Resolution range (Å)	45.91 - 1.95 (2.02 - 1.95)
Total number of reflections	253115
Number of unique reflections	59294
Average redundancy	4.27 (4.18)
Completeness (%)	99.7 (100.0)
R_{merge}^{c}	0.075 (0.398)
Reduced ChiSquared	0.98 (1.02)
Output <I/sigI>	10.9 (3.4)

Note: Values in () are for the last resolution shell.
$R_{merge}^{c} = \sum | I_{obs} - I_{avg} | / \sum I_{avg}$

Nevertheless, the resultant data set was of high quality as evidence by the significant data processing statistics in Table 5-2. The complete data set exhibited a high average redundancy of 4.27 (Total number of reflections/Number of unique reflections) with 10.9 signal to noise ratio and R_{merge}^{c} value of 0.075 (0.398). The refined unit cell dimension of the GmhA crystal were a = 83.93 Å, b = 89.61 Å, c = 106.91 Å, with angles of $\alpha = \beta = \gamma = 90°$ as listed on Table 5-2. The resolution of the protein crystal enables us to observe disulfide bond between residue 57 of chain A and residue 57 of chain D (Figure 5-1). On the other hand, another disulfide bond exists between residue 57 of chain B and residue 57 of chain C. The structure also shows crosslinking between the A

and C chains also by disulfide bridging between residues 90 from A and 90 from C. However, there was no cross-linking observed between the B and D chains.

The model for the GmhA with substrate bound was generated using the model from the GmhA without the substrate bound since both crystals are from the same protein of *E. coli* only with substrate bound to one crystal. A complete data set to 2.79 Å resolution was collected for the GmhA-sedoheptulose-7-phosphate crystals. The complex crystallized in the $P2_1$ space group with a 2.63 average redundancy and 98.6% completeness. The signal to noise ratio was 6.7, R_{merge}[c] value of 0.111 (0.360) and the refined unit cell dimensions of the crystal with substrate were a = 73.04 Å, b = 76.54 Å, c = 78.32 Å with angles of $\alpha = \gamma = 90°$ and $\beta = 106.13°$ (Table 5-2).

The tetramer protein structure showed the same disulfide bridging between chains A and D, and between chains B and C on residues 57. However, no disulfide bonds observed between chains A and C and chains B and D, instead, the structure showed disordered loops (Figure 5-1).

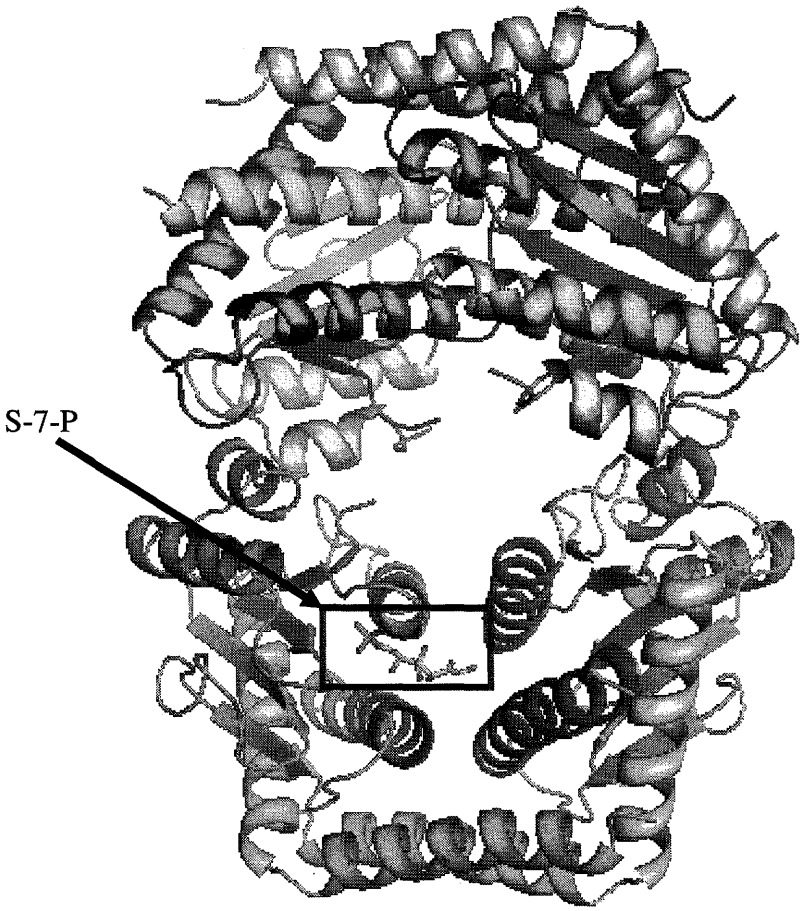

Figure 5-2. Three dimensional protein structure of *E. coli* phosphoheptose isomerase (GmhA) with bound substrate, sedoheptulose-7-phosphate (S-7-P). The tertiary structure of *E. coli* GmhA bound with the substrate sedoheptulose-7-phosphate showed a tetramer consists of four chains A, B, C and D. The structure was solved using molecular replacement with a search model dimer used to solve the GmhA structure without the bound S-7-P (Figure 5-1). The substrate S-7-P is in the red box and labeled S-7-P.

Table 5-3. Data collection statistics for *E. coli* GmhA with the bound substrate sedoheptulose-7-phosphate.

Information	**Statistics**
Space group	$P2_1$
Unit cell dimensions (Å)	a = 73.04 b = 76.54 c = 78.32 α = 90° β = 106.13° γ = 90°
Resolution range (Å)	47.39 - 2.79 (2.89 - 2.79)
Total number of reflections	53944
Number of unique reflections	20533
Average redundancy	2.63 (2.68)
Completeness (%)	98.6 (99.4)
R_{merge}[c]	0.111 (0.360)
Reduced ChiSquared	0.98 (0.94)
Output <I/sigI>	6.7 (2.6)

Note: Values in () are for the last resolution shell.

$R_{merge}^{c} = \sum | I_{obs} - I_{avg} | / \sum I_{avg}$

A complete data set to 2.79 Å resolution was collected for the GmhA-substrate crystals. The complex crystallized in the $P2_1$ space group which, tetramer showed the same disulfide bridging between chains A and D and chains B and C on residues. However, no disulfide bonds observed between chains A and C and chains B and D, instead, the structure showed disordered loops (Figure 5-2).

Possible residues interacting with the phosphate at the C7 position of S-7-P are 119 (Ser), 124 (Ser), 55 (Ser), 120 (Thr), 169 (Asp) in the B chain and 180 (His) and 65 (Glu) in the C chain.

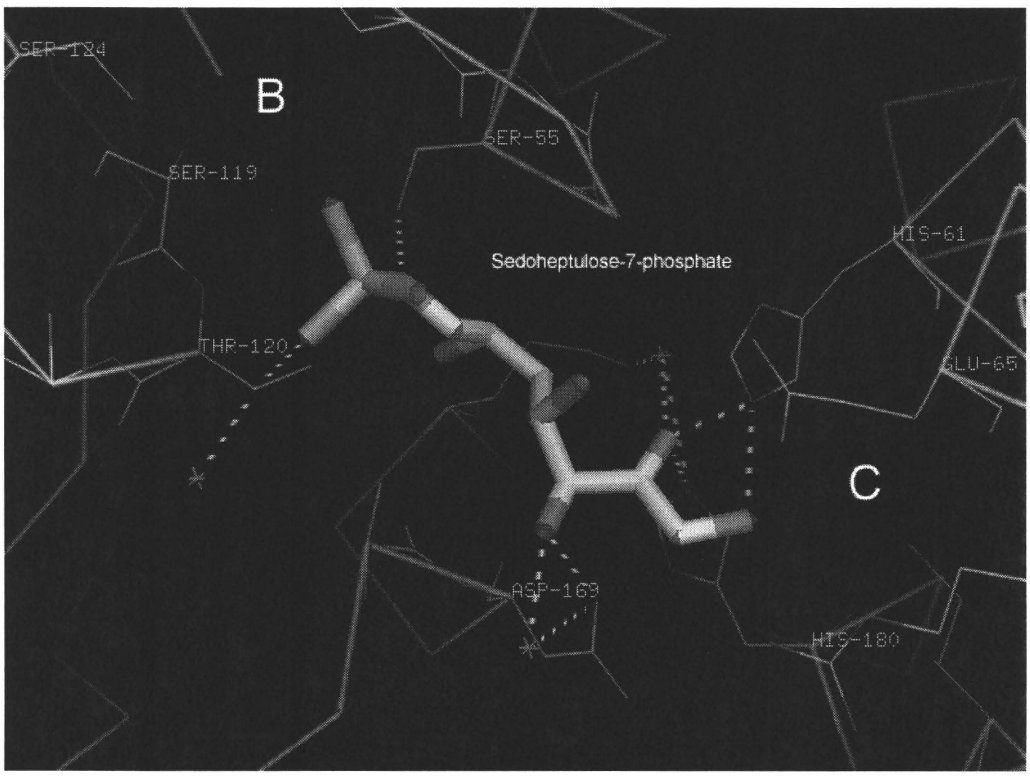

Figure 5-3. Tertiary structure of GmhA in complex with sedoheptulose-7-phosphate in *E. coli*. The substrate, sedoheptulose-7-phosphate is painted in yellow (carbon), red (oxygen) and orange (phosphate). The amino acid residues proposed to interact with the substrates are labeled in both chains B and C. This picture was produce using Pymol.

The tertiary structure of the GmhA protein bound with sedoheptulose -7-phosphate is the first reported crystal structure with the substrate bound. The crystal structure of the GmhA bound with the product however, has been solved to 2.5Å resolution (Figure 5-4) (58)

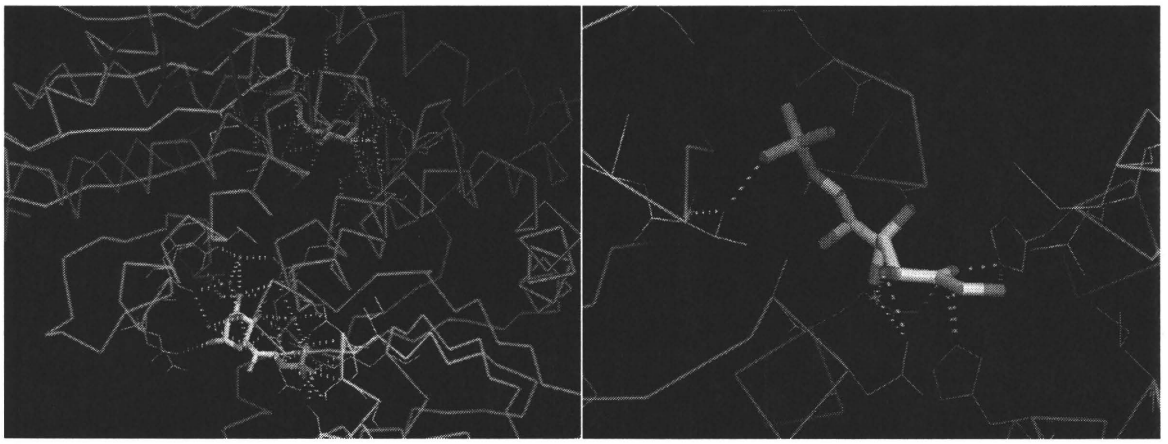

Figure 5-4. Closer look on the GmhA active site bound with the product (left) in *P. aeruginosa* and bound with the substrate (right) in *E. coli*. The tertiary structure of GmhA in complex with the product, D-glycero-α,β-D-manno-heptose-7-phosphate, has been solved with 2.5 Å resolution (left) (ref). The structure shows the cyclic heptose sugar in comparison to it linear sugar isomer sedoheptulose-7-phosphate observed in the active site of GmhA in *E.coli* with 2.8Å resolution (right). Substrate and product are color-coded as in Figure 4-3. The figure was also produced using Pymol .

References

1. **Adams, G. A., Quadling, C., and Perry, M.B.** 1967. Lipopolysaccharides from Gram-negative bacteria. Can. J. Micro **13.:**13, 1605-1613.
2. **Bareich, D. C., I. Nazi, and G. D. Wright.** 2003. Simultaneous in vitro assay of the first four enzymes in the fungal aspartate pathway identifies a new class of aspartate kinase inhibitor. Chem Biol **10:**967-73.
3. **Bauer, M. E., and R. A. Welch.** 1997. Pleiotropic effects of a mutation in rfaC on *Escherichia coli* hemolysin. Infect Immun **65:**2218-24.
4. **Blow, D. M., N. E. Chayen, L. F. Lloyd, and E. Saridakis.** 1994. Control of nucleation of protein crystals. Protein Sci **3:**1638-43.
5. **Brooke, J. S., and M. A. Valvano.** 1996. Biosynthesis of inner core lipopolysaccharide in enteric bacteria identification and characterization of a conserved phosphoheptose isomerase. J Biol Chem **271:**3608-14.
6. **Chatterjee, A. K., K. E. Sanderson, and H. Ross.** 1976. Influence of temperature on growth of lipopolysaccharide-deficient (rough) mutants of *Salmonella typhimurium* and *Salmonella minnesota*. Can J Microbiol **22:**1540-8.
7. **Cogan, E. B., Birrell, G.B. and Griffith, O.H.** 1999. A robotics-based automated assay for inorganic and organic phosphates. Anal Biochem **271:**29-35.
8. **Copeland, R. A.** 2003. Mechanistic considerations in high-throughput screening. Anal Biochem **320:**1-12.
9. **Corterton, J. W., Stewart, P.S., Greenberg, E.P.** 1999. Bacterial Biofilms: A common Cause of Persistent Infections. Science **284:**1318-1322.
10. **Davies, J. C.** 2002. *Pseudomonas aeruginosa* in cystic fibrosis: pathogenesis and persistence. Paediatric Respiratory Reviews **3:**128-134.
11. **Eidels, L., and M. J. Osborn.** 1971. Lipopolysaccharide and aldoheptose biosynthesis in transketolase mutants of *Salmonella typhimurium*. Proc Natl Acad Sci U S A **68:**1673-7.
12. **Eidels, L., and M. J. Osborn.** 1974. Phosphoheptose isomerase, first enzyme in the biosynthesis of aldoheptose in *Salmonella typhimurium*. J Biol Chem **249:**5642-8.
13. **Ernst, R. K., E. C. Yi, L. Guo, K. B. Lim, J. L. Burns, M. Hackett, and S. I. Miller.** 1999. Specific lipopolysaccharide found in cystic fibrosis airway *Pseudomonas aeruginosa*. Science **286:**1561-5.
14. **Ferguson, A. D., W. Welte, E. Hofmann, B. Lindner, O. Holst, J. W. Coulton, and K. Diederichs.** 2000. A conserved structural motif for lipopolysaccharide recognition by procaryotic and eucaryotic proteins. Structure Fold Des **8:**585-92.
15. **Heinrichs, D. E., J. A. Yethon, and C. Whitfield.** 1998. Molecular basis for structural diversity in the core regions of the lipopolysaccharides of *Escherichia coli* and *Salmonella enterica*. Mol Microbiol **30:**221-32.
16. **Jacob, S. W., and D. C. Wood.** 1967. Dimethyl sulfoxide (DMSO): toxicology, pharmacology, and current clinical usefulness. Arzneimittelforschung **17:**1553-60.

17. **Jin, U. H., T. W. Chung, Y. C. Lee, S. D. Ha, and C. H. Kim.** 2001. Molecular cloning and functional expression of the *rfaE* gene required for lipopolysaccharide biosynthesis in *Salmonella typhimurium*. Glycoconj J **18:**779-87.
18. **Jovine, L., T. Hainzl, C. Oubridge, and K. Nagai.** 2000. Crystallization and preliminary X-ray analysis of the conserved domain IV of *Escherichia coli* 4.5S RNA. erratum. Acta Crystallogr D Biol Crystallogr **56:**1512.
19. **Kadrmas, J. L., and C. R. Raetz.** 1998. Enzymatic synthesis of lipopolysaccharide in *Escherichia coli*. Purification and properties of heptosyltransferase i. J Biol Chem **273:**2799-807.
20. **Kelly, K. L., Kimball, B.A., Johnston, J.J.** 1995. Quantitation of digitoxin, digoxin, and their metabolites by high-performance liquid chromatography using pulsed amperometric detection. Journal of Chromatography **711:**289-295.
21. **Kneidinger, B., Graninger, M., Puchbergers, M., Kosma, P.m and Messner, P.** 2001. Biosynthesis of Nucleotide-activated D-*glycero*-D-*manno*-Heptose. Journal of Biological Chemistry **276:**20935-20944.
22. **Kneidinger, B., C. Marolda, M. Graninger, A. Zamyatina, F. McArthur, P. Kosma, M. A. Valvano, and P. Messner.** 2002. Biosynthesis pathway of ADP-L-*glycero*-beta-D-*manno*-heptose in *Escherichia coli*. J Bacteriol **184:**363-9.
23. **Leatherbarrow, R. J.** 2000. Grafit Ver 4.0.12. Erithacus Software LTD, Staines, UK.
24. **Lee, S., Kirschning, Muller, M., Way, C., and Floss, H.G.** 1998. Enzymatic sunthesis of [7-14C,73H]-and [1-13C] sedoheptulose-7-phospahte and [1-13C] iso-heptulose 7-phosphate. Journal of Molecular Catalysis B; Enzymatic **6:**369-377.
25. **Leive, L.** 1974. The barrier function of the gram-negative envelope. Ann N Y Acad Sci **235:**109-29.
26. **Lindsay, S. S., B. Wheeler, K. E. Sanderson, J. W. Costerton, and K. J. Cheng.** 1973. The release of alkaline phosphatase and of lipopolysaccharide during the growth of rough and smooth strains of *Salmonella typhimurium*. Can J Microbiol **19:**335-43.
27. **Macgregor, D. R., and P. R. Elliker.** 1958. A comparison of some properties of strains of P*seudomonas aeruginosa* sensitive and resistant to quaternary ammonium compounds. Can J Microbiol **4:**499-503.
28. **McGrath, B. C., and M. J. Osborn.** 1991. Evidence for energy-dependent transposition of core lipopolysaccharide across the inner membrane of *Salmonella typhimurium*. J Bacteriol **173:**3134-7.
29. **McPherson, A., A. J. Malkin, and Y. G. Kuznetsov.** 1995. The science of macromolecular crystallization. Structure **3:**759-68.
30. **Nikaido, H.** 1996. *Escherichia coli* and *Salmonella* Cellular and Molecular Biology, vol. 2. American Society of Microbiology, Washington, DC.
31. **Nikaido, H.** 1985. Molecular Basis of Bacterial Outer Membrane Permeability. Microbiological Reviews **49:**1-32.
32. **Nikaido, H.** 2003. Molecular Basis of Bacterial Outer Membrane Permeability Revisited. Microbiology and Molecular Biology Reviews **67:**593-656.

33. **Nikaido, H.** 1996. Multidrug efflux pumps of gram-negative bacteria. J Bacteriol **178:**5853-9.
34. **Nikaido, H.** 2001. Preventing drug access to targets: cell surface permeability barriers and active efflux in bacteria. Semin Cell Dev Biol **12:**215-23.
35. **Nikaido, H., K. Nikaido, and S. Harayama.** 1991. Identification and characterization of porins in *Pseudomonas aeruginosa.* J Biol Chem **266:**770-9.
36. **Parker, C. T., Kloser, A.W., Schnaitman, C.A., Stein, M.A., Gottesman, S. and Gibson, B.W.** 1992. Role of the *rfaG* and *rfaP* Genes in Determinng the Lipopolysaccharide Core Structure and Cell Surface Properties of *Escherichia coli* K-12. Journal of Bacteriology **174:**2525-2538.
37. **Parsek, M. R., and P. K. Singh.** 2003. Bacterial biofilms: an emerging link to disease pathogenesis. Annu Rev Microbiol **57:**677-701.
38. **Raetz, C.** 1996. Bacterrial Lipopolysacharides: a remarkable family of bioactive maroamphiphiles, vol. 2.
39. **Raetz, C. R., and C. Whitfield.** 2002. Lipopolysaccharide endotoxins. Annu Rev Biochem **71:**635-700.
40. **Raetz, C. R. H.** 1996. *Escherichia coli* and *Salmonella.* Cellular and Molecular Biology, vol. 2. American Society of Microbiology, Washington, DC.
41. **Saiman, L., and J. Siegel.** 2004. Infection control in cystic fibrosis. Clin Microbiol Rev **17:**57-71.
42. **Sambrook, J., Fritsch, E.F. and Maniatis,T.** 1989. *In* C. Nolan (ed.), Molecular Cloning - A Laboratory manual. Cold Spring Harbor Laboratory Press, Plainview, New York.
43. **Schnaitman, C. A., and J. D. Klena.** 1993. Genetics of lipopolysaccharide biosynthesis in enteric bacteria. Microbiol Rev **57:**655-82.
44. **Seetharaman, J., Swaminathan, S.** 2004, posting date. Crystal Structure of a Hypothetical Protein. Protein Data Bank. [Online.]
45. **Sen, K., and H. Nikaido.** 1991. Lipopolysaccharide structure required for in vitro trimerization of *Escherichia coli* OmpF porin. J Bacteriol **173:**926-8.
46. **Singh, P. K., Parsek, M.R., Greenberg, E.P., WElsh, M.J.** 2002. A component of innate immunity prevents bacterial biofilm development. Nature **417:**552-554.
47. **Singh, P. K., A. L. Schaefer, M. R. Parsek, T. O. Moninger, M. J. Welsh, and E. P. Greenberg.** 2000. Quorum-sensing signals indicate that cystic fibrosis lungs are infected with bacterial biofilms. Nature **407:**762-4.
48. **Sprenger, G. A., U. Schorken, G. Sprenger, and H. Sahm.** 1995. Transketolase A of *Escherichia col*i K12. Purification and properties of the enzyme from recombinant strains. Eur J Biochem **230:**525-32.
49. **Stanley, P. L., P. Diaz, M. J. Bailey, D. Gygi, A. Juarez, and C. Hughes.** 1993. Loss of activity in the secreted form of *Escherichia coli* haemolysin caused by an *rfaP* lesion in core lipopolysaccharide assembly. Mol Microbiol **10:**781-7.
50. **Tefsen, B., J. Geurtsen, F. Beckers, J. Tommassen, and H. de Cock.** 2005. Lipopolysaccharide transport to the bacterial outer membrane in spheroplasts. J Biol Chem **280:**4504-9.

51. **Tong, J. a. M., T.J.** 2004. Structure of Supported Bilayers Composed of Lipopolysaccharides and Bacterial Phospholipids: Raft Formation and Implications for Bacterial Resistance. Biophysical Journal **86:**3759-3771.
52. **Vaara, M.** 1992. Agents that increase the permeability of the outer membrane. Microbiol Rev **56:**395-411.
53. **Vaara, M.** 1993. Antibiotic-supersusceptible mutants of *Escherichia coli* and *Salmonella typhimurium*. Antimicrob Agents Chemother **37:**2255-60.
54. **Vaara, M.** 1996. Lipid A: target for antibacterial drugs. Science **274:**939-40.
55. **Valvano, M. A., C. L. Marolda, M. Bittner, M. Glaskin-Clay, T. L. Simon, and J. D. Klena.** 2000. The *rfaE* gene from *Escherichia coli* encodes a bifunctional protein involved in biosynthesis of the lipopolysaccharide core precursor ADP-L-*glycero*-D-*manno*-heptose. J Bacteriol **182:**488-97.
56. **Valvano, M. A., P. Messner, and P. Kosma.** 2002. Novel pathways for biosynthesis of nucleotide-activated *glycero-manno*-heptose precursors of bacterial glycoproteins and cell surface polysaccharides. Microbiology **148:**1979-89.
57. **Voet, D. a. V., J.G.** 1995. Rates of Enzymatic Reactions, p. 345-371, Biochemistry, 2 ed. John Wiley and Sons Inc., Etobicoke, Ontario.
58. **Walker, J. R., Evdokimova, E., Kudritska M., Edwards, A.,Savchenko, A.** 2004, posting date. Crystal Structure of *Psedomonas aeruginosa* phosphoheptose isomerase In Complex with reaction product D-*glycero*-D-*manno*pyranose-7-phosphate. Protein Data Bank. [Online.]
59. **WHO** 2000, posting date. World Health Organization infectious disease report. [Online.]
60. **Yethon, J. A., and C. Whitfield.** 2001. Lipopolysaccharide as a target for the development of novel therapeutics in gram-negative bacteria. Curr Drug Targets Infect Disord **1:**91-106.
61. **Zhang, J., Chung, T.D.Y., Oldenburg, K.R.** 1999. A Simple Statistical Parameter for use in Evaluation and Validation of High Troughput Screening Assays. Journal of Biomolecular Screening **4:**67-73.